P.O. Box 63
Lycoming, New York 13093

Constellation Energy Group

Nine Mile Point
Nuclear Station

January 15, 2003
NMP1L 1708

U.S. Nuclear Regulatory Commission
Attn: Document Control Desk
Washington, DC 20555

SUBJECT: Nine Mile Point Unit 1
Docket No. 50-220

Transmittal of Neutron Transport Calculations Benchmarking Report
TAC Nos. MB6687 and MB6703

Gentlemen:

The purpose of this letter is to transmit the Reactor Pressure Vessel (RPV) neutron transport calculations benchmarking report for NRC review and approval for qualification of the calculational methodology utilized in the neutron fluence determinations applicable to Nine Mile Point Unit 1 (NMP1). As further discussed below, submittal of the benchmarking report also satisfies a commitment contained in a Technical Specification (TS) amendment application, dated November 15, 2002 (Reference: TAC Nos. MB6687 and MB6703).

By letter dated November 15, 2002 (NMP1L 1697), Nine Mile Point Nuclear Station, LLC, (NMPNS) transmitted an application for amendment to the NMP1 Technical Specifications (TSs) as set forth in Appendix A of Operating License DPR-63. The application proposed changes that would revise the Reactor Coolant System (RCS) Pressure-Temperature (P-T) limit curves and associated limit tables specified in Section 3/4 2 2, "Minimum Reactor Vessel Temperature for Pressurization," of the TSs. The proposed P-T limit curves and tables were developed using the alternate methodology of American Society of Mechanical Engineers (ASME) Boiler and Pressure Vessel (B&PV) Code Case N-640 and would be valid for 28 Effective Full Power Years (EFPY). The neutron fluence values for the RPV are unchanged from those calculated and approved for the current P-T limit curves and tables. Therefore, the proposed P-T limit curves and tables were developed using the ASME B&PV N-640 Code Case in conjunction with the currently approved neutron fluence values.

The current P-T limit curves and tables were developed in 1998 following the 1997 withdrawal and testing of the 210 degree surveillance capsule. The calculations supporting the current P-T limit curves and tables utilized RPV neutron fluence values calculated consistent with the methodology of Draft Regulatory Guide DG-1053, which was a previous draft for Regulatory Guide 1.190, "Calculational and Dosimetry Methods

A001
A047

for Determining Pressure Vessel Neutron Fluence." The supporting calculations are documented in Appendix B of Report No. MPM-108679, "Nine Mile Point Unit 1 Shroud Neutron Transport and Uncertainty Analysis," dated October 1998, which was submitted to the NRC for review in Letter NMP1L 1373, dated October 22, 1998. Note that Draft Regulatory Guide DG-1053 was the most recent guidance for neutron fluence calculations available in 1998.

In March 2001, the NRC issued Regulatory Guide 1.190, which requires the benchmarking of the methodology used for fluence determinations. The neutron fluence calculations supporting both the current and proposed P-T limit curves and tables have been verified to be fully compliant with Regulatory Guide 1.190, except for the benchmark reporting requirement for methods qualification.

In the November 15, 2002 TS amendment application, NMPNS committed to submit to the NRC by January 15, 2003 the report documenting the results of the RPV neutron fluence benchmark measurements and calculations applicable to the methods used for NMP1. Contained herein as Attachment 1 is the benchmarking report (MPM-402781) for NRC review and approval. Note that this report applies to the methodology used to calculate the RPV and core shroud fluence for both NMP1 and Nine Mile Point Unit 2 (NMP2). As previously indicated, the fluence calculations for NMP1 are documented in Report No. MPM-108679, dated October 1998, which was submitted to the NRC for review in 1998. The fluence calculations for NMP2 are documented in Report Nos. MPM-301624 and MPM-301624A, dated January 2003. The NMP2 reports are being submitted as Attachments 2 and 3 to this letter, respectively, as they have not been previously submitted to the NRC for review. These NMP2 reports are incorporated by reference into the MPM-402781 benchmarking report.

Upon approval of the RPV neutron fluence benchmarking report and corresponding calculational methodology, NMPNS requests that the NRC staff remove any restrictions on the application of the P-T limit curves and tables for NMP1 that were imposed pending such approval.

Since the attached analyses are copyright protected by the author, enclosed is a copyright release permitting limited distribution within the NRC.

Sincerely,

Bruce S. Montgomery
Manager Engineering Services

BSM/CDM/jm
Enclosure

Attachments:
1. Report No. MPM-402781
2. Report No. MPM-301624
3. Report No. MPM-301624A

cc: Mr. H. J. Miller, NRC Regional Administrator, Region I
Mr. G. K. Hunegs, NRC Senior Resident Inspector
Mr. P. S. Tam, Senior Project Manager, NRR (2 copies)

Copyright Notice

The publications listed below bears a 2003 Copyright Notice. MPM Technologies, Inc., holder of the copyright, hereby grants the Nuclear Regulatory Commission (NRC) the authority to make the number of copies of this copyrighted material which are necessary for its internal use and to fulfill its legal responsibilities as regards public disclosure. This authorization is granted with the understanding that any copies of the publication made by the NRC will continue to bear the following copyright notice, which will be reproduced along with any portion of the publication:

The reports listed below contains material copyrighted by MPM Technologies, Inc.. Material reproduced by permission of MPM Technologies, Inc..

1. "Nine Mile Point Unit 2 Shroud Neutron Transport and Uncertainty Analysis," Report MPM-301624, MPM Technologies, Inc., 2161 Sandy Drive, State College, PA 16803-2283, January, 2003.
2. "Nine Mile Point Unit 2 Shroud Neutron Transport and Uncertainty Analysis:Addendum", Report MPM-301624A, MPM Technologies, Inc., 2161 Sandy Drive, State College, PA 16803-2283, January, 2003.
3. "Benchmarking of Neutron Transport Calculations for Boiling Water Reactor Analyses," Report MPM-402781, MPM Technologies, Inc., 2161 Sandy Drive, State College, PA 16803-2283, January, 2003.

MPM Technologies, Inc.

M P Manahan, Sr.

M. P. Manahan, Sr.
President

ATTACHMENT 1

REPORT NO. MPM-402781

BENCHMARKING OF NINE MILE POINT UNIT 1 AND UNIT 2 NEUTRON TRANSPORT CALCULATIONS

Benchmarking of Nine Mile Point Unit 1 and Unit 2 Neutron Transport Calculations

© Copyright 2003 MPM Technologies, Inc.
All Rights Reserved

MPM Technologies, Inc.

. .serving client needs through advanced technology ..

January, 2003

Report Number MPM-402781

Final Report

entitled

Benchmarking of Nine Mile Point Unit 1 and Unit 2 Neutron Transport Calculations

prepared for

Constellation Generation Group
Nine Mile Point Units 1 and 2
Lake Road
Lycoming, NY 13093

by

MPM Technologies, Inc.
2161 Sandy Drive
State College, PA 16803-2283

January, 2003

Preparer	**Checker**
1/7/03	**1/7/03**
Date	**Date**

MPM Approval

1/7/03

Date

© Copyright 2003 MPM Technologies, Inc.
All Rights Reserved

Nuclear Quality Assurance Certification

This document certifies that MPM has performed all work under Nine Mile Point Station Purchase Order Number 01-35807-001 in accordance with the requirements of the Purchase Order. All work has been performed under the MPM Nuclear Quality Assurance Program.

M P Manahan, Sr.

M. P. Manahan, Sr.
President
1/7/03

Date

S. Clinger

S. Clinger
QA Manager
1/7/03

Date

Executive Summary

In March 2001, the Nuclear Regulatory Commission (NRC) issued Regulatory Guide (RG) 1.190, "Calculational and Dosimetry Methods for Determining Pressure Vessel Neutron Fluence." Although specifically developed to address calculation of fluence to the vessel, the guide can be considered to apply to other reactor components such as the shroud or surveillance capsule. One of the requirements of RG 1.190 is the benchmarking of the methodology used in the fluence determination. This report documents calculations performed to qualify the MPM methodology as applied for fluence determination for Nine Mile Point Unit 1 and Unit 2.

In order to meet the methods qualification requirement of RG 1.190, the MPM calculational methodology has been validated by comparison with measurement and calculational benchmarks. Comparisons of calculations with measurements have been made in the Pool Critical Assembly (PCA) pressure vessel simulator benchmark and in the Nine Mile Point Units 1 and 2 (NMP-1 and NMP-2) operating plants. Comparisons with a BWR calculational benchmark have also been completed.

The PCA has high-accuracy measurement results extending from inside a simulated thermal shield through to the outside of a simulated vessel. The calculational results in the PCA show a slight consistent bias (less than 10%) with respect to the measurements, but no significant change in bias is observed with change in irradiation position. This indicates that the transport methodology is calculating the flux attenuation outside the core region with high accuracy. The observed bias is consistent with that obtained by other synthesis calculations.

The calculational benchmark was a typical BWR geometry similar to those of NMP-1 and NMP-2. Comparisons were made between the MPM calculations and the benchmark calculational results which indicated very good agreement. In the capsule the average results were about 3% low, and at the vessel inner radius (IR) and within the vessel, the average results were about 2-3% high. All compared results fell within ±10%.

Additional comparisons were made with surveillance capsule measurements from NMP-1 and NMP-2 and with shroud boat sample measurements from NMP-1. In all cases, agreement with measured results were shown to be less than ±20%. This meets the criterion set by RG 1.190 for acceptability of the calculations.

In summary, it is concluded that the RG 1.190 requirement for qualification of the MPM methodology used for Nine Mile Point Units 1 & 2 by comparisons to measurement and calculational benchmarks has been fully satisfied.

Contents

Executive Summary ..... **Preface Page iii**

1.0 Introduction ..... **Page Number 1**

2.0 Neutron Flux Calculational Method ..... **Page Number 3**
- 2.1 Neutron Transport Model ..... Page Number 3
- 2.2 Compliance with RG 1.190 ..... Page Number 4

3.0 PCA Benchmark Calculation ..... **Page Number 10**

4.0 BWR Calculational Benchmark ..... **Page Number 19**

5.0 Plant Specific Benchmarking ..... **Page Number 27**
- 5.1 NMP-1 Benchmarks ..... Page Number 27
- 5.2 NMP-2 Benchmark ..... Page Number 30

6.0 Summary and Conclusions ..... **Page Number 42**

7.0 Nomenclature ..... **Page Number 43**

8.0 References ..... **Page Number 44**

1.0 Introduction

In March 2001, the Nuclear Regulatory Commission (NRC) issued Regulatory Guide (RG) 1.190, "Calculational and Dosimetry Methods for Determining Pressure Vessel Neutron Fluence" [1]. This guide is the final version of two previous draft guides, DG-1053 and DG-1025. The guide was developed to provide state-of-the-art calculational and measurement procedures that are acceptable to the NRC staff for determining pressure vessel fluence. Although specifically developed to address calculation of fluence to the vessel, the guide can be considered to apply to other reactor components such as the shroud and the surveillance capsules.

One of the requirements of RG 1.190 is the benchmarking of the methodology used in the fluence determination. Specifically, RG 1.190 has the following requirement:

> *Methods Qualification. The calculational methodology must be qualified by both (1) comparisons to measurement and calculational benchmarks and (2) an analytic uncertainty analysis. The methods used to calculate the benchmarks must be consistent (to the extent possible) with the methods used to calculate the vessel fluence. The overall calculational bias and uncertainty must be determined by an appropriate combination of the analytic uncertainty analysis and the uncertainty analysis based on the comparisons to the benchmarks.*

Fluences in various reactor components for Nine Mile Point Units 1 and 2 (NMP-1 and NMP- 2) have been evaluated in several reports [2,3,4] prepared prior to the issuance of RG 1.190 in March, 2001. In addition, an update of the NMP-2 shroud fluence evaluation has been issued [5,6]. The fluence analyses in these reports were fully compliant with RG 1.190 except for part of the benchmarking requirement for methods qualification. This report completes that requirement and, thereby, makes all the analyses totally consistent with RG 1.190.

Benchmarking the methodology requires more than one analysis. Because fluence measurements cannot be made at all of the actual points of interest in an operating plant, neutron transport calculations are necessary to obtain the fluence at all important locations. Since the calculations involve many parameters, agreement of calculations with measurements at one point in space cannot guarantee the same calculational accuracy at other points. This report contains documentation of several benchmark analyses pertinent to BWR calculations. Taken together, they provide a validation of the calculational method for accurate determination of the fluence at all regions between the core and the outside of the reactor vessel.

The first benchmark is a calculation of the Pool Critical Assembly (PCA) simulated reactor vessel [7]. This benchmark provides validation of the transport through typical reactor structures and the simulated reactor vessel in a simple geometry. It provides a test of the transport methodology in a reactor geometry and enables a comparison of the calculational results within the vessel structure with measurements.

The second benchmark is a calculational benchmark for a typical BWR geometry [8]. While this benchmark does not provide verification of the methodology by comparison with measurements, it does enable a check for the consistency of the methodology with results calculated by NRC contractors using standard techniques. Agreement with this benchmark ensures that the transport results obtained for BWR plants includes all important factors for accurate transport in BWR plants. BWR analyses involve more complex modeling situations than encountered in PWR plant analyses such as those that arise from asymmetric geometry, fuel burnup, and fuel region void fractions.

The third set of benchmarks is a comparison with dosimetry measurements in actual BWR plants. While the other benchmarks provide validation of the methodology, only comparisons with actual plant measurements can verify that the correct plant information has been included in the analysis. Plant-specific comparisons enable biases to be identified that arise from uncertainties in the plant dimensions, power distributions, operating conditions, etc.

Successful completion of the analyses described above, as indicated by agreement with measurements or other calculations within tolerance, completely satisfies the methodology qualification requirement. In addition, application of the methodology to a specific plant requires an analytic uncertainty analysis for each plant-specific case. These uncertainty analyses are included in the report prepared for each specific plant.

2.0 Neutron Flux Calculational Method

2.1 Neutron Transport Model

The neutron exposure of reactor structures is determined by a neutron transport calculation, or a combination of neutron transport calculations, to represent the distribution of neutron flux in three dimensions. The calculation determines the distribution of neutrons of all energies from their source from fission in the core region to their eventual absorption or leakage from the system. The calculation uses a model of the reactor geometry that includes the significant structures and geometrical details necessary to define the neutron environment at locations of interest.

The transport calculations reported here were carried out using the DORT two-dimensional discrete ordinates code [9] and the BUGLE-96 cross-section library [10]. Other codes used for DORT input preparations included the DOTSOR code (available as part of the LEPRICON code package [11], which was used to convert core power distributions from X,Y to R,θ coordinates and place the source in each mesh cell, and the ORIGEN 2.1 code [12], which was used to calculate the effects of burnup on the neutron source. The computer codes and data libraries were obtained from the Radiation Safety Information Computational Center (RSICC) at Oak Ridge National Laboratory (ORNL). Each code was then compiled on the computer used by MPM for the calculations and a series of test cases were run to verify the code performance. The test cases all agreed within allowable tolerance with established results. This verification was conducted under the MPM Nuclear Quality Assurance Program.

The DORT code is an update of the DOT code which has been in use for this type of problem for many years. It is routinely used and has been used by others for benchmarking calculations [7,8,13,14]. In the analyses, anisotropic scattering was treated with a P_3 expansion of the scattering cross-sections, and the angular discretization was modeled with an S_8 order of angular quadrature. These procedures are in accordance with RG 1.190 and ASTM Standard E-482 [15].

The BUGLE-96 library is a 47 energy group ENDF/B-VI based data set produced specifically for light water reactor shielding and pressure vessel dosimetry applications (an update of the earlier SAILOR library). The energy group boundaries for the 47 groups are given in Table 2-1. This library contains cross-sections collapsed using flux spectra from both BWR and PWR reactor models. Within the core region, cross section sets are collapsed using a PWR core spectrum and a BWR core spectrum. Outside the core, cross sections are produced using a PWR downcomer spectrum, a PWR vessel 1/4 T spectrum, and a concrete spectrum. Reference [8] details the data testing of the BUGLE libraries and validation of their applicability for LWR shielding calculations.

As indicated above, the DORT code calculates the neutron transport in two dimensions. In order to estimate the fluence rate in the three-dimensional geometry, the following equation was used to synthesize the flux ϕ for each case of cylindrical geometry:

$$\phi(R,\theta,Z) = \phi(R,\theta) * \phi(R,Z) / \phi(R)$$

In this equation, $\phi(R,\theta)$ is taken from the DORT R,θ calculation (normalized to the power at midplane in the model region), and $\phi(R,Z)$ is from the R,Z calculation normalized to the power in the entire core. A third calculation determined $\phi(R)$ using a one-dimensional cylindrical model normalized at core midplane. The one-dimensional calculation uses the same radial geometry and source distribution as the R,Z calculation at core midplane. In the case of the PCA benchmark, the calculation was carried out in X, Y, Z geometry and a similar synthesis equation was used.

For each calculation, a detailed model of the reactor geometry was developed. The models contain all of the significant reactor structures and use a mesh structure that is fine enough to give good flux convergence. Typically, the radial mesh will be the most critical because of the large flux attenuation of neutrons as they are transported from the core to the vessel region. Most radial mesh intervals outside the core are smaller than 1 cm. This is particularly important in steel structures for calculation of the flux above 1 MeV. Models of large reactor geometries, such as for BWRs, will have 140 to 200 radial mesh points. In the azimuthal direction models have 40 to 80 mesh points to cover an octant of the reactor, depending on the structures to be defined. In the axial direction, models may have as many as 150 mesh points, or more. Modeling smaller reactor geometries, such as the PCA, do not require as many points.

2.2 Compliance with RG 1.190

Regulatory Guide 1.190 covers recommended practices for neutron transport calculations and applies to other reactor components in addition to the primary emphasis on the pressure vessel. The regulatory positions in the guide that pertain to calculational methodology are summarized in Table 2-2 which is taken directly from the guide. The table references paragraphs in the guide that give more detailed information on each position. The compliance of the MPM calculational methodology with the guide is summarized below.

Fluence Determination: All calculations were performed using an absolute fluence calculation. Meets guide requirement.

Modeling Data: All the data used in the models are documented and verified. Meets guide requirement.

Nuclear Data: The calculations use the BUGLE-96 cross section set which is based on the latest version (VI) of the Evaluated Nuclear Data File (ENDF/B). The BUGLE-96 set has undergone extensive testing and benchmarking to ensure its validity for LWR calculations.

Meets guide requirement.

Cross-Section Angular Representation: The calculations use a P3 angular expansion in accordance with the guide.
Meets guide requirement.

Cross-Section Group Collapsing: The calculations use the BUGLE-96 library without additional collapsing. Benchmarking has shown that the 47 group structure is adequate for LWR neutron transport calculations.
Meets guide requirement.

Neutron Source: Isotopic variation is accounted for in the neutron spectrum, neutrons per fission, and energy per fission within the modeling limitations. Moderator density is included in detail.
Meets guide requirement.

End-of-Life Predictions: No fluence projections are made in this benchmarking effort. Fluence projections for plant analyses use best-estimate fuel loadings.
Meets guide requirement.

Spatial Representation: Mesh intervals are adopted to ensure that flux changes within intervals are small enough to allow for accurate results. Radial intervals in the outer core region and in the region between the core and the outside of the vessel are generally about 1 cm except near boundaries where a finer mesh is used in some cases. Inside the core, where flux changes are small, larger intervals are used. In the azimuthal direction, between 40 and 80 meshes are used, depending on the complexity of structures to be modeled. In the axial direction, a coarse mesh is acceptable in regions where the flux changes slowly. Finer meshing is used near boundaries. The quadrature used was S8.
Meets guide requirement.

Multiple Transport Calculations: It was not necessary to use bootstrapping for these calculations so this requirement does not apply.

Point Estimates: This requirement only applies to Monte Carlo calculations which are not used here.

Statistical Tests: This requirement only applies to Monte Carlo calculations which are not used here.

Variance Reduction: This requirement only applies to Monte Carlo calculations which are not used here.

Spectral Effects on RT_{NDT}: This requirement only applies to extrapolation through the vessel and does not affect the benchmark calculations. However, when fluence within the vessel is

required, the displacement per atom (dpa) methodology is applied to vessel calculations as specified in RG 1.99, Revision 2 [16] (see, for example, Reference [3]).
Meets guide requirement.

Cavity Calculations: With the exception of the one dosimetry measurement at the rear of the PCA vessel, no cavity results have been applied for this benchmarking effort. In the event that cavity dosimetry measurements are analyzed in the future, it will be necessary to ensure that the quadrature is adequate. Utilization of cavity flux calculations is not anticipated at this time.
Meets guide requirement.

Methods Qualification: These calculations and comparisons provide the required methods qualification. This includes verification of vessel fluence calculations using the PCA simulator measurements, the BWR calculational benchmark, and comparisons with plant specific BWR measurements. No uncertainty analysis was performed for the PCA calculation or for the BWR calculational benchmark since no uncertainty data is given with these problems. Comparisons with measurements or with standard results provide validation of the accuracy of the calculations. A complete analytical uncertainty analysis was carried out in accordance with the guide for the NMP-1 and NMP-2 calculations. This uncertainty analysis indicated that calculational errors for vessel fluences in the beltline region were about 15%, well within the 20% accuracy requirement specified by RG 1.190.
Meets guide requirement.

Fluence Calculational Uncertainty: An extensive evaluation of all contributors to the uncertainty in the calculated fluence was made for the NMP-1 and NMP-2 calculations. This evaluation indicated that the uncertainty in calculated fluences in the reactor beltline region is below 20% as specified in the guide. In addition, the comparisons with measurements indicate agreement well within the 20% limit. Thus, fluence evaluations using the present methodology applied to NMP-1 and NMP-2 will use the calculated results with no bias applied.
Meets guide requirement.

Table 2-1 Neutron Energy Group Structure – 47 Groups.

Energy Group	Upper Energy (MeV)	Energy Group	Upper Energy (MeV)
1	1.733E+01	25	2.972E-01
2	1.419E+01	26	1.832E-01
3	1.221E+01	27	1.111E-01
4	1.000E+01	28	6.738E-02
5	8.607E+00	29	4.087E-02
6	7.408E+00	30	3.183E-02
7	6.065E+00	31	2.606E-02
8	4.966E+00	32	2.418E-02
9	3.679E+00	33	2.188E-02
10	3.012E+00	34	1.503E-02
11	2.725E+00	35	7.102E-03
12	2.466E+00	36	3.355E-03
13	2.365E+00	37	1.585E-03
14	2.346E+00	38	4.540E-04
15	2.231E+00	39	2.145E-04
16	1.920E+00	40	1.013E-04
17	1.653E+00	41	3.727E-05
18	1.353E+00	42	1.068E-05
19	1.003E+00	43	5.044E-06
20	8.208E-01	44	1.855E-06
21	7.427E-01	45	8.764E-07
22	6.081E-01	46	4.140E-07
23	4.979E-01	47	1.000E-07
24	3.688E-01		1.000E-11

Table 2-2 Summary of Regulatory Positions on Fluence Calculation Methods [1].

	Regulatory Position
Fluence Determination. Absolute fluence calculations, rather than extrapolated fluence measurements, must be used for the fluence determination.	1.3
Modeling Data. The calculation modeling (geometry, materials, etc.) should be based on documented and verified plant-specific data.	1.1.1
Nuclear Data. The latest version of the Evaluated Nuclear Data File (ENDF/B) should be used for determining nuclear cross- sections. Cross-section sets based on earlier or equivalent nuclear-data sets that have been thoroughly benchmarked are also acceptable. When the recommended cross-section data change, the effect of these changes on the licensee-specific methodology must be evaluated and the fluence estimates updated when the effects are significant.	1.1.2
Cross-Section Angular Representation. In discrete ordinates transport calculations, a P_3 angular decomposition of the scattering cross-sections (at a minimum) must be employed.	1.1.2
Cross-Section Group Collapsing. The adequacy of the collapsed job library must be demonstrated by comparing calculations for a representative configuration performed with both the master library and the job library.	1.1.2
Neutron Source. The core neutron source should account for local fuel isotopics and, where appropriate, moderator density. The neutron source normalization and energy dependence must account for the fuel exposure dependence of the fission spectra, the number of neutrons produced per fission, and the energy released per fission.	1.2
End-of-Life Predictions. Predictions of the vessel end-of-life fluence should be made with a best-estimate or conservative generic power distribution. If a best estimate is used, the power distribution must be updated if changes in core loadings, surveillance measurements, or other information indicate a significant change in projected fluence values.	1.2
Spatial Representation. Discrete ordinates neutron transport calculations should incorporate a detailed radial- and azimuthal-spatial mesh of ~2 intervals per inch radially. The discrete ordinates calculations must employ (at a minimum) an S_8 quadrature and (at least) 40-80 intervals per octant.	1.3.1
Multiple Transport Calculations. If the calculation is performed using two or more "bootstrap" calculations, the adequacy of the overlap regions must be demonstrated.	1.3.1

Table 2-2 Summary of Regulatory Positions on Fluence Calculation Methods [1] (Continued).

	Regulatory Position
Point Estimates. If the dimensions of the tally region or the definition of the average-flux region introduce a bias in the talley edit, the Monte Carlo prediction should be adjusted to eliminate the calculational bias. The average-flux region surrounding the point location should not include material boundaries or be located near reflecting, periodic or white boundaries.	1.3.2
Statistical Tests. The Monte Carlo estimated mean and relative error should be tested and satisfy all statistical criteria.	1.3.2
Variance Reduction. All variance reduction methods should be qualified by comparison with calculations performed without variance reduction.	1.3.2
Capsule Modeling. The capsule fluence is extremely sensitive to the geometrical representation of the capsule geometry and internal water region, and the adequacy of the capsule representation and mesh must be demonstrated	1.3.3
Spectral Effects on RT_{NDT}. In order to account for the neutron spectrum dependence of RT_{NDT}, when it is extrapolated from the inside surface of the pressure vessel to the T/4 and 3T/4 vessel locations using the > 1-MeV fluence, a spectral lead factor must be applied to the fluence for the calculation of ΔRT_{NDT}.	1.3.3
Cavity Calculations. In discrete ordinates transport-calculations, the adequacy of the S_8 angular quadrature used in cavity transport calculations must be demonstrated.	1.3.5
Methods Qualification. The calculational methodology must be qualified by both (1) comparisons to measurement and calculational benchmarks and (2) an analytic uncertainty analysis. The methods used to calculate the benchmarks must be consistent (to the extent possible) with the methods used to calculate the vessel fluence. The overall calculational bias and uncertainty must be determined by an appropriate combination of the analytic uncertainty analysis and the uncertainty analysis based on the comparisons to the benchmarks.	1.4.1, 1.4.2, 1.4.3
Fluence Calculational Uncertainty. The vessel fluence (1 sigma) calculational uncertainty must be demonstrated to be 20% for RT_{PTS} and RT_{NDT} determination. In these applications, if the benchmark comparisons indicate differences greater than ~20%, the calculational model must be adjusted or a correction must be applied to reduce the difference between the fluence prediction and the upper 1-sigma limit to within 20%. For other applications, the accuracy should be determined using the approach described in Regulatory Position 1.4, and an uncertainty allowance should be included in the fluence estimate as appropriate in the specific application.	1, 1.4.3

3.0 PCA Benchmark Calculation

The PCA pressure vessel simulator was constructed to provide a well-characterized geometry that is a mockup of typical reactor geometries. A view of this benchmark facility is shown in Figure 3-1 (from Reference [7]). Measurements were made with this simulator arranged in a variety of geometries, including in some cases simulated surveillance capsules, but the recommended benchmark described in Reference [7] consists of a single geometry. The reference provides a complete description of the benchmark including the geometry and source distribution. The geometry has a 12 cm gap between the reactor core and thermal shield plate, and a 13 cm gap between the thermal shield and the vessel simulator. A schematic of this geometry is shown in Figure 3-2 (from Reference [7]). This geometry, while more typical of PWRs than BWRs, can be used to evaluate the adequacy of the calculational methodology to accurately determine fluence from the core to the rear of the pressure vessel. In particular, measurements within the pressure vessel mockup provide validation of the calculations in this region where dosimetry measurements cannot normally be made.

Results in the PCA were calculated using X,Y,Z geometry. The results were synthesized from an X,Y calculation (X is the horizontal direction and Y is the direction out from the core through the mockup), a Y,Z calculation (Z is the vertical direction), and a one-dimensional calculation in Y. The synthesis equation is:

$$\phi\,(X,Y,Z) = \phi(X,Y) * \phi(Y,Z) / \phi(Y).$$

The X,Y model was set up using 79 meshes in the X direction and 130 meshes in the Y direction. The 79 X meshes consist of 17 meshes in the water on each side of the core and 45 meshes within the core. The line of symmetry at X=0 was ignored and the whole width of the core was included in the model. The Y direction starts at the line of symmetry in the middle of the core and extends through to the water at the rear of the void box. The mesh spacing is defined similar to that which is normally used to ensure good convergence of the calculated flux. Similarly, the Y,Z model was set up using the same Y dimensions and meshes and 61 meshes in the vertical direction. The model extends from the water region below the fuel to the water region above the fuel. Both the X,Y and Y,Z models include water regions outside the thermal shield and pressure vessel simulator and thus take into account streaming that can occur around these structures due to their finite size.

The fuel region was modeled as a homogeneous material, calculated from the dimensions of the fuel plates and other structures. The fuel elements are made up of slightly curved fuel plates. This curvature was ignored in the model and the fuel elements were taken to have a rectangular cross section (8.100 cm in the Y direction by 7.709 cm in the X direction). The fuel height of the core region was taken to be the fuel element length (62.548 cm), but the source was confined to the length of the fueled region in the fuel plates (60.008 cm).

The power distribution in the horizontal plane was defined by a 3x3 array for each fuel element. This distribution was used directly for the X,Y calculation. In the vertical direction,

the power distribution was specified by a cosine function:

$$p(z) = C \cos[B_z(z-z_o)]$$

where C is a normalization constant, B_z is equal to 0.0442 cm^{-1} and z_o is equal to -4.20 cm [7]. The overall normalization of the calculations is a source of 1 neutron/cm-s produced in the core. The fuel enrichment is 93% U235 and it was assumed that 100% of the fissions were from U235.

Measurements in the mockup can be made by inserting dosimetry into tubes extending down through the water and through the mockup region. Both active and passive dosimetry measurements were made (using several different techniques). Results are available for seven measurement positions ranging from the front of the thermal shield to the back of the vessel. These positions are listed and described in Table 3-1.

All measurements were normalized to a reactor power of one fission neutron per second produced in the core. The measurements were related to similar measurements made in a U235 fission spectrum and are presented in the units of "equivalent fission flux", which is the detector response in the PCA divided by the detector response in a U235 fission flux. By expressing the measurement in this way, a number of uncertainties are eliminated from the measurement (e.g. fission yield, gamma yield, and detector efficiency). Thus, some measurement uncertainties are reported to be as low as 1% or less [7]. Most of the non-fission radiometric dosimeter measurements have uncertainties between 1% and 3%. The fission measurements have higher uncertainties (5% to 9%), which may be due in part to differences in results obtained with the different techniques. The benchmark specifications do not give any estimate of uncertainties in positioning (or reproducibility of positioning) of the mockup, and this could be an important consideration in an uncertainty evaluation of comparisons of calculations with the measurements.

Results were calculated for the measured dosimetry reactions at each of the locations in Table 3-1. The reaction rates were calculated assuming 1 fission neutron per second produced in the core from U235 fission. The reaction rates were then converted to give an equivalent fission flux by dividing by a calculated reaction rate in a unit U235 fission spectrum. The results are presented in Table 3-2 for each of six reactions for each location. Comparisons are then made with the measured values from Reference [7].

The rhodium reaction is not one that is commonly used in reactor dosimetry analyses because of the very short half-life. Therefore not much attention has been paid to the dosimetry cross section for this reaction and the BUGLE-96 cross section is probably not very accurate. Thus, data from this reaction should be rejected and these data were not used in calculating an average bias at each location. Note that in Reference [7] the rhodium results show more consistency using a different reaction cross section.

It is also noted that the U238 calculated results are consistently low compared to the other reactions. This is not likely to be an error in calculation of the flux spectrum since dosimeters

with energy responses above and below the U238 energy response do not support any trend in deviation of the results. The dosimeter cross sections used here are the ones collapsed using a fine group spectrum calculated at the 1/4T position in a pressure vessel. The fine group calculation includes structure in the flux spectrum around 1 MeV, a region where the U238 cross section is changing rapidly with energy. The result is that the BUGLE-96 cross section at the 1/4T position is lower in energy group 18 (the one just above 1 MeV) than is the case if flat weighting is used. This group is the most important one for the U238 response. Results here and in PWR cases indicate that the U238 cross section may be too low in this region. This does not affect any of the other dosimetry reactions and U238 is not typically used in BWR dosimetry packages and was not used in any of the NMP-1 nor NMP-2 dosimetry. Because of the greater C/M ratio deviation and the concerns expressed above, the U238 results were also ignored in calculating an average bias at each location.

Average C/M ratios were calculated at each location using all the measurements available except the Rh103 and U238. These results are shown in Table 3-3. The calculation is consistently low by 3 to 8%. There is no obvious trend to the bias in going from the location nearest the core to the one at the back of the vessel. Table 3-3 also contains C/M ratios calculated by Remec [7] using BUGLE-93. The MPM C/M ratios are seen to be very consistent with Remec's ratios except at the A7 position which only has the Np237 reaction. At this position, the MPM results here are in better agreement with the measurements. Results calculated using BUGLE-96 are also reported in Reference [13]. Results in this reference using the synthesis approach show a slight increase in bias going through the pressure vessel, and a three-dimensional calculation was made which eliminated this bias. The latter reference did not use the BUGLE-96 dosimetry cross sections and also made comparisons with a slightly different set of measured data. The fact that the three-dimensional calculation eliminated some of the bias illustrates that the synthesis method may contribute a small amount of bias. However, this would be a small effect in evaluating the fluence within the beltline region of a power reactor where streaming is very small except possibly in the reactor cavity.

The overall conclusion is that the methodology employed here obtains results consistent with calculations performed by qualified NRC contractors and with measurements reported for the PCA. The results show some consistent bias (possibly due to errors in dimensions or source distributions) but this bias is within acceptable tolerance. The results indicate that the calculation produces consistent results in flux variation from the thermal shield through the outside of the vessel.

Table 3-1 PCA Dosimetry Locations.

Location	Distance from Core Face of Aluminum Window (cm)	Location Description
A1	12.0	water at front surface of simulated thermal shield
A2	23.8	water at rear surface of simulated thermal shield
A3	29.7	water at front surface of pressure vessel simulator
A4	39.5	1/4 T position in pressure vessel simulator
A5	44.7	½ T position in pressure vessel simulator
A6	50.1	3/4 T position in pressure vessel simulator
A7	59.1	void box at rear of pressure vessel simulator

Table 3-2 Comparison of Calculated and Measured Results for PCA.

	Equivalent Fission Flux (n/cm^2-s)		
Reaction	Measured Results	Calculated Results	C/M
Location A1			
Np237(n,f)	6.64E-06	5.92E-06	0.891
U238(n,f)[a]	-	4.71E-06	-
Rh103(n,n')[a]	5.54E-06	6.14E-06	1.109
In115(n,n')	5.61E-06	5.16E-06	0.921
Ni58(n,p)	5.83E-06	5.46E-06	0.937
Al27(n,α)	7.87E-06	7.24E-06	0.920
Location A2			
Np237(n,f)	-	6.76E-07	-
U238(n,f)[a]	-	4.91E-07	-
Rh103(n,n')[a]	-	7.92E-07	-
In115(n,n')	6.06E-07	5.63E-07	0.929
Ni58(n,p)	6.18E-07	5.86E-07	0.949
Al27(n,α)	1.02E-06	9.38E-07	0.919
Location A3			
Np237(n,f)	2.27E-07	2.20E-07	0.970
U238(n,f)[a]	-	1.81E-07	-
Rh103(n,n')[a]	-	2.22E-07	-
In115(n,n')	1.99E-07	1.94E-07	0.973
Ni58(n,p)	2.31E-07	2.26E-07	0.977
Al27(n,α)	4.48E-07	4.30E-07	0.959
Location A4			
Np237(n,f)	9.27E-08	8.49E-08	0.916
U238(n,f)[a]	6.11E-08	4.97E-08	0.814
Rh103(n,n')[a]	7.74E-08	1.43E-07	1.844
In115(n,n')	5.87E-08	5.77E-08	0.984
Ni58(n,p)	5.3E-08	5.04E-08	0.951
Al27(n,α)	1.02E-07	9.56E-08	0.938
Location A5			
Np237(n,f)	5.18E-08	4.69E-08	0.906
U238(n,f)[a]	2.74E-08	2.13E-08	0.778
Rh103(n,n')[a]	4.35E-08	9.39E-08	2.158
In115(n,n')	2.76E-08	2.64E-08	0.955
Ni58(n,p)	2.09E-08	1.98E-08	0.948
Al27(n,α)	4.1E-08	3.84E-08	0.937

Table 3-2 Comparison of Calculated and Measured Results for PCA (Continued).

	Equivalent Fission Flux (n/cm^2-s)		
Reaction	Measured Results	Calculated Results	C/M
Location A6			
Np237(n,f)	2.7E-08	2.37E-08	0.879
U238(n,f)[a]	1.12E-08	8.56E-09	0.764
Rh103(n,n')[a]	2.19E-08	5.37E-08	2.454
In115(n,n')	1.17E-08	1.13E-08	0.962
Ni58(n,p)	7.43E-09	7.34E-09	0.987
Al27(n,α)	1.54E-08	1.46E-08	0.946
Location A7			
Np237(n,f)	7.25E-09	6.71E-09	0.926
U238(n,f)[a]	-	2.52E-09	-
Rh103(n,n')[a]	-	1.51E-08	-
In115(n,n')	-	3.06E-09	-
Ni58(n,p)	-	2.05E-09	-
Al27(n,α)	-	4.94E-09	-

[a] These reactions were not included in the average C/M ratio determination because of cross section uncertainties. Further details are given in the text.

Table 3-3 Comparison of Calculated and Measured Results for PCA.

Location	Average C/M Ratio[a] for MPM Analysis	Average C/M Ratio[b] for ORNL Analysis [7]
A1	0.917	0.93
A2	0.932	0.92
A3	0.970	0.96
A4	0.947	0.95
A5	0.936	0.92
A6	0.944	0.91
A7	0.926	0.84

a. Rhodium and U238 results excluded.
b. Results from Reference [7]. Np results are excluded from the averages at the A1 and A3 positions.

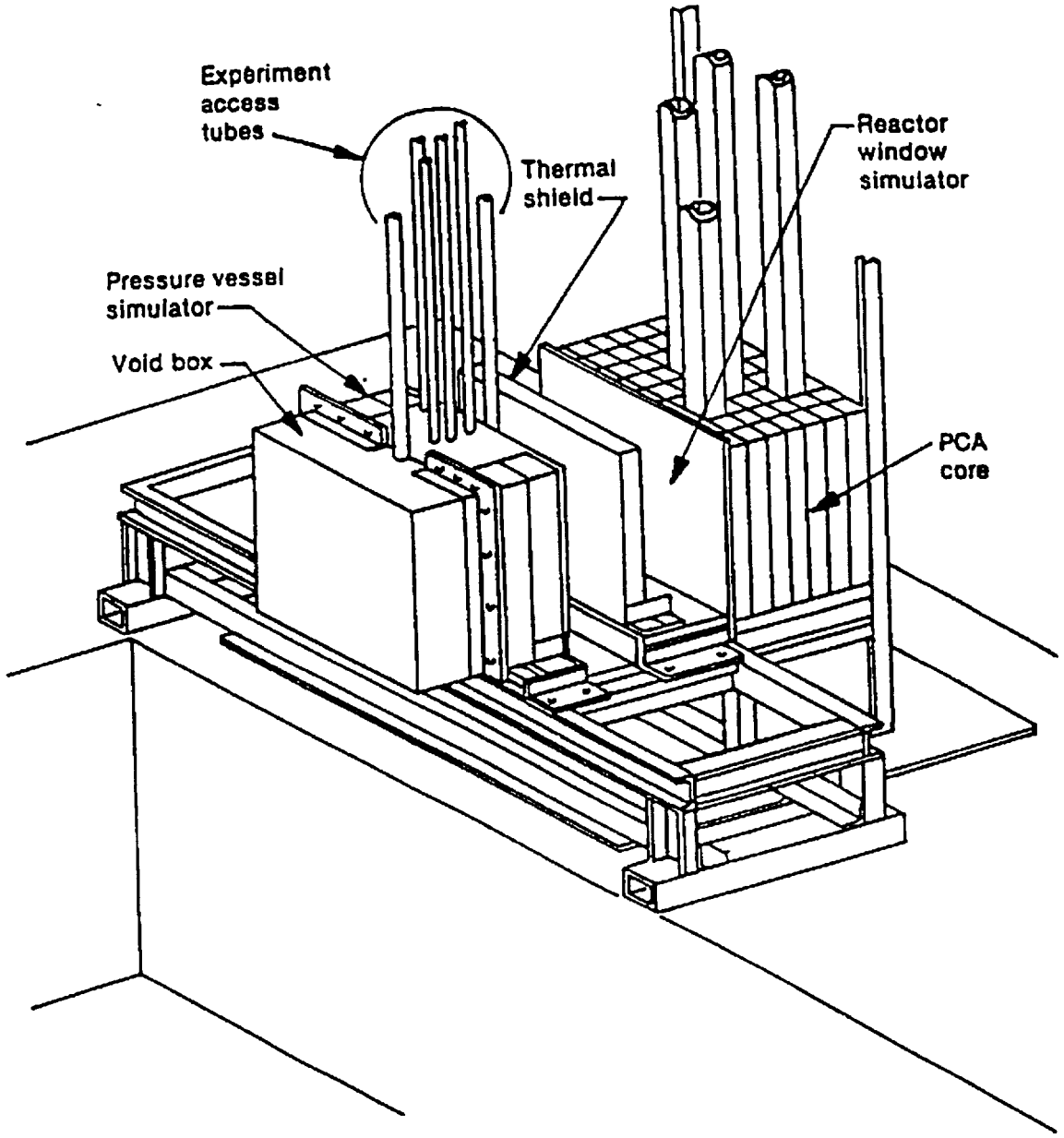

Figure 3-1 PCA Pressure Vessel Wall Benchmark Facility (Reference [7]).

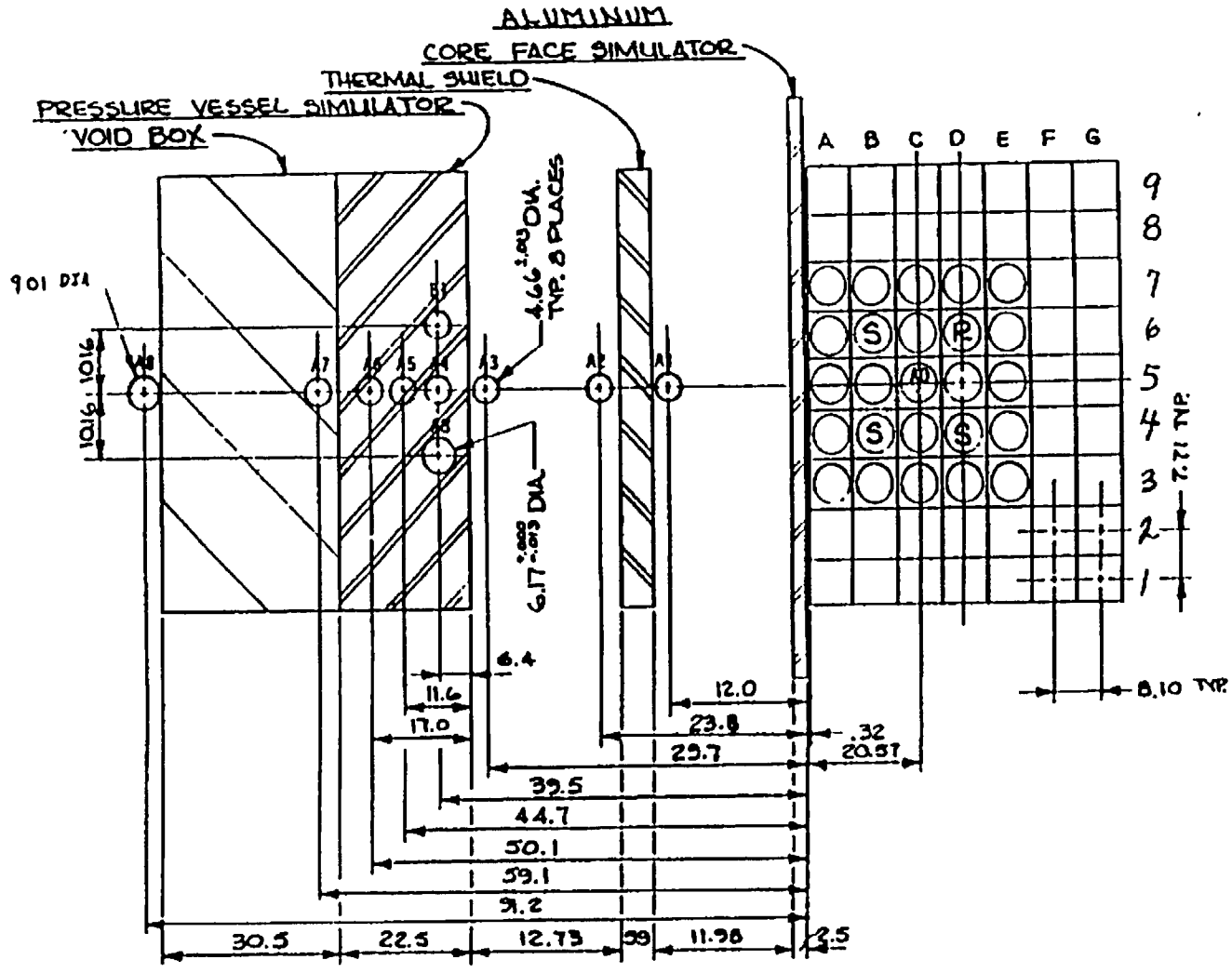

Figure 3-2 Horizontal Cross Section of PCA 12/13 Configuration (Reference [7]).

4.0 BWR Calculational Benchmark

In addition to benchmarking against measurements, RG 1.190 has a requirement to benchmark the methodology against a calculational benchmark. The calculational benchmarks needed to satisfy this requirement are documented in Reference [8]. Although this is a draft report, the final version of this report is not expected to contain any significant differences from the draft version [17]. Therefore, the calculation and comparisons reported here are considered to be final results. It will, of course, be necessary to verify that the final issuance of Reference [8] does not contain significant differences as compared to the draft version which was analyzed in the present work.

The calculational benchmark problems include 3 different PWR geometries and a single BWR problem. It is intended that the analyst select the benchmark problem or problems appropriate to the plant being analyzed. Accordingly, the BWR problem has been calculated since this problem is the one particularly appropriate for NMP-1 and NMP-2 as well as other BWRs. The benchmark problems are designed to ensure that two major difficulties encountered in neutron transport analysis are addressed. First is the strong attenuation of the neutron flux between the edge of the core and the vessel, and through the vessel. This large attenuation makes the vessel fluence dependent on the cross section sets used as well as the numerical procedures to approximate the Boltzmann transport equation. The second calculational difficulty is the evaluation of the neutron source which includes taking into account the irregular (in cylindrical coordinates) core boundary, conversion of the source geometry from X,Y to R,θ coordinates, and the burnup dependence of the source data. In addition, in the case of the BWR problem, the changing amount of water in the axial direction due to steam formation must be taken into account.

The BWR vessel fluence benchmark problem is for a typical BWR geometry. The core has 800 fuel bundles that have an axial height of 381 cm. Structures between the core and vessel that are included are the shroud, jet pumps and risers, and a surveillance capsule. The model extends outside the vessel into an outer concrete biological shield. The core power distribution and burnup are for a typical equilibrium cycle. The problem specification includes the dimensions of all components, material compositions by region, and the core neutron source.

The layout for the BWR benchmark problem is shown in Figures 4-1 and 4-2 (taken from Reference [8]). The present calculation used 198 radial meshes to represent the region from the center of the core to about 40 cm inside the concrete shield. In the azimuthal direction, 76 meshes were used, and in the axial direction 154 meshes were used to cover the region as shown in Figure 4-2. This mesh meets the requirements specified in RG 1.190 and is sufficiently fine to give an accurate transport result.

The neutron source was calculated from the information provided in the benchmark documentation [8]. This information included the location and fuel burnup for each assembly in the octant representation. Pin powers for the peripheral assemblies were supplied in an 8x8

array. Assemblies one row in from the periphery have the power variation defined in a 4x4 array, and two rows in use a coarser 2x2 array. The assemblies inside the outer three rows are given a flat weighting. Axial power distributions are given in three radial zones for 25 axial segments of the core, each 6 inches in extent. The R,Z model includes the three radial zones and expands the 25 power points into 94 meshes. The meshes are spaced at 2-inch intervals near the middle of the core where the power changes with height are small. Extra mesh points are included near the top and bottom of the core to define the more rapid changes in flux.

The benchmark problem gave fission fractions as a function of fuel burnup. Using these data, the fission fractions were determined using the average burnup for the outer core assemblies. The resultant average fission fractions were used to define the neutron spectrum, the number of neutrons per fission, and the energy per fission. The single neutron spectrum was used for the entire core, but the use of the outer assemblies only to define this spectrum is justified since almost all the neutrons leaking radially out of the core originate in these outer assemblies.

The calculated results were synthesized to produce the flux values and activities in the surveillance capsule and in the reactor vessel. The results were then compared with those tabulated in Reference [8] for the benchmark calculation. These comparisons are summarized in Tables 4-1 through 4-3.

The calculations reported in Reference [8] were carried out using a similar methodology to that used here. In addition, Monte Carlo transport results are reported to confirm the DORT code results. The mesh structure used in the Reference [8] DORT model is detailed, but this mesh was not used in the present calculation. This is because it was desired to check the methodology using the standard methods used by MPM in BWR neutron transport analyses. Another difference from the benchmark calculation in [8] is the use of a different code (DOTSOR rather than MESH) to convert the source from X,Y to R,θ coordinates. Also, MPM used the BUGLE-96 cross sections rather than the BUGLE-93 cross sections used in the Reference [8] analyses. These differences would be expected to produce variations in calculated flux from the benchmark case, but the results should be within tolerances of 5-10%.

Table 4-1 presents the results for activities calculated in the surveillance capsule which is centered at 3°. These results are interpolated to the radial and azimuthal center of the capsule and are for the maximum axial position in each case. In the present calculation, the axial peak is in the mesh centered at 61 cm above core midplane. However, the difference in activity between this location and the neighboring axial mesh is small. In the benchmark case, the peak is about 66 cm above midplane. The comparisons indicate very good agreement for all the reactions. The non-fission reaction rates agree to within 3%. The fission reactions show a slightly bigger difference which is likely due to differences between the BUGLE-96 and BUGLE-93 dosimetry cross sections for these reactions as observed in Reference [7]. The BUGLE-96 dosimetry cross-sections are an improvement over BUGLE-93. Unfortunately, the NUREG analysis used BUGLE-93 cross-sections which leads to differences with the MPM results which are based on BUGLE-96. The existence of these differences is indicated by comparisons in the PCA report

[7]. The average ratio for all six reactions is 0.968 with a standard deviation of 0.016.

Tables 4-2 and 4-3 give results for the flux (E > 1.0 MeV) in the vessel. Results are given for the vessel inner radius (IR), at 1/4 thickness (T) intervals through the vessel, and at the vessel outer radius (OR). In Table 4-2, flux results are tabulated for the peak axial position and ratios to the benchmark results are given. The calculated results are very consistent with the benchmark, but do show some scatter. This is presumably due to differences in the source calculation which can affect the relative flux at different angles. The average deviation is about +2%. Variation through the vessel also shows some scatter, but no trends are evident. The scatter in this case is probably due to differences in the model.

Results in the vessel have also been calculated for core midplane. These results are given in Table 4-3. The comparisons with the benchmark calculation are similar to those at the axial maximum. The average deviation is about +3% in this case.

The results for the capsule and vessel comparisons with the benchmark indicate agreement at most points to within ±5%, with differences slightly larger at some angles. All results agree with the benchmark to within ±10%. It is concluded that the comparisons between the present calculations and the benchmark calculation are within acceptable tolerances and that the present calculational method applied to BWR geometries is therefore validated.

Table 4-1 Comparison of Calculated and Benchmark Dosimeter Activities at the Middle of the Surveillance Capsule at the Peak Axial Location.

Reaction	MPM Calculated Activity	Reference [8] Benchmark Value	Ratio Calculated/ Benchmark
U238(n,f)	4.234E-16	4.414E-16	0.959
Np237(n,f)	1.847E-15	1.972E-15	0.936
Ti46(n,p)	3.399E-17	3.464E-17	0.981
Fe54(n,p)	1.481E-16	1.518E-16	0.976
Ni58(n,p)	1.899E-16	1.950E-16	0.974
Cu63(n,α)	2.345E-18	2.387E-18	0.983

Table 4-2 Comparison of Calculated and Benchmark Results for the Reactor Vessel Calculated at Reactor Axial Midplane.

angle[a]	IR	1/4T	1/2T	3/4T	OR
	MPM Calculated Flux (E > 1.0 MeV) n/cm^2-s				
0	7.738E+08	5.241E+08	3.140E+08	1.782E+08	8.728E+07
15	5.780E+08	3.953E+08	2.417E+08	1.417E+08	7.607E+07
30	1.012E+09	6.892E+08	4.170E+08	2.390E+08	1.168E+08
peak	1.456E+09	9.872E+08	5.916E+08	3.337E+08	1.546E+08
45	1.420E+09	9.629E+08	5.796E+08	3.289E+08	1.535E+08
	Reference [8] Benchmark Flux (E > 1.0 MeV) n/cm^2-s				
0	8.047E+08	5.382E+08	3.207E+08	1.809E+08	8.539E+07
15	5.515E+08	3.810E+08	2.347E+08	1.378E+08	7.253E+07
30	1.015E+09	6.671E+08	4.207E+08	2.405E+08	1.140E+08
peak	1.441E+09	9.679E+08	5.772E+08	3.235E+08	1.459E+08
45	1.323E+09	9.081E+08	5.495E+08	3.185E+08	1.432E+08
	Ratio: MPM Calculation/Benchmark Calculation				
0	0.962	0.974	0.979	0.985	1.022
15	1.048	1.038	1.030	1.029	1.049
30	0.997	1.033	0.991	0.994	1.024
peak	1.010	1.020	1.025	1.032	1.060
45	1.073	1.060	1.055	1.033	1.072

a. Results at 0 and 45 degrees are at the center of the initial and final azimuthal mesh. These angles are slightly different for the two calculations. The peak angle refers to the angle with the peak azimuthal flux (about 43 degrees for the present calculation and 42.5 for the benchmark calculation).

Table 4-3 Comparison of Calculated and Benchmark Results for the Reactor Vessel Calculated at Reactor Axial Midplane.

angle[a]	IR	1/4T	1/2T	3/4T	OR
	MPM Calculated Flux (E > 1.0 MeV) n/cm^2-s				
0	7.077E+08	4.798E+08	2.880E+08	1.642E+08	8.185E+07
15	5.286E+08	3.619E+08	2.217E+08	1.305E+08	7.133E+07
30	9.256E+08	6.310E+08	3.825E+08	2.202E+08	1.095E+08
peak	1.331E+09	9.039E+08	5.426E+08	3.074E+08	1.450E+08
45	1.299E+09	8.816E+08	5.316E+08	3.030E+08	1.439E+08
	Reference [8] Benchmark Flux (E > 1.0 MeV) n/cm^2-s				
0	7.267E+08	4.860E+08	2.901E+08	1.641E+08	7.916E+07
15	4.980E+08	3.441E+08	2.122E+08	1.250E+08	6.725E+07
30	9.169E+08	6.268E+08	3.806E+08	2.182E+08	1.057E+08
peak	1.301E+09	8.739E+08	5.222E+08	2.935E+08	1.353E+08
45	1.194E+09	8.198E+08	4.971E+08	2.889E+08	1.328E+08
	Ratio: MPM Calculation/Benchmark Calculation				
0	0.974	0.987	0.993	1.001	1.034
15	1.062	1.052	1.045	1.045	1.061
30	1.010	1.007	1.005	1.009	1.036
43	1.023	1.034	1.039	1.047	1.071
45	1.088	1.075	1.069	1.049	1.084

a. Results at 0 and 45 degrees are at the center of the initial and final azimuthal mesh. These angles are slightly different for the two calculations. The peak angle refers to the angle with the peak azimuthal flux (about 43 degrees for the present calculation and 42.5 for the benchmark calculation).

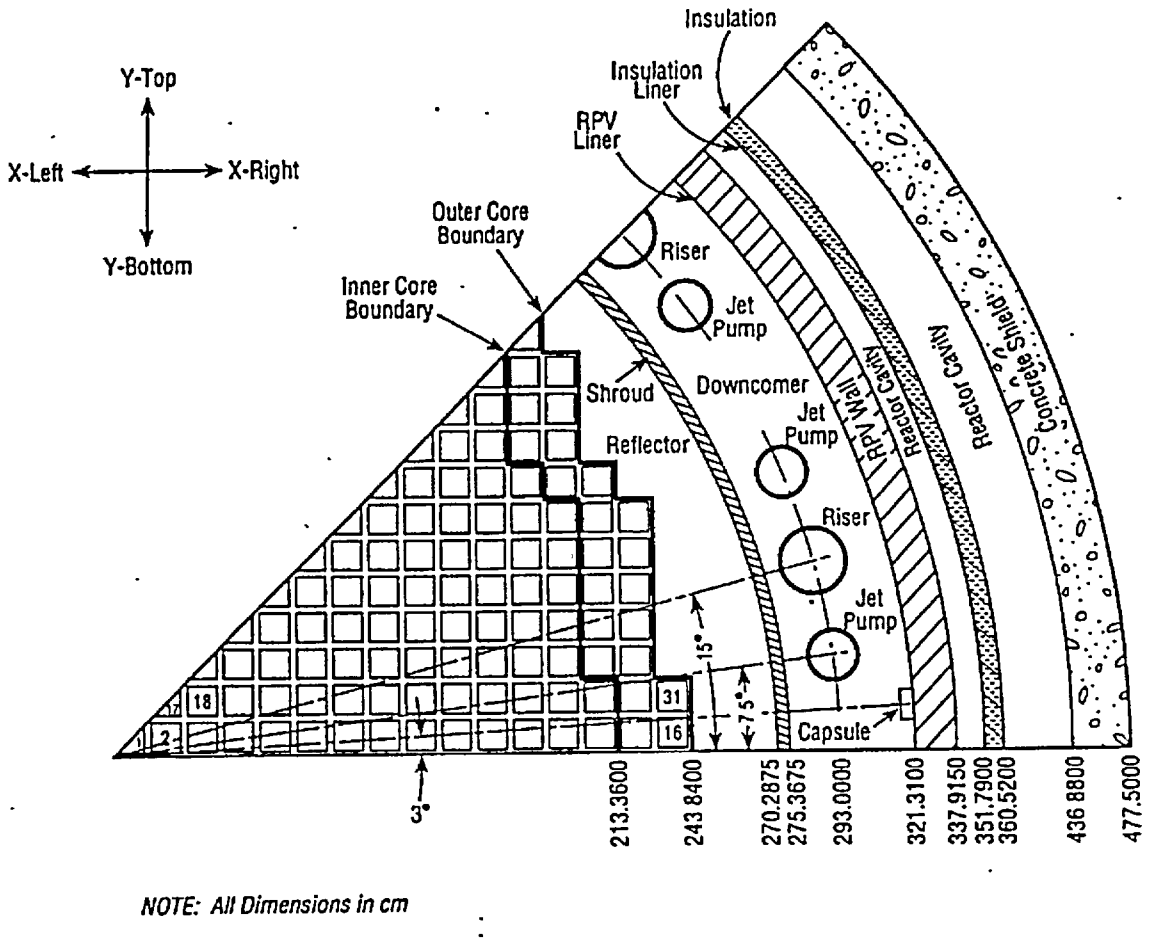

Figure 4-1 BWR Benchmark Problem Horizontal View (Reference [8]).

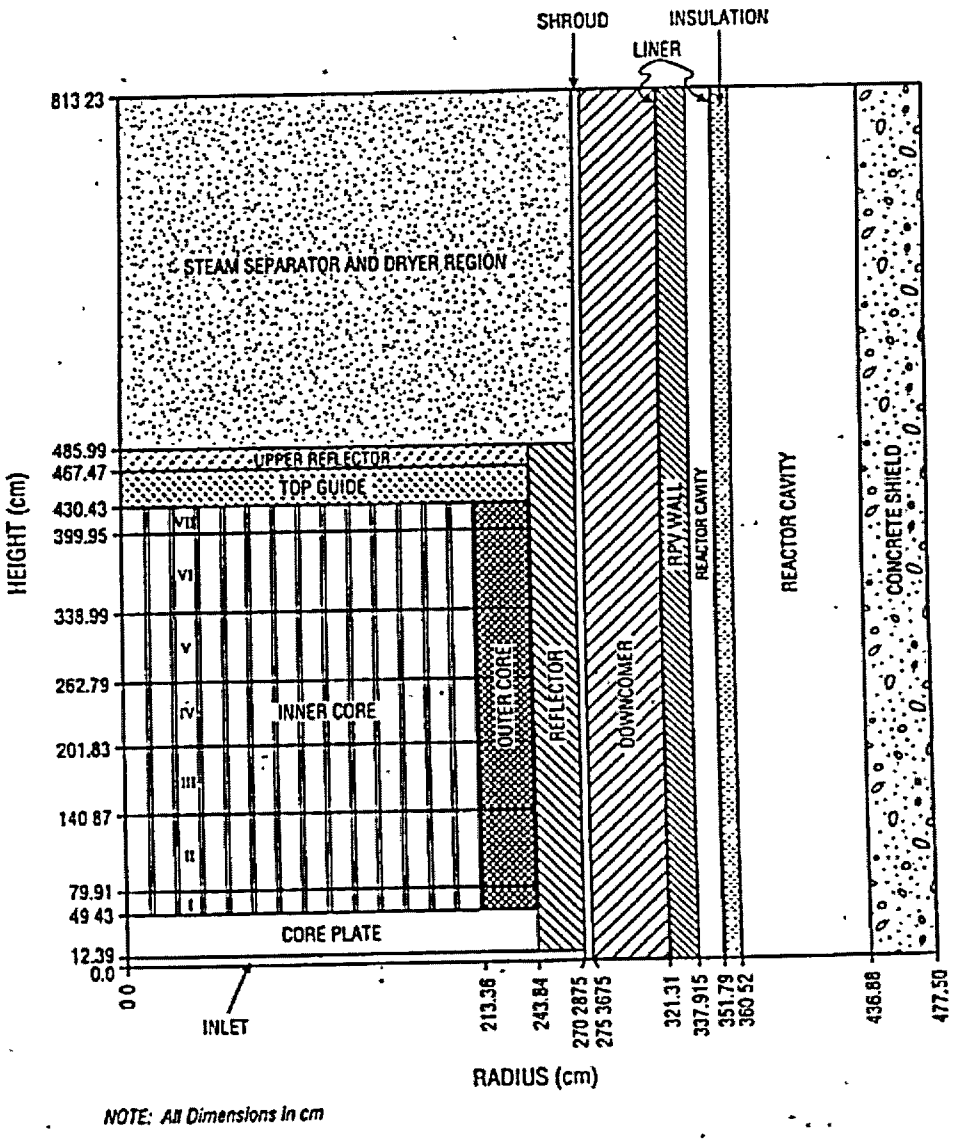

Figure 4-2 BWR Benchmark Problem Axial View (Reference [8]).

5.0 Plant Specific Benchmarking

The second element of neutron transport method benchmarking is to compare calculations with dosimetry measurements from the actual plant of interest, or with one that has similar geometry and fuel power distributions. It is, of course, preferred that this element of benchmarking be performed using data from the plant itself. Measurements have been made in both NMP-1 and NMP-2 in order to provide verification of the accuracy of fluence evaluations in these plants. These measurements enable possible errors not detected by the other benchmarking efforts to be identified and properly addressed. Such errors may arise from uncertainties in plant dimensions, fuel power distributions, time variations in flux level, or void fractions in outer fuel bundles.

5.1 NMP-1 Benchmarks

At the end of NMP-1 fuel cycle 12 (March 1997), the surveillance capsule located at 210° was removed for analysis. This capsule contained Fe, Ni, and Cu dosimeters and the measurement results are reported in Reference [2]. At the same time, in order to determine the material properties of the shroud, and to provide dosimetry data, boat samples were removed from the shroud at two locations. One was cut from the inner diameter (ID) surface of axial weld V9 at an elevation of 26.4 inches above core midplane. This sample was intended to provide near peak flux data for the weld. The other sample was cut from the shroud outer diameter (OD) surface at an elevation of 8.3 inches below core midplane. This sample was intended to provide relatively low flux data. Both samples were taken at azimuthal positions equivalent to 20°. The boat samples were evaluated by Framatome Technologies and the fast fluence was determined based on the Fe54(n,p)Mn54 and Ni58(n,p)Co58 reactions [18]. An inconsistency was found to exist between the Fe and Ni reactions at the boat sample locations. Further, MPM's analysis of the capsule dosimetry indicated, to a lesser extent, an inconsistency in the copper reaction for the capsule. Based on these findings, NMPC contracted with MPM to have an in-depth analysis performed of both the boat sample and the capsule dosimetry data for cycle 12.

Since the Fe and Ni reactions have a similar neutron response as a function of neutron energy, MPM proposed that the most likely cause of the difference between these results is a change in the flux level relative to reactor power at the sample location (i.e. the reaction rate of the dosimeter material with the reactor at full power varies during the fuel cycle). Such a flux level change can occur due to changes in radial or axial power shape, or due to changes in leakage from the core due to water density changes. As fuel burnup occurs, or as reactor control rod patterns change, these types of effects can be expected. Accordingly, a detailed investigation was made of cycle 12 to evaluate the cycle changes that affect the flux level at the dosimetry locations.

Neutron transport calculations were performed for five cases representing different time intervals of cycle 12. The core power distributions and void fractions were calculated by NMPC for 68 cases during the fuel cycle. Plots were made of axial power distributions for the corner assembly nearest 20° and for a core average. Inspection of these plots indicated that the

variations were not uniform with time, but significant changes occurred at discrete times, presumably due to changes in operation (such as control rod patterns). To account for these changes, the operating time was divided into 5 intervals which contained cases with similar profiles. A typical case for each interval was then selected from near the middle of that operating period. An R-θ calculation was then carried out for each case with a midplane neutron source and void fraction distribution calculated for that case. The effect of flux variations in earlier cycles has much less effect on the dosimetry results. To limit the effort, the earlier cycles (1 through 9) were assumed to be represented by a single analysis performed for cycle 7. In cycle 10, a transition to a new fuel management scheme began, and it was assumed that this cycle could be represented by an average of the cycle 7 result and an average of the 5 cycle 12 results. Cycle 11 was assumed to be equal to the cycle 12 average.

The R-θ layout is shown in Figure 5-1. In this figure all structures outside the core were modeled with a cylindrical symmetry except for the inclusion of a surveillance capsule centered at 30°. The R-θ model included 142 mesh points in the radial direction covering the range from the center of the core to the outside of the reactor vessel. In the azimuthal direction, 42 mesh points were used to model a single octant of the reactor. Inspection of the fuel loading patterns indicated that only minor deviations from an octant symmetry were present. The region external to the vessel was not modeled in the Unit 1 calculation. This will cause some error at the 3/4T position and outside of the vessel. It does not affect the comparisons with measurements or shroud and vessel IR results which were the main focus of the calculations. Thus, it was not deemed necessary to include the cavity region in the model at the time the Unit 1 calculation was done.

The core region used a homogenized material distribution which includes the fuel, fuel cladding, and the water. The water region in the fuel contains both liquid water and steam. The fraction occupied by steam is known as the void fraction and varies by assembly and axial position within the fuel. Values of void fraction for cycle 12 were supplied by NMPC for each fuel bundle at 24 axial nodes [19]. Inspection of these values indicated that significant variation in the void fraction occurred, but that some groups of neighboring fuel bundles had close to the same void fraction. To model the void fraction variation, the outer rows of fuel bundles were divided into six regions of approximately uniform water material density, and the average water density for the fuel bundles in each of these regions was calculated by multiplying the base water density (46.0415 lb/ft3) by 1.0 minus the void fraction. The fuel bundles in each of these regions are indicated by the region numbers shown in Figure 5-1. Water density in the bypass region was taken to be the same as in the core except with zero void fraction. The downcomer water density was calculated for a temperature of 530 °F and a pressure of 1050 psia.

Generic pin power distributions were used to define the power variation within the fuel bundles. The pin power distributions vary with burnup and void fraction, but, since the variations are relatively small, it was deemed sufficient to use a single set of normalized pin power distributions for each of the cases. The relative pin powers were taken at a burnup corresponding to the mid-cycle burnup average and void fraction average for the outer fuel bundles. The source per group was defined by an average fission spectrum calculated for a

fission breakdown by isotope determined for the average burnup of the outer fuel bundles in cycle 12. This is a good approximation to the fission spectrum because the outer fuel bundles were all burned fuel bundles and the fission spectrum only slowly varies with burnup. The average burnup was also used to determine the average value of the neutrons per fission and the average energy per fission. The main isotopes that contribute to the fission spectrum are U235 and Pu239, but contributions from U238, Pu240, and Pu241 were also included.

For the R,Z calculation, the core was divided into 4 radial regions. Three of these regions consisted of each of the outer three rows of fuel bundles averaged over the octant. The fourth region consisted of the inner part of the core. The neutron source in each of these regions was calculated using a radial source averaged over the octant calculated by DOTSOR together with an average axial power shape for each region. The axial power distribution was supplied for each assembly in 24 nodes, each representing 6 inches of core height. Neutron source outside the equivalent core radius was eliminated.

Each radial region was also divided into axial regions according to variation in void fraction. The void fraction was also given for each assembly in 24 axial nodes. Except for nodes near the bottom of the core which had zero void fraction, each node was modeled as a separate region for the calculation. Because the void fraction distribution in the outer two rows of fuel bundles was similar (as was done for the R-θ model), these were combined for the void fraction definition. This resulted in a total of 67 regions in the core, each with a distinct cross section set. For the R-Z model, the core radius was taken to be that which gave the equivalent core volume. Regions above and below the core were not modeled exactly but consisted of a one-foot high water reflector with vacuum boundaries at the top and bottom of the model. The model had 142 mesh points in the radial direction as in the R-θ model except with slightly different boundaries near the core edge. In the axial direction, the model had 68 mesh points with 38 in the core region.

Further details on the transport calculations and the analytic uncertainty analysis are given in Reference [2]. The results are used for evaluation of the capsule and shroud dosimetry measurements as well as for fluence projections.

The boat samples taken from the shroud contained stainless steel material that extended from the surface of the shroud to about the middle of the shroud wall. Samples for dosimetry analysis were removed from 3 radial locations from each boat sample and analyzed for Mn54 and Co58 activity, making a total of 12 samples for each weld. Results in units of μCi/gm of target isotope (i.e. Fe54 or Ni58) are given in Table 5-1 (taken from reference [20]). This table also provides the radial location of each sample in units of inches from the shroud inner surface. The shroud thickness is 1.5 inches.

The measured disintegration rate (μCi/gm) is converted to reaction rate at full power (reactions per target nucleus per second) using a position dependent flux time-history evaluated by adjusting the reactor power history by the relative calculated flux distribution. The reaction rate is defined here as the average rate for the 12 cycles of operation. Using the calculated cross

sections (averaged above 1 MeV) for iron and nickel, the average flux seen by each sample is calculated and given in the table.

Inspection of the results in Table 5-1 indicates that the iron results and nickel results are in good agreement. The average of the ratio of the flux as calculated from the nickel measurements to that from the iron is 0.991 with a standard deviation of 3.3%. This should be considered excellent agreement when compared with the estimated measurement accuracy of about 6%.

The averages of the four measurement results for the flux at each of the six locations are given in Table 5-2. These results are compared with the calculated flux for each location. The results indicate that the calculations for the average flux at the shroud boat sample locations are consistently high relative to the measurements. This bias averages 15.7% with a standard deviation of 3.1%. This is considered to be excellent consistency and the bias falls within expected bounds of calculational accuracy for the flux at a given point in the shroud. The analytical uncertainty analysis indicated the uncertainty in the calculated shroud fluence to be 16%. The most important contributors to this uncertainty are uncertainties in the shroud inner radius value, the fuel power distribution, and the uncertainty in power history. However, the most likely cause of the C/M bias is uncertainty in the azimuthal location of the welds. Since the 20 degree position was assumed to represent the weld azimuthal location, and the 20 degree position is very close to the azimuthal peak of 19.38 degrees, the calculated flux can only increase upward by about 1 %. However, if the welds were located at the assumed 5 degree limit of uncertainty, then the calculated fluence could be lower by as much as 30 %.

The 210° capsule dosimetry results are presented in Table 5-3 [2]. Measurement results for three dosimeters of each type were obtained, and a flux derived for each. The flux measurements for each reaction were averaged and an overall average flux was obtained by averaging all the results with equal weight. The reaction rates were again evaluated by a position dependent flux history, and the use of the five sub-periods in cycle 12 produced a slight discrepancy of 6% between the iron and nickel results. Using the same flux level for all of cycle 12 increases this discrepancy to 25%. Some bias may still be present (maybe due to the fact that the earlier cycles were not calculated in detail), but the results are consistent enough so that the use of an average of all the dosimeters produces a reasonable flux estimate. Comparing the flux derived from the measurements to the calculated value gives a C/M ratio of 0.84. When the reaction rate uncertainty of 8% and the estimated capsule fluence calculation uncertainty of 14% are considered, it is concluded that the results are consistent within uncertainty.

5.2 NMP-2 Benchmark

The NMP-2 capsule located at 3° was removed at the end of the seventh fuel cycle (March, 2000) and the dosimetry was analyzed. This dosimetry consisted of two iron wires and two copper wires. To analyze the dosimetry, a detailed analysis of reactor operation was performed to evaluate changes in neutron flux level at the dosimetry location due to changes in fuel composition, power distributions within the core, and water void fraction. These changes

occur between fuel cycles due to changes in fuel loading and fuel design, and within a fuel cycle due to fuel burnup and resultant changes in power shape, control rod position, fission contributions by nuclide, and void fraction vs. axial height in each fuel bundle. For the final fuel cycle (cycle 7), five cases were selected to characterize changes during the cycle. These points were distributed throughout the cycle so that each of these was taken to represent an average of the neutron flux level for about 1/5 of the operating time for the cycle. For the other fuel cycles, which have less effect on the dosimetry results, the assumption was made that conditions at the middle of each cycle were an adequate estimation of the average over the cycle and a single calculation was performed for each of these cycles.

The layout for the R-θ calculation is shown in Figure 5-2. In this figure, all structures outside the core were modeled with a cylindrical symmetry except for the inclusion of a surveillance capsule centered at 3° and jet pump structures located in the downcomer region. The latter are not to scale in the figure. The jet pumps are only approximate models of two pumps with a central pipe (riser) in between.

The R-θ model included 186 mesh points in the radial direction covering the range from the center of the core to ten inches into the biological shield. This large number of mesh points was used to accurately calculate the neutron flux transport from the core edge to the outside of the vessel. In the azimuthal direction, 48 mesh points were used to model a single octant of the reactor. Inspection of the fuel loading patterns indicated that only minor deviations from an octant symmetry were present and these were ignored. The 48 points provided good definition of the variation of the core edge with angle and defined the azimuthal flux variation.

The core region used a homogenized material distribution which includes the fuel, fuel cladding, and the water. The water region in the fuel contains both liquid water and steam. The fraction occupied by steam is known as the void fraction and varies by assembly and axial position within the fuel. Inspection of the void fraction values indicated that while some assemblies exhibit significant variation in the void fraction, some groups of neighboring assemblies had close to the same void fraction. To model the void fraction variation in the R-θ model, the outer rows of assemblies were divided into seven regions of approximately uniform water material density, and the average water density for the assemblies in each of these regions was calculated by multiplying the base water density (0.7365 g/cc) by 1.0 minus the void fraction. The assemblies in each of these regions are indicated by the region numbers defined in Figure 5-2. Each one of these regions had a void fraction assigned as the average midplane void fraction value for the assemblies in the region. These average void fraction values were different for each case analyzed.

Water density in the bypass region was varied between 0.7585 g/cc at the inlet and 0.7394 g/cc at the outlet. The value at midplane was taken to be an average of these values. The downcomer water density was calculated for a temperature of 534 °F and a pressure of 1037 psia.

The source calculations used the appropriate power distribution for all the fuel bundles in the first octant together with pin power distributions for the outer rows of bundles. The pin

power distributions were used to model the spatial variation of the source within the bundles and took into account the gaps between bundles and water rods in the center. Equal pin power weighting was used for interior fuel bundles. In the calculations, the variation in relative pin power distributions within similar bundles between cycles was determined to be small [4] and so the cycle 7 9x9 mid-cycle pin power distributions were used in the calculations for all the cases. The neutron source per group was defined by an average fission spectrum calculated for a fission breakdown by isotope determined for the average burnup of the outer assemblies for each case. This is a good approximation to the fission spectrum because the outer assemblies were all assemblies with similar burnup, and the fission spectrum only slowly varies with burnup. Almost all of the neutrons that reach the capsule and vessel originate in the outer rows of fuel bundles.

The ORIGEN 2.1 code [12] was used to calculate the effects of burnup on the neutron source. This was carried out using an ORIGEN BWR cross section library appropriate for high burnup fuel. The results were validated by comparison to NMP-2 calculated fuel compositions as a function of fuel burnup. The initial fuel composition for each cycle was taken to be the average initial composition for the outer assemblies. The effects of the varying axial initial enrichment, burnup, and void fraction were ignored in this calculation and are assumed to have negligible impact because the effects of the change in parameters are minor. The ORIGEN code calculated the fission fraction by isotope and the average energy deposited in the reactor per fission (κ). The isotopic fission fractions were used to determine the fission spectrum and the average number of neutrons per fission (ν). The normalization of the neutron source in the DORT calculations is directly proportional to ν/κ which slowly varies with burnup.

For the calculation in R-Z geometry, the core was divided into 3 radial regions. Two of these regions consisted of each of the outer two rows of assemblies averaged over the octant. The third region consisted of the inner part of the core. The neutron source in each of these regions was calculated using a radial source averaged over the octant together with an average axial power shape for each region. The axial power distribution was supplied for each assembly in 25 nodes, each representing 6 inches of core height. Neutron source outside the equivalent core radius was eliminated.

Each radial region was also divided into axial regions according to variation in void fraction. The void fraction was also given for each assembly in 25 axial nodes. Except for nodes near the bottom of the core which had zero void fraction, each node was modeled as a separate region for the calculation. This resulted in a total of 70 regions in the core, each with a distinct cross section set. In addition, the GE11 fuel bundles contain 8 part length fuel pins that end at 96 inches above the bottom of the active fuel. The volume of these pins was replaced with water at axial meshes above the 96 inch level. The bypass region was also modeled with a varying axial water density. The bypass region was divided into 12 subregions within the core height, each with a different water density.

For the R-Z model, the core radius was taken to be that which gave the equivalent core volume. Since the focus of the calculations was on obtaining accurate results at shroud and

vessel locations within the beltline axial region, the regions above and below the core in the R-Z model were not modeled using an exact representation of the structures above and below the beltline region. The model was extended above and below the core for 12 inches (30 cm) to provide a reflector region and to allow leakage out to the shroud and vessel. The region below the core (which corresponds to the core plate region in NUREG/CR-6115) was approximated by water with the same density as the downcomer, in contrast to the NUREG model which had a mixture of stainless steel and water. Omission of the stainless steel is conservative for high energy neutron transport. Similarly, the region above the core was approximated using water with the density determined using the core outlet water density. The model had 186 mesh points in the radial direction as in the R-θ model except with slightly different boundaries near the core edge. In the axial direction, the model had 68 mesh points with 38 in the core region. Further details of the calculations are given in Reference [3].

The dosimetry results that relate to fast fluence are given in Table 5-4 [3]. The dosimeter measurements are presented in units of disintegrations per second per milligram (dps/mg), adjusted to the end-of-irradiation (March 3, 2000 at 14:17 EST). Using the power history and the reaction rates for Fe and Cu determined by the DORT calculation for each cycle and the five cycle 7 cases, the activity at the end of the irradiation was calculated for a point at the geometrical center of the capsule. The results were obtained by multiplying the calculated reaction rate for each of the two reactions (obtained from the synthesis procedure for each case) by the effective full power seconds (EFPS) for each monthly time interval and then accounting for radioactive decay during the interval and to the end-of-irradiation time.

The C/M ratios for each dosimeter measurement and the average are tabulated in Table 5-4. The average C/M ratio of 1.07, based on the assumption that the dosimetry is at the capsule center, indicates good agreement between the calculation and the measurement. However, the Fe and Cu dosimetry results do show a large difference with the Fe showing a C/M over 20 %. It should be noted that 95% of the iron response is from the last two irradiation cycles, while 48% of the copper response is from earlier cycles. In addition, copper has a much higher reaction threshold and so only responds to a small fraction of the fast neutrons while the iron responds to a larger fraction. In addition, the copper cross section is not as well known as the iron cross section. Since these observations are not expected to explain all of the discrepancy, additional measurements and analyses were made to better quantify the C/M ratio.

The location of the dosimeters in BWR capsules is uncertain. Unlike most PWR capsule designs, the BWR dosimeters are not placed in sealed containers inside the capsule. Instead, the bare wires are held by spring load near the top or bottom of the capsule for most BWR capsules. For NMP-2, the intended location is near the front top of the capsule at the right side as viewed from the core. This would place the dosimeters at about 0.48 cm towards the core from the capsule radial center and about 6 inches above core midplane. The radial correction would increase the calculated activity by 4.6% for copper and 7.4% for iron. The axial correction varies during the fuel cycle and between cycles, but the activities 6 inches above midplane average about 4% higher. The azimuthal difference is small, but the activity to the right (higher angles in the first octant) increases by about 1% from that at the center of the capsule. If all

these factors are included, the calculated copper activity at the indicated dosimeter position is higher by about 10% compared to the capsule center and the iron by 13%. This results in average C/M ratios of 1.02 for copper and 1.37 for iron, and an average C/M of 1.19.

However, it may also be postulated that the copper dosimeter is positioned towards the core side of the capsule, while the iron is positioned towards the vessel side. This condition could occur if the dosimeters shifted during capsule assembly or if the dosimeters moved during irradiation in the plant. If this assumption is made, then the iron average C/M ratio is 1.19 and the average of the two dosimeter types is 1.11. It is also possible to assume that the dosimeter wires dropped to the bottom of the capsule. This would lower the calculated activity by 4% compared to the capsule axial midplane (instead of increasing it as noted above for the correction to the top of the capsule). The average C/M ratio would then be about 1.02.

Since the bottom of the NMP-2 capsule was cut during capsule disassembly and the wires were located somewhere in the capsule above the cut location, it is not possible to determine the dosimeter wire locations during irradiation. Therefore, to reduce the dosimeter location uncertainty and to obtain a meaningful C/M ratio, an additional measurement was made using a sample cut from a Charpy bar. The sample was a complete slice across the specimen taken near the fracture surface and thus is radially centered and located very near the azimuthal center of the capsule. The sample was modeled at the radial center of the capsule because the counting geometry for the slice approximates a point source at the radial center. Unfortunately, the axial location within the capsule could not be determined because the specimens were not recorded for axial position during disassembly. This is not a serious problem because the axial uncertainty is only a few percent. The measurement result, adjusted to the reference time, is 30.62 dps/mg. The Charpy is not pure iron, but has been determined to have an iron fraction of 0.9694. Using this value, the dps/mg of iron is then 31.59. This result is 12% higher than the result from the iron dosimeters and gives a C/M ratio of 1.08. This indicates that the iron dosimeters are located towards the rear of the capsule, and most likely at the bottom. The results using this location for the iron dosimeter, and assuming the copper location towards the core, are shown in the last column of Table 5-4. The average C/M for copper is 0.95 and for iron is 1.09, for an overall average of 1.02, indicating excellent agreement of the calculation with measurement.

Uncertainty in the calculation and measurement is considered in detail in Reference [3]. The uncertainty in the calculated flux at the center of the surveillance capsule was evaluated to be 15.3%. Uncertainty in the measured result must include the uncertainty in activity measurements, dosimeter position uncertainty, dosimeter cross section uncertainty, and the flux history uncertainty. The activity measurements have a total uncertainty of about 3%. As discussed above, the dosimeter position uncertainty can be as large as 10-13%. However, use of the Charpy measurement, which has a better known position, reduces this uncertainty to about 5%. The dosimeter cross section uncertainty is limited by correlation with benchmark measurements. It can be assumed that typical iron and copper reaction integral cross sections are known to within 3% [21]. The flux history uncertainty will vary with the half-life, but can be conservatively assumed to be less than 8% [3]. The total uncertainty in the measurement relative to the calculation is then about 10%.

It is seen that the Charpy bar C/M value of 1.08 is well within both the measurement uncertainty and the calculation uncertainty. It is concluded that the measurement provides an excellent validation of the adequacy of the calculation.

Table 5-1 Tabulation of NMP-1 Shroud Boat Sample Dosimetry Results [20].

Weld V9	Dosimeter Identification	Location[a] in Shroud (in)	Specific Activity (uCi/g)	Reaction Rate (r/s/nucleus)	Cross Section (cm^{-1})	Fast (E>1MeV) Flux ($n/cm^2/s$)
1	Fe	0.000	1.94E+04	8.061E-14	1.207E-25	6.677E+11
2	Fe	0.000	1.93E+04	8.020E-14	1.207E-25	6.643E+11
3	Ni	0.000	2.01E+04	9.976E-14	1.583E-25	6.304E+11
4	Ni	0.000	2.15E+04	1.067E-13	1.583E-25	6 743E+11
5	Fe	0.337	1.60E+04	6.648E-14	1.152E-25	5.772E+11
6	Fe	0.337	1.68E+04	6.981E-14	1.152E-25	6.060E+11
7	Ni	0.337	1.91E+04	9.480E-14	1.516E-25	6.255E+11
8	Ni	0.337	1.83E+04	9.083E-14	1.516E-25	5.993E+11
9	Fe	0.850	1.31E+04	5.443E-14	1.099E-25	4.955E+11
10	Fe	0.850	1.32E+04	5.485E-14	1.099E-25	4.993E+11
11	Ni	0.850	1.44E+04	7.147E-14	1.451E-25	4.926E+11
12	Ni	0.850	1.51E+04	7.494E-14	1.451E-25	5.166E+11
Weld V10	**Dosimeter Identification**	**Location[a] in Shroud (in)**	**Specific Activity (uCi/g)**	**Reaction Rate (r/s/nucleus)**	**Cross Section (cm^{-1})**	**Fast (E>1MeV) Flux ($n/cm^2/s$)**
1	Fe	0.882	8.98E+03	4.080E-14	1.098E-25	3.715E+11
2	Fe	0.882	9.14E+03	4.153E-14	1.098E-25	3.781E+11
3	Ni	0.882	9.72E+03	5.468E-14	1.450E-25	3.770E+11
4	Ni	0.882	9.91E+03	5.575E-14	1.450E-25	3.843E+11
5	Fe	1.063	8.34E+03	3.790E-14	1.097E-25	3.456E+11
6	Fe	1.063	8.26E+03	3.753E-14	1.097E-25	3.423E+11
7	Ni	1.063	8.42E+03	4.736E-14	1.448E-25	3.271E+11
8	Ni	1.063	8.52E+03	4.793E-14	1.448E-25	3.310E+11
9	Fe	1.500	6.74E+03	3.063E-14	1.111E-25	2.757E+11
10	Fe	1.500	6.74E+03	3.063E-14	1.111E-25	2.757E+11
11	Ni	1.500	6.75E+03	3.797E-14	1.465E-25	2.592E+11
12	Ni	1.500	6 80E+03	3.825E-14	1.465E-25	2.611E+11

a. measured from shroud ID surface
b. fluence evaluated from reactor startup through end of cycle 12

Table 5-2 Measured and Calculated Boat Sample Flux Values from Nine Mile Point Unit 1 [2].

Radial Location[a] (in)	Axial Location[b] (in)	Flux (E > 1 MeV) n/cm²/s		C/M Ratio
		Measured[c] (M)	Calculated (C)	
Vertical Weld V9				
0.000	26.4	6.59E+11	7.55E+11	1.14567526555
0.337	26.4	6.02E+11	6.86E+11	1.13953488372
0.850	26.4	5.01E+11	5.62E+11	1.12175648703
Average C/M				1.136
Vertical Weld V10				
0.882	-8.3	3.78E+11	4.61E+11	1.21957671958
1.062	-8.3	3.36E+11	3.88E+11	1.15476190476
1.500	-8.3	2.68E+11	3.11E+11	1.16044776119
Average C/M				1.179

a. Measured from shroud ID surface.
b. Measured from fuel axial midplane.
c. Average of flux derived from 2 iron and 2 nickel measurements at each location. The flux is determined from the measurements by dividing the average reaction rate (calculated from the measured decay rate per mg. of sample using the reactor power history as adjusted by the relative flux calculation) by the spectrum average cross section.

Table 5-3 Tabulation of 210° Capsule Dosimetry Results for NMP-1 [2].

Wire	dps/mg	Reaction Rate (s^{-1})	Flux (E > 1 MeV) n/cm^2-s
Cu-1	20.66	4.898E-18	1.909E+09
Cu-2	20.81	4.934E-18	1.923E+09
Cu-3	19.43	4.607E-18	1.796E+09
Avg	20.30	4.813E-18	1.876E+09
Fe-1	149.4	2.998E-16	1.757E+09
Fe-2	138.6	2.781E-16	1.630E+09
Fe-3	135.7	2.723E-16	1.596E+09
Avg	141.2	2.834E-16	1.661E+09
Ni-1	1725	3.580E-16	1.638E+09
Ni-2	1636	3.395E-16	1.554E+09
Ni-3	1592	3.304E-16	1.512E+09
Avg	1651	3.426E-16	1.568E+09
Average flux for all dosimeters			1.702E+09
Calculated capsule flux			1.440E+09

Table 5-4 Tabulation of NMP-2 3° Surveillance Capsule Dosimetry Results [3,4].

Dosimeter	Measured Activity (dps/mg)	Calculated Activity (dps/mg) [a]	Ratio (C/M) [a] Capsule Center Assumption	Ratio (C/M) [b] Best Estimate Position
Cu-1	4.97	4.50	0.91	0.92
Cu-2	4.62	4.50	0.97	0.99
Avg Cu	4.80	4.50	0.94	0.95
Fe-1	27.84	34.10	1.22	1.10
Fe-2	28.49	34.10	1.20	1.08
Avg Fe	28.16	34.10	1.21	1.09
Capsule Average			1.07	1.02
Charpy Bar (Slice Near Fracture Surface)	31.59[c]	34.10	1.08[c]	N/A

a. There is uncertainty in the NMP-2 capsule dosimetry location. The results in this column are based on the assumption that the dosimetry is at the capsule center.

b. The results in this column are based on the assumption that the dosimetry is at the best estimate positions. Dosimetry results from the Charpy bar indicate that the dosimetry wires may have moved from their intended locations within the capsule.

c. The Charpy bar dosimetry results have been corrected for iron composition. A slice was taken from the Charpy bar parallel to and near fracture surface. This approach resulted in an approximate point source near the radial and azimuthal center of the capsule.

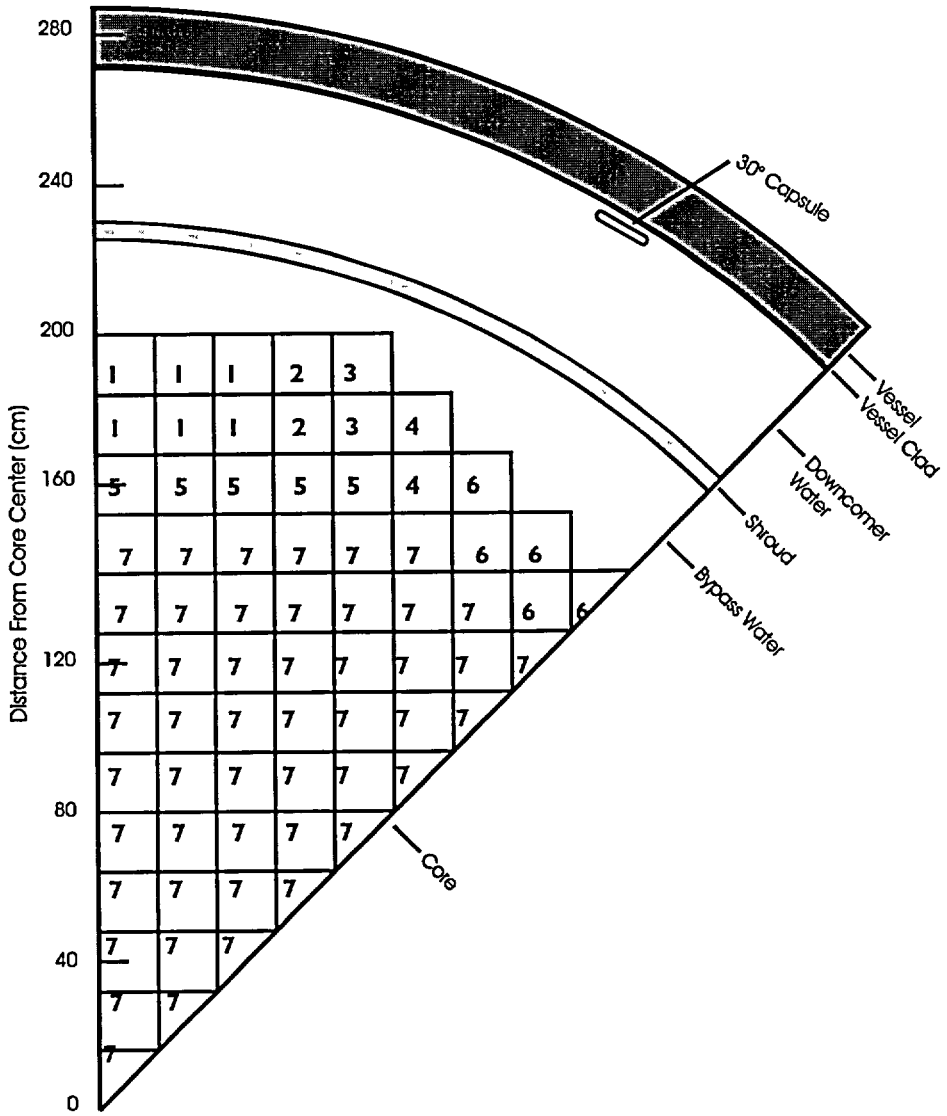

Figure 5-1 Nine Mile Point Unit 1 R-θ Geometry Used in the DORT Calculations.
(capsule not drawn to scale)

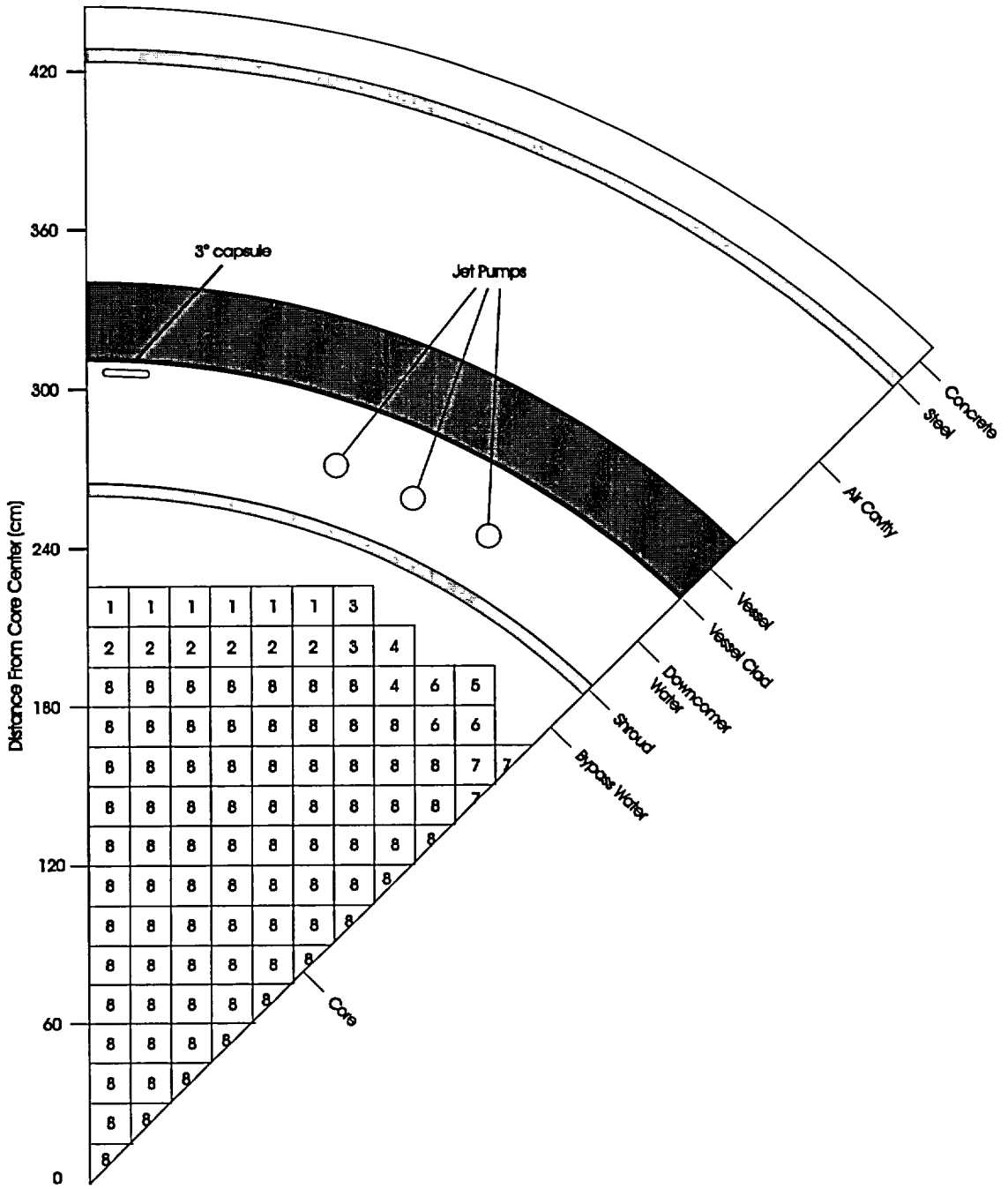

Figure 5-2 Nine Mile Point Unit 2 R-θ Geometry Used in the DORT Calculations.
(jet pumps and capsule are not drawn to scale)

6.0 Summary and Conclusions

In order to meet the methods qualification requirements of RG 1.190, the MPM calculational methodology used for Nine Mile Point Unit 1 (Reference 2) and Unit 2 (References 4, 5, and 6) has been validated by comparison with measurement and calculational benchmarks. These include the PCA pressure vessel simulator benchmark, which has high-accuracy measurement results extending from inside a simulated thermal shield through to the outside of a simulated vessel. The calculational results in the PCA show a slight consistent bias (less than 10%) with respect to the measurements, but no significant change in bias is observed with change in irradiation position. This indicates that the transport methodology is calculating the flux attenuation outside the core region with high accuracy. The observed bias is consistent with that obtained by other synthesis calculations.

The calculational benchmark was a typical BWR geometry similar to those for NMP-1 and NMP-2. Comparisons were made between the MPM calculations and the benchmark calculational results which indicated very good agreement. In the capsule, the average results were about 3% low, and at the vessel IR and within the vessel the average results were about 2-3% high. All compared results fell within ±10%. Additional comparisons were made with surveillance capsule measurements in NMP-1 and NMP-2 and with shroud measurements in NMP-1. In all cases, agreement with measured results within uncertainty was obtained. Uncertainties were shown to be less than ±20%. This meets the criterion set by RG 1.190 for acceptability of the calculations.

As a result of the work performed and documented in this report, it is concluded that the RG 1.190 requirement for qualification of the MPM methodology used for Nine Mile Point Unit 1 (Reference 2) and Unit 2 (References 4, 5, and 6) by comparisons to measurement and calculational benchmarks has been fully satisfied.

7.0 Nomenclature

BWR	boiling water reactor
C/M	calculated to measured ratio
dpa	displacements per atom
EFPS	effective full power seconds
ID	inner diameter
IR	inner radius
LWR	light water reactor
MPM	MPM Technologies, Inc.
NMPC	Niagara Mohawk Power Corporation
NMP-1	Nine Mile Point Unit 1
NMP-2	Nine Mile Point Unit 2
NRC	U. S. Nuclear Regulatory Commission
OD	outer diameter
OR	outer radius
ORNL	Oak Ridge National Laboratory
PCA	pool critical assembly
PWR	pressurized water reactor
RG	Regulatory Guide
RSICC	Radiation Safety Information Computational Center
T	vessel wall thickness

8.0 References

1. Regulatory Guide 1.190, *Calculational and Dosimetry Methods for Determining Pressure Vessel Neutron Fluence*, U. S. Nuclear Regulatory Commission, March, 2001.
2. "Nine Mile Point Unit 1 Shroud Neutron Transport and Uncertainty Analysis," Report Number MPM-108679, MPM Technologies, Inc, 2161 Sandy Drive, State College, PA 16803-2283, October, 1998.
3. "Nine Mile Point Unit 2 Shroud Neutron Transport and Uncertainty Analysis," Report MPM-200623, MPM Technologies, Inc., 2161 Sandy Drive, State College, PA 16803-2283, February, 2000.
4. "Nine Mile Point Unit 2 3-Degree Pressure Vessel Surveillance Capsule Report," Report MPM-1200676, MPM Technologies, Inc., 2161 Sandy Drive, State College, PA 16803-2283, December, 2000.
5. "Nine Mile Point Unit 2 Shroud Neutron Transport and Uncertainty Analysis," Report MPM-301624, MPM Technologies, Inc., 2161 Sandy Drive, State College, PA 16803-2283, January, 2003.
6. "Nine Mile Point Unit 2 Shroud Neutron Transport and Uncertainty Analysis", Report MPM-301624A, MPM Technologies, Inc., 2161 Sandy Drive, State College, PA 16803-2283, January, 2003.
7. Remec, I. and Kam, F.B.K., *Pool Critical Assembly Pressure Vessel Facility Benchmark*, NUREG/CR-6454, (ORNL/TM-13205), USNRC, July 1997.
8. Carew, J. F., Hu, K., Aronson, A., Prince, A., and Zamonsky, G., PWR and BWR Pressure Vessel Fluence Calculational Benchmark Problems and Solutions, NUREG/CR-6115 (BNL-NUREG-52395), Draft completed May 20, 1997.
9. RSICC Computer Code Collection, CCC-543, TORT-DORT-PC, Two- and Three-Dimensional Discrete Ordinates Transport Version 2.7.3, available from the Radiation Safety Information Computational Center, Oak Ridge National Laboratory, Oak Ridge, TN, June, 1996.
10. RSICC Data Library Collection, DLC-185, BUGLE-96, Coupled 47 Neutron, 20 Gamma Ray Group Cross Section Library Derived from ENDF/B-VI for LWR Shielding and Pressure Vessel Dosimetry Applications, available from the Radiation Safety Information Computational Center, Oak Ridge National Laboratory, Oak Ridge, TN, March, 1996.
11. RSICC Peripheral Shielding Routine Code Collection, PSR-277, LEPRICON, PWR Pressure Vessel Surveillance Dosimetry Analysis System, available from the Radiation Safety Information Computational Center, Oak Ridge National Laboratory, Oak Ridge, TN, June, 1995.

12. RSICC Computer Code Collection, CCC-371, "ORIGEN 2.1, Isotope Generation and Depletion Code Matrix Exponential Method," available from the Radiation Safety Information Computational Center, Oak Ridge National Laboratory, Oak Ridge, TN, May, 1999.

13. Fero, A.H., Anderson, S.L. and Roberts, G.K., "Analysis of the ORNL PCA Benchmark Using TORT and BUGLE-96," Reactor Dosimetry: Radiation Metrology and Assessment, ASTM STP 1398, John G. Williams, David W. Vehar, Frank H. Ruddy, and David Gilliam, Eds., American Society for Testing and Materials, West Conshohocken, PA, 2001.

14. Remec, I. and Kam, F.B.K., *H. B. Robinson-2 Pressure Vessel Benchmark*, NUREG/CR-6453 (ORNL/TM-13204), Oak Ridge National Laboratory, Oak Ridge, TN 37831, February, 1998.

15. ASTM Designation E482-89, *Standard Guide for Application of Neutron Transport Methods for Reactor Vessel Surveillance*, in ASTM Standards, Section 12, American Society for Testing and Materials, Philadelphia, PA, 2000.

16. Regulatory Guide 1.99, Revision 2, Radiation Embrittlement of Reactor Vessel Materials, U. S. Nuclear Regulatory Commission, May, 1988.

17. Carew, J. F., private communication, June, 2001.

18. S. King, K. Hour, "Fluence Analysis Report for Boat Samples, Nine Mile Point 1", January 29, 1998.

19. Letter SA-98-8, Anthony M. Salvagno to M.P. Manahan, "Data for NMP-1 Neutron Transport Analysis," February 10, 1998.

20. Framatome Report 86-1266298-00, "Fluence Analysis Report for Boat Samples", January, 1998.

21. ASTM Designation E261-94, *Standard Practice for Determining Neutron Fluence, Fluence Rate, and Spectra by Radioactivation Techniques*, in ASTM Standards, Section 12, American Society for Testing and Materials, Philadelphia, PA, 2000.

ATTACHMENT 2

REPORT NO. MPM-301624

NINE MILE POINT UNIT 2
SHROUD NEUTRON TRANSPORT AND UNCERTAINTY ANALYSIS

Nine Mile Point Unit 2 Shroud Neutron Transport and Uncertainty Analysis

© Copyright 2003 MPM Technologies, Inc.
All Rights Reserved

MPM Technologies, Inc.

...serving client needs through advanced technology .

Report Number MPM-301624
Revision 1

January, 2003

Report Number MPM-301624
Revision 1

Final Report

entitled

Nine Mile Point Unit 2 Shroud Neutron Transport and Uncertainty Analysis

prepared for

Niagara Mohawk Power Corporation
Nine Mile Point Unit 2
Lake Road
Lycoming, NY 13093

by

MPM Technologies, Inc.
2161 Sandy Drive
State College, PA 16803-2283

January, 2003

Preparer	**Checker**
1/7/03	**1/7/03**
Date	**Date**

MPM Approval

1/7/03

Date

© Copyright 2003 MPM Technologies, Inc.
All Rights Reserved

Nuclear Quality Assurance Certification

This document certifies that MPM has performed all work under NMPC Purchase Order Number 00-30028 in accordance with the requirements of the Purchase Order. All work has been performed under the MPM Nuclear Quality Assurance Program.

M P Manahan, Sr.

M. P. Manahan, Sr.
President
1/7/03

Date

S. Clinger

S. Clinger
QA Manager
1/7/03

Date

Executive Summary

This work was undertaken to calculate the best estimate neutron fluence, and its uncertainty, to the NMP-2 core shroud horizontal and vertical welds. The calculations were carried out using a synthesis of 2 dimensional neutron transport calculations, including plant specific R-θ and R-Z calculations, for each fuel cycle through the end of cycle 7. The power and void fraction distributions selected from near the middle of each cycle were used to represent an average for each of the cycles calculated except cycle 7. Cycle 7 was calculated in more detail using conditions at 5 points spanning the cycle to facilitate dosimetry analysis for the 3-degree surveillance capsule which was withdrawn at the end of cycle 7. Each case consisted of three transport analyses R-θ, R-Z, and R) which were synthesized to provide a three dimensional flux profile at the shroud. The calculations were used to determine detailed fluence profiles at the end of cycle 7, and projected to the end of cycle 8 (around March 2002). The calculational procedures meet standards specified by the NRC and ASTM as appropriate. In particular, the analysis meets the requirements of Regulatory Guide 1.190.

Table ES-1 summarizes the calculated maximum fluences to the shroud welds. The fluences were calculated at the ID surface of the shroud welds. As previously mentioned, the fluence is evaluated at the end of cycle 7 and the projected end of cycle 8 (cycle 8 is assumed to operate for 23 months at a capacity factor of 95%). For the weld locations above and below the core region, the calculational model did not include geometrical details or extend far enough to accurately determine the fluence to these points. The fluence values given for these welds are upper limit estimates based on extrapolation of the flux through additional water. For the welds above the core, this extrapolation is uncertain due to water mixing in this region and a resultant uncertain void fraction. As shown in the table, all shroud weld fluences are below 5.0E+20 n/cm^2 through the end of cycle 7, but weld H4 is projected to exceed this value during cycle 8.

The calculations were also used to evaluate fluence for the surveillance capsules and for the reactor vessel. Comparisons with dosimetry measurements at the surveillance capsule location were made and excellent agreement was found. The surveillance capsule fluence lead factor for the vessel inner radius maximum fluence location was calculated to be 0.43. Maximum fluence to the reactor vessel was calculated to be 1.98 E17 n/cm^2 (E > 1 MeV) at the end of cycle 7, and 5.71 E17 n/cm^2 (E > 1 MeV) after 22 efpy.

Fluence values for the capsule and for the vessel and shroud in the beltline region except for the very top and bottom of the core are estimated to have an uncertainty of about 15-16%. These uncertainties are within the value of 20% specified by RG 1.190. Moreover, the calculations are benchmarked against NMP-2 capsule dosimetry measurements which are in excellent agreement. Additional benchmarking is provided by comparisons of previous calculations using the same methodology with NMP-1 capsule and shroud measurements (boat samples were cut from the shroud). These latter measurements provide specific benchmarking of shroud fluence estimates that support the analytical uncertainty analysis. It is concluded that the calculations of shroud, vessel, and capsule fluence meet all the requirements of RG 1.190.

Table ES-1 Estimated Maximum Exposure to NMP-2 Shroud Welds.

Weld Identification	Location of Maximum			End of Cycle 7 Fast (E > 1 MeV) Fluence (n/cm^2)	End of Cycle 8 Fast (E > 1 MeV) Fluence (n/cm^2)
	ID Surface Radius (in)	Height Above BAF (in)	angle (degrees)		
Vertical Welds					
V24,V25[1]	98.38	-29.43	0	1.4E+19	1.7E+19
V18-V23[1]	101.56	-25.43	0, 30	9.2E+18	1.2E+19
V16,V17	101.56	7.07	45	3.64E+19	4.41E+19
V14,V15	101.56	80.69	0	7.47E+19	9.11E+19
V12,V13	101.56	111.00	45	1.51E+20	1.85E+20
V6,V9	101.56	143.57	0	3.27E+19	3.85E+19
V7,V8,V10, V11	101.56	143.57	30	1.31E+20	1.59E+20
V4,V5	101.56	146.07	5	2.89E+19	3.40E+19
V1-V3[1]	108.00	181.69	5, 25, 35	2.8E+19	3.4E+19
Horizontal Welds					
H7	98.38	-29.43	24.6	1.4E+19	1.7E+19
H6	101.56	-25.43	24.6	9.2E+18	1.2E+19
H5	101.56	7.07	24.6	1.26E+20	1.58E+20
H4	101.56	80.69	24.6	4.77E+20	6.04E+20
H3	101.56	143.57	24.6	2.06E+20	2.51E+20
H2	101.56	146.07	24.6	1.63E+20	1.97E+20
H1	108.00	181.69	24.6	2.8E+19	3.4E+19

[1] At elevations above and below the active fuel, the objective is to determine a bounding fluence for all welds at that elevation. Accordingly, the azimuthal position is not relevant for these welds. Vertical weld azimuthal locations were extracted from GE Report GE NE-B13-02047-00-17-01.

Contents

Executive Summary ..... **Preface Page iii**

1.0 Introduction ..... **Page Number 1**

2.0 Neutron Flux Calculation ..... **Page Number 4**
- 2.1 Introduction ..... Page Number 4
- 2.2 Neutron Transport Model ..... Page Number 5
- 2.3 Neutron Transport Results ..... Page Number 9
- 2.4 Chapter 2 References ..... Page Number 10

3.0 Fluence to Capsule and Vessel ..... **Page Number 29**
- 3.1 Surveillance Capsule Results ..... Page Number 29
- 3.2 Reactor Vessel Results ..... Page Number 29
- 3.3 Capsule Measurement Results ..... Page Number 30
- 3.4 Chapter 3 References ..... Page Number 33

4.0 Uncertainty Analysis ..... **Page Number 40**
- 4.1 Uncertainty Assumptions ..... Page Number 40
- 4.2 Uncertainty Evaluation ..... Page Number 44
- 4.3 Chapter 4 References ..... Page Number 45

5.0 Methodology Validation ..... **Page Number 54**
- 5.1 Compliance With RG 1.190 ..... Page Number 54
- 5.2 Benchmarking of Methodology ..... Page Number 55
- 5.3 Chapter 5 References ..... Page Number 57

6.0 Summary and Conclusions ..... **Page Number 62**

7.0 Nomenclature ..... **Page Number 63**

1.0 Introduction

The Nine Mile Point Unit 2 (NMP-2) shroud fluence is needed for use with stress corrosion crack growth models. Figure 1-1 shows the NMP-2 shroud weld designations. These designations are used throughout the report to identify the vertical and horizontal welds of interest. In a previous report [1-1], a detailed evaluation of the fluence distribution in the shroud was described. This earlier evaluation was based on calculations performed for fuel power distributions at the midpoint of fuel cycles 3, 4, and 7. These flux distributions were used to integrate the flux over the reactor operating history to the end of cycle 7 and projected to the end of cycle 8.

The current work was undertaken to update the best estimate neutron fluence, and its uncertainty, to the NMP-2 core shroud horizontal and vertical welds. The calculations were carried out using a synthesis of 2 dimensional neutron transport calculations, including plant specific R-θ and R-Z calculations. Each case consisted of three transport analyses R-θ, R-Z, and R) which were synthesized to provide a three dimensional flux profile at the shroud. The calculations were used to determine detailed fluence profiles at the end of cycle 7 and projected to the end of cycle 8 which is expected to be around March 2002.

After the end of fuel cycle 7, a surveillance capsule was removed and dosimetry measurements were made to provide data to confirm the calculated fluence evaluation. In order to improve the accuracy of the transport results at the 3-degree capsule location, it was decided to perform additional calculations to better define the flux for each cycle, and to provide a detailed evaluation of the flux variation with time during cycle 7. The detailed evaluation of cycle 7 is necessary to obtain an accurate relationship between measured shorter-lived radioactive products and the capsule fluence. The previous analyses for cycles 3 and 4 were used, and new analyses were performed for cycles 1, 2, 5, 6, and for 5 fuel power distributions during cycle 7. The results of the capsule and vessel fluence evaluations are described in [1-2]. This report uses these results to update the shroud fluence evaluation which is reported in Reference [1-1]. In addition, the NMP-2 capsule and vessel results are summarized, along with other dosimetry analysis results for Nine Mile Point Unit 1 (NMP-1) in an effort to benchmark the MPM calculational methods.

The calculational procedures meet standards specified by the NRC and ASTM as appropriate. In particular, the analysis and results meet the requirements of Regulatory Guide (RG) 1.190 [1-3]. This is discussed further in Section 5.

1.1 Chapter 1 References

[1-1] "Nine Mile Point Unit 2 Shroud Neutron Transport and Uncertainty Analysis," Report MPM-200623, MPM Technologies, Inc., 2161 Sandy Drive, State College, PA 16803-2283, February 2000.

[1-2] "Nine Mile Point Unit 2 3-Degree Pressure Vessel Surveillance Capsule Report," Report MPM-1200676, MPM Technologies, Inc., 2161 Sandy Drive, State College, PA 16803-2283, December 2000.

[1-3] Regulatory Guide 1.190, *Calculational and Dosimetry Methods for Determining Pressure Vessel Neutron Fluence*, U. S. Nuclear Regulatory Commission, March 2001.

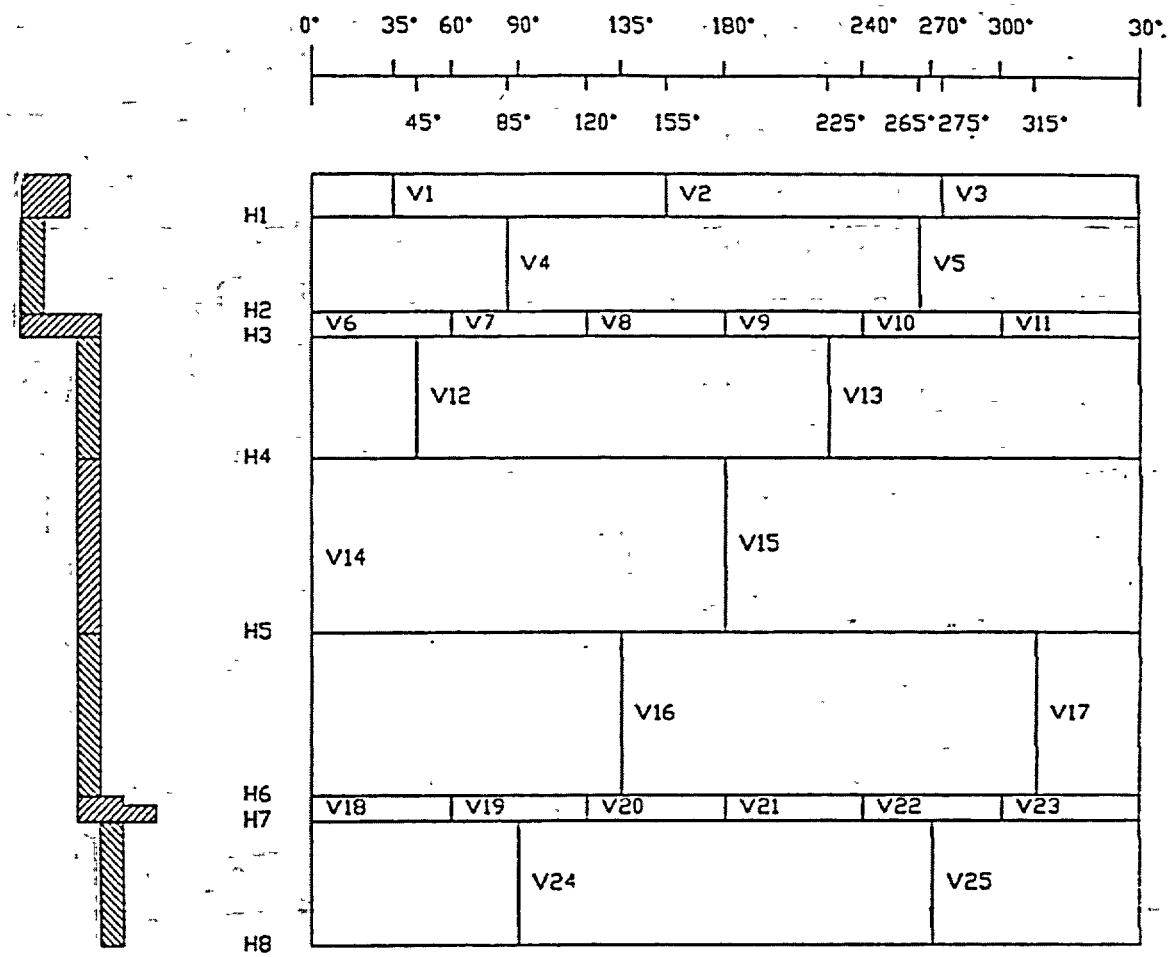

Figure 1-1 **Weld Designations for Nine Mile Point Unit 2.**
(weld azimuths are typical, and may not be located exactly as specified in the above figure; this drawing was extracted from GE report GENE-B13-02047-00-17-01)

2.0 Neutron Flux Calculation

2.1 Introduction

The neutron exposure of reactor structures is determined by a neutron transport calculation, or a combination of neutron transport calculations, to represent the distribution of neutron flux in three dimensions. The calculation determines the distribution of neutrons of all energies from their source from fission in the core region to their eventual absorption or leakage from the system. The calculation uses a model of the reactor geometry that includes the significant structures and geometrical details necessary to define the neutron environment at locations of interest.

A previous set of calculations was carried out for NMP-2 to determine the shroud exposure [2-1]. These calculations also included the surveillance capsule and vessel. The shroud fluence estimates were based on neutron transport calculations performed using fuel power and void fraction distributions taken at the midpoint of cycles 3, 4, and 7. In a subsequent analysis performed to evaluate the fluence for the vessel and the surveillance capsule removed at the end of cycle 7 [2-2], determination of the fluence was carried out using the previous results for cycles 3 and 4, and new calculations were performed using fuel power and void fraction distributions at the middle of each of cycles 1, 2, 5, and 6, and at five representative times during cycle 7. The detailed evaluation of the variation in flux level due to changes in fission distributions and void fraction distributions during cycle 7 was made to allow for accurate determination of dosimeter activities from the surveillance capsule that was withdrawn at the end of this cycle. It also provides an indication of the variation in flux level that occurs during a fuel cycle. The updated results are used in this report to provide a better estimate of the shroud exposure.

During reactor operation, the neutron flux level at any point in the shroud or vessel will vary due to changes in fuel composition, power distributions within the core, and water void fraction. These changes occur between fuel cycles due to changes in fuel loading and fuel design, and within a fuel cycle due to fuel burnup and resultant changes in power shape, control rod position, fission contributions by nuclide, and void fraction vs. axial height in each fuel bundle. In order to ensure that the fuel cycle data input to the model was representative, NMPC performed an analysis of the axial power shapes. For cycles 1 through 6, the core average axial power shape was plotted versus cycle exposure. An exposure-weighted cycle average power shape was calculated based on all of the individual power shapes. Power shapes close to the middle of cycle (MOC) were compared with the cycle average shape to determine which shape was representative of the entire cycle.

For cycle 7, NMPC once again examined the core average axial power shapes and the shapes were plotted throughout the cycle. Five cases were selected: beginning-of-cycle (BOC); before middle-of-cycle (BMOC); middle-of-cycle (MOC); after middle-of-cycle (AMOC); and near the end-of-cycle (NEOC). An axial shape which was most representative of each regime was chosen

to represent that segment of cycle exposure.

The NMPC approach for selecting power shape inputs results in power shapes that are representative of the fuel cycle (or fuel cycle segment). Power shape throughout a typical cycle's worth of operation has similar characteristics from cycle-to- cycle. Power starts out being preferentially produced in the bottom of the core via rod pattern manipulation, causing a spectral shift and enhanced Pu production. The Pu produced in the early part of the cycle is beneficial for "squeezing" extra energy out of the core toward the EOC when control blades are not available for power shaping. During MOC, the axial segments of the core which were burned harder in the early cycle cause the power shape to flatten. As the cycle comes to a close, and rods are nearly fully withdrawn, the power shifts to the top of the core and the reactor is subsequently shut down for refueling as EOC is achieved. These cycle characteristics are repeatable for all cycles which allows one to choose a MOC shape which is representative of the average over the entire cycle.

2.2 Neutron Transport Model

The transport calculations for NMP-2 were carried out in R-θ and R-Z geometry using the DORT two-dimensional discrete ordinates code [2-3] and the BUGLE-96 cross-section library [2-4]. The DORT code is an update of the DOT code which has been in use for this type of problem for many years. The BUGLE-96 library is a 47 energy group ENDF/B-VI based data set produced specifically for light water reactor applications (an update of the earlier SAILOR library). The energy group boundaries for the 47 groups are given in Table 2-1. This library contains cross-sections collapsed using a BWR core spectrum which were used for the core region. Outside the core region, cross sections collapsed using PWR downcomer and PWR vessel spectra were used. The difference between BWR and PWR collapsing in these regions is not significant. In these analyses, anisotropic scattering was treated with a P_3 expansion of the scattering cross-sections, and the angular discretization was modeled with an S_8 order of angular quadrature. These procedures are in accordance with ASTM Standard E-482 [2-5].

The computer codes were obtained from the Radiation Safety Information Computational Center (RSICC) at Oak Ridge National Laboratory. Each code was then compiled on the computer used by MPM for the calculations and a series of test cases were run to verify the code performance. The test cases all agreed within allowable tolerance with established results. This verification was conducted under the MPM Nuclear Quality Assurance Program. The calculational procedures meet standards specified by the NRC and ASTM as appropriate. In particular, the analysis (including all modeling details and cross-sections) is consistent with RG 1.190 [2-6] and the calculations have been benchmarked to measured plant specific BWR data as described in Section 5.

R-θ Calculations

The R-θ layout is shown in Figure 2-1. Dimensions for the various structures are given in Table 2-2. Dimensions were obtained from plant drawings [2-7] which are referenced in Table

2-2. Additional data on the jet pumps and biological shield were supplied in [2-8] and confirmation of all the data in Table 2-2 by NMP-2 staff is in [2-9]. As shown in Figure 2-1, all structures outside the core were modeled with a cylindrical symmetry except for the inclusion of a surveillance capsule centered at 3° and jet pump structures located in the downcomer region. The latter are not to scale in the figure. The jet pumps are only approximate models of two pumps with a central pipe (riser) in between. These structures were modeled as 2 slabs of stainless steel each centered at a radius of approximately 112.28 inches (from drawing 732E143). The slabs representing the pumps are at about 22 and 36.5 degrees, and the riser is at about 29.3 degrees. The slabs extend over approximately 3.85 degrees and have a thickness of 0.477 inches. The pipe slab extends over about 4.25 degrees and is 0.523 inches thick.

The R-θ model included 186 mesh points in the radial direction covering the range from the center of the core to ten inches into the biological shield. This large number of mesh points was used to accurately calculate the neutron flux transport from the core edge to the outside of the vessel. In the azimuthal direction, 48 mesh points were used to model a single octant of the reactor. Inspection of the fuel loading patterns indicated that only minor deviations from an octant symmetry were present and these were ignored. The 48 points provided good definition of the variation of the core edge with angle and defined the azimuthal flux variation in the shroud. In the discussion below, all angles are referred to in the first octant (i.e. relative to the nearest cardinal axis) and thus welds at both 45° and 225° are referred to as a 45° location. It should be noted that the azimuthal flux shape between 45° and 90° is the mirror image of that between 0° and 45° (i.e. an angle of 50° corresponds to 40° in the first octant).

The core region [2-10, 2-11] used a homogenized material distribution which includes the fuel, fuel cladding, and the water. The water region in the fuel contains both liquid water and steam. The fraction occupied by steam is known as the void fraction and varies by assembly and axial position within the fuel. Values of void fraction for each cycle at the middle of the cycle, and at the additional times during the cycle for cycle 7, were supplied by Niagara Mohawk for each assembly at 25 axial nodes [2-12, 2-13, 2-14]. Inspection of these values indicated that while some assemblies exhibit significant variation in the void fraction, some groups of neighboring assemblies had close to the same void fraction. To model the void fraction variation in the R-θ model, the outer rows of assemblies were divided into seven regions of approximately uniform water density, and the average water density for the assemblies in each of these regions was calculated by multiplying the base water density (0.7365 g/cc) by 1.0 minus the void fraction. The assemblies in each of these regions are indicated by the region numbers defined in Figure 2-1. Each one of these regions had a void fraction assigned as the average midplane void fraction value for the assemblies in the region. These average void fraction values were different for each case analyzed. Values for the average axial midplane void fractions by region for each case are given in Table 2-3.

Water density in the bypass region was varied between 0.7585 g/cc at the inlet and 0.7394 g/cc at the outlet. The value at midplane was taken to be an average of these values. The downcomer water density was calculated for a temperature of 534 °F and a pressure of 1037 psia.

The DOTSOR code (available as part of the LEPRICON code package [2-15]), was used to convert the cycle power distributions from x,y to R,θ coordinates and place the source in each mesh cell. The source per group was defined by an average fission spectrum calculated for a fission breakdown by isotope determined for the average burnup of the outer fuel bundles for each case. The main isotopes that contribute to the fission spectrum are U-235 and Pu-239, but contributions from U-238, Pu-240, and Pu-241 were also included. Use of the outer bundle average is a good approximation to the fission spectrum because the outer bundles were all burned assemblies with similar burnup, and the fission spectrum only slowly varies with burnup. Almost all of the neutrons that reach the capsule and vessel originate in the outer rows of fuel bundles. The average core burnup was used to determine the average value of the neutrons per fission and the average energy per fission.

The source calculations used the appropriate power distribution for all the fuel bundles in the first octant together with pin power distributions for the outer rows of bundles. The pin power distributions were used to model the spatial variation of the source within the bundles and took into account the gaps between bundles and water rods in the center. Equal pin power weighting was used for interior fuel bundles. In the calculations, the variation in relative pin power distributions within similar bundles between cycles was determined to be small [2-1] and so the cycle 7 9x9 MOC pin power distributions were used in the calculations for all the cases.

The calculation of the fuel fission parameters was handled differently from the previous calculations. The ORIGEN 2.1 code [2-16] was used to calculate the effects of burnup on the neutron source. This was carried out using an ORIGEN BWR cross section library appropriate for high burnup fuel. The results were validated by comparison to NMP-2 calculated fuel compositions as a function of fuel burnup.

For the ORIGEN calculations, the initial fuel composition for each cycle was taken to be the average initial composition for the outer assemblies. The effects of the varying axial initial enrichment, burnup, and void fraction were ignored in this calculation and are assumed to have negligible impact because the effects of the change in parameters are minor. The ORIGEN code calculated the fission fraction by isotope and the average energy deposited in the reactor per fission (κ). The isotopic fission fractions were used to determine the fission spectrum and the average number of neutrons per fission (ν). The normalization of the neutron source in the DORT calculations is directly proportional to ν/κ which slowly varies with burnup.

Since the average burnup of the outer assemblies was used for the source normalization, this is an updated method compared to [2-1] where the average core burnup was used. The present assumption more accurately represents the neutrons that escape from the core. This effect is small enough that it was ignored for the cycle 3 and 4 cases. The source calculations used the MOC power distribution for all the fuel bundles in the first octant together with pin power distributions for the outer rows of bundles. The pin power distributions were used to model the spatial variation of the source within the bundles and took into account the gaps between bundles and water rods in the center. Equal pin power weighting was used for interior fuel bundles. In the calculations, the variation in pin power distributions between cycles was determined to be

small and so it was decided to use the cycle 7 9x9 pin power distributions in the calculations for the other cycles. Since this conclusion on the effect of the pin power variation was made using engineering judgement, it was necessary to test this assumption by performing a calculation for cycle 3 with the cycle 3 pin power distribution to compare with that made with the cycle 7 pin power distribution. It was found that the pin power difference caused differences in the shroud flux of 1.3% or less with an average deviation of 0.2%. Of most interest is the effect at the peak flux position where the difference was only 0.05%. These differences are much less than the uncertainty in the flux value and it is concluded that it is not necessary to evaluate the pin power distribution for every cycle.

R-Z Calculations

A second set of transport calculations were performed for each case in R-Z geometry. For this calculation, the core was divided into 3 radial regions. Two of these regions consisted of each of the outer two rows of assemblies averaged over the octant. The third region consisted of the inner part of the core. The neutron source in each of these regions was calculated using a radial source averaged over the octant (calculated by DOTSOR as for the R,θ case) together with an average axial power shape for each region. The axial power distribution was supplied for each assembly in 25 nodes, each representing 6 inches of core height. Neutron source outside the equivalent core radius was eliminated.

Each radial region was also divided into axial regions according to variation in void fraction. The void fraction was also given for each assembly in 25 axial nodes. Except for nodes near the bottom of the core which had zero void fraction, each node was modeled as a separate region for the calculation. This resulted in a total of 70 regions in the core, each with a distinct cross section set. The bypass region was also modeled with a varying axial water density. The bypass region was divided into 12 subregions within the core height, each with a different water density.

For the R-Z model, the core radius was taken to be that which gave the equivalent core volume. Regions above and below the core were not modeled exactly but consisted of a one-foot high water reflector with vacuum boundaries at the top and bottom of the model. The model had 186 mesh points in the radial direction as in the R-θ model except with slightly different boundaries near the core edge. In the axial direction, the model had 68 mesh points with 38 in the core region.

Flux Synthesis

As indicated above, the calculations were carried out in 2 dimensions. In order to estimate the fluence rate in the 3 dimensional geometry, the following equation was used to evaluate the flux ϕ for each cycle case:

$$\phi(R,\theta,Z) = \phi(R,\theta) * \phi(R,Z) / \phi(R)$$

In this equation, $\phi(R,\theta)$ is taken from the DORT R,θ calculation (normalized to the power at

midplane in the model region), and $\phi(R,Z)$ is from the R,Z calculation normalized to the power in the entire core. A third calculation determined $\phi(R)$ using a one-dimensional cylindrical model normalized at core midplane. The model for the one-dimensional calculation used the same radial geometry as the R,Z calculation.

2.3 Neutron Transport Results

Selected results of the 3-dimensional flux synthesis are presented here. Detailed tables of the fluence to all the horizontal and vertical shroud welds that are located in the beltline region are contained in an addendum to this report [2-17]. Fluence values were calculated at two times: at the end of Cycle 7 (8.72 EFPY) and projected to the end of cycle 8 in about March 2002. Cycle 8 is assumed to be 1.82 EFPY (5.75E7 s) in length at a power of 3467 MWth.

Table 2-4 summarizes the calculated maximum fluences to the shroud welds. These fluences were calculated at the ID surface of the shroud welds. As shown in the table, all shroud weld fluences are below 5.0E+20 n/cm^2 through the end of cycle 7, but weld H4 is projected to exceed this value during cycle 8.

The fluence to shroud welds outside the beltline region were not calculated using the RG 1.190 procedures because of limitations of the synthesis method and because the regions above and below the core were not accurately modeled since only conservative upper limit fluences are needed. Therefore, conservative upper limit fluences were determined. The fluence to weld H1 was calculated by using the calculated fluence and the fluence slope (which is approximately exponential) at a reference point about 6 inches above the core. Since the neutron flux arrives at the weld from the whole top of the core, an effective increased distance to the weld was calculated by considering the distance from the center of the core at the top of the fuel to the nearest point of the weld, and then subtracting the distance to the reference point. The slope was then used to adjust the weld fluence using this increased distance. This calculation is conservative since most neutrons will travel longer incremental paths to arrive at the weld. In addition, the fluence was determined relative to that at the maximum azimuthal point without taking any credit for streaming which will lower the relative peak fluence. Thus, more detailed fluence calculations would be expected to result in significantly lower fluence estimates for the top weld. Similar calculations were carried out for the bottom welds, H6 and H7. Upper limits for the vertical welds V1-V3 and V18-V25 were set equal to the upper limits for the horizontal weld nearest the core that borders each of these vertical welds. The azimuthal position of the vertical welds was not taken into account in determining these upper limits.

Figure 2-2 is a plot of the flux (E > 1 MeV) evaluated at the middle of 3 cycles (2, 3, and 7) calculated at the inner radius (IR) of the shroud as a function of height. Cycles 2 and 3 bound the range of flux magnitudes obtained for the seven cycles. Cycle 7 falls between these limits and is used for projection of fluence into the future. The azimuth chosen for this plot is at 24.6°, which is the maximum azimuthal flux point in the shroud. It is seen from the plot that the maximum flux occurs at about a distance of 111 inches above the bottom of the active fuel (BAF). It is also seen that there are significant differences between the three cycles. For

convenience, the flux level for all cycles was normalized to the uprated power of 3467 MWth. Thus differences between the cycles in this comparison are not affected by the power uprate.

In the previous analysis [2-1], it was shown that differences in shroud flux level can be quantitatively explained by considering differences in power level in the outer fuel bundles. Lower power in the outer bundles has two effects which act in concert. First, since these outer bundles are the most important for the leakage flux, the source of high energy neutrons reaching the shroud is reduced. Second, the lower power in the outer bundles causes the void fraction to be lower and this also reduces the leakage.

Figure 2-3 is a plot of the shroud flux for the same 3 cycles discussed earlier as a function of the azimuth at the axial position of weld H4 (about 5 inches above the core axial midplane). The shape of the azimuthal traverse for the different cycles is consistent, with the main difference being the flux level. A similar comparison for 3 of the cycle 7 cases is shown in Figure 2-4. The cases plotted are for fuel power distributions near the beginning of the cycle, near the middle of the cycle, and near the end of the cycle. This figure indicates the changes in shroud exposure rate that occur during a cycle.

Figures 2-5 and 2-6 show the calculated fluence (E > 1 MeV) to the shroud horizontal weld H4 as a function of azimuthal angle at the end of cycle 7 and projected to the end of cycle 8, respectively. The fluence is shown at the shroud IR, the radial middle of the shroud, and at the outer radius (OR). Data plotted in these figures are given in tables in the addendum to this report. Weld H4 is the weld calculated to receive the highest fluence. Similarly, Figures 2-7 and 2-8 show the calculated fluence for horizontal weld H5.

Figures 2-9 through 2-12 show the calculated fluence (E > 1 MeV) to the shroud vertical welds encompassing most of the beltline region. Fluence is plotted for the IR, middle, and OR of the shroud as a function of height above the bottom of the active fuel. Fluence results at the end of cycle 7 and projections to the end of cycle 8 are shown. Data plotted in these figures are also given in tables in the addendum to this report (Reference [2-17]).

2.4 Chapter 2 References

[2-1] "Nine Mile Point Unit 2 Shroud Neutron Transport and Uncertainty Analysis," Report MPM-200623, MPM Technologies, Inc., 2161 Sandy Drive, State College, PA 16803-2283, February 2000.

[2-2] "Nine Mile Point Unit 2 3-Degree Pressure Vessel Surveillance Capsule Report," Report MPM-1200676, MPM Technologies, Inc., 2161 Sandy Drive, State College, PA 16803-2283, December 2000.

[2-3] RSICC Computer Code Collection, CCC-543, TORT-DORT-PC, Two- and Three-Dimensional Discrete Ordinates Transport Version 2.7.3, available from the Radiation Safety Information Computational Center, Oak Ridge National Laboratory, Oak Ridge,

TN, June 1996.

[2-4] RSICC Data Library Collection, DLC-185, BUGLE-96, Coupled 47 Neutron, 20 Gamma Ray Group Cross Section Library Derived from ENDF/B-VI for LWR Shielding and Pressure Vessel Dosimetry Applications, available from the Radiation Safety Information Computational Center, Oak Ridge National Laboratory, Oak Ridge, TN, March 1996.

[2-5] ASTM Designation E482-89, *Standard Guide for Application of Neutron Transport Methods for Reactor Vessel Surveillance*, in ASTM Standards, Section 12, American Society for Testing and Materials, Philadelphia, PA, 1997.

[2-6] Regulatory Guide 1.190, *Calculational and Dosimetry Methods for Determining Pressure Vessel Neutron Fluence*, U. S. Nuclear Regulatory Commission, March 2001.

[2-7] Letter, Shashi K. Dhar to M. P. Manahan, File Code ESB2-M99-034, June 17, 1999.

[2-8] Letter, Shashi K. Dhar to M. P. Manahan, File Code ESB2-M99-048, August 17, 1999.

[2-9] Letter, Shashi K. Dhar to M. P. Manahan, "Input Data for NMP-2 Fluence/Transport Calculations - Final," File Code ESB2-M99-058, October 26, 1999.

[2-10] Letter, Shashi K. Dhar to M. P. Manahan, File Code ESB2-M99-043, July 29, 1999.

[2-11] Letter, Shashi K. Dhar to M. P. Manahan, File Code ESB2-M99-047, August 9, 1999.

[2-12] Winklebleck, J., Email with attached files, entitled, "NMP-2 Cycles 4, 5, & 7 Core Neutronics Data", From J. Winklebleck to M. P. Manahan, Sr., August 6, 1999.

[2-13] Winklebleck, J., Email with attached files, entitled, "NMP-2 Cycle 3 Core Neutronics Data", From J. Winklebleck to M. P. Manahan, Sr., January 13, 2000.

[2-14] Email from J. Winkelbleck to M. P. Manahan, Sr.: Power and Void Fraction, casematrix.xls - 9/20/00, nmp2flue.zip - 9/27/00; Cycle 7 Power History, cycle7_pow.xls - 10/2/00, cycle7thermal.xls - 10/11/00; Cycle 1 Power and Void Fraction, c1mocmap_rev01.txt - 11/15/00.

[2-15] RSICC Peripheral Shielding Routine Code Collection, PSR-277, LEPRICON, PWR Pressure Vessel Surveillance Dosimetry Analysis System, available from the Radiation Safety Information Computational Center, Oak Ridge National Laboratory, Oak Ridge, TN, June 1995.

[2-16] RSICC Computer Code Collection, CCC-371, "ORIGEN 2.1, Isotope Generation and Depletion Code Matrix Exponential Method," available from the Radiation Safety

Information Computational Center, Oak Ridge National Laboratory, Oak Ridge, TN, May 1999.

[2-17] "Nine Mile Point Unit 2 Shroud Neutron Transport and Uncertainty Analysis: Addendum", Report MPM-301624A, MPM Technologies, Inc., 2161 Sandy Drive, State College, PA 16803-2283, October 2001.

Table 2-1 Neutron Energy Group Structure – 47 Groups.

Energy Group	Upper Energy (MeV)	Energy Group	Upper Energy (MeV)
1	1.733E+01	25	2.972E-01
2	1.419E+01	26	1.832E-01
3	1.221E+01	27	1.111E-01
4	1.000E+01	28	6.738E-02
5	8.607E+00	29	4.087E-02
6	7.408E+00	30	3.183E-02
7	6.065E+00	31	2.606E-02
8	4.966E+00	32	2.418E-02
9	3.679E+00	33	2.188E-02
10	3.012E+00	34	1.503E-02
11	2.725E+00	35	7.102E-03
12	2.466E+00	36	3.355E-03
13	2.365E+00	37	1.585E-03
14	2.346E+00	38	4.540E-04
15	2.231E+00	39	2.145E-04
16	1.920E+00	40	1.013E-04
17	1.653E+00	41	3.727E-05
18	1.353E+00	42	1.068E-05
19	1.003E+00	43	5.044E-06
20	8.208E-01	44	1.855E-06
21	7.427E-01	45	8.764E-07
22	6.081E-01	46	4.140E-07
23	4.979E-01	47	1.000E-07
24	3.688E-01		1.000E-11

Table 2-2 Nine Mile Point Unit 2 Radial Dimensions.

Component	Dimension (in)	Dimension (cm)	Reference
Fuel Bundle Size	6.000	15.240	DB-0003.04
Core edge at 0 degrees	89.759	227.988	15 times fuel bundle size minus outside water gap of 0.241 inches (DB-0003.04)
Shroud IR	101.56	257.962	105E1347A
Shroud OR	103.56	263.042	105E1347A
Vessel Clad IR	126.5	321.310	VPF#3516-213-2 and VPF#3516-214-4
Vessel Base Metal IR	126.6875	321.786	
Vessel OR	133.125	338.138	
Bio Shield Iron IR	168.75	428.625	USAR Section 3.8.3.1.3
Bio Shield Concrete IR	170.25	432.435	
Capsule IR	125.60	319.024	105D5036, 105D5017, 112D1065 and VPF3516-304-3
Capsule OR	126.14	320.396	

Table 2-3 Fuel Region Void Fractions at Midplane for Each R-θ Calculation.

Case	Void Fraction by Region							
	1	2	3	4	5	6	7	8
Cycle 1	0.363	0.521	0.239	0.333	0.074	0.362	0.425	0.530
Cycle 2	0.183	0.150	0.010	0.072	0.014	0.145	0.119	0.417
Cycle 3	0.368	0.432	0.275	0.258	0.083	0.317	0.171	0.486
Cycle 4	0.169	0.293	0.068	0.184	0.030	0.272	0.271	0.470
Cycle 5	0.264	0.257	0.055	0.232	0.136	0.381	0.288	0.509
Cycle 6	0.310	0.341	0.080	0.203	0.057	0.283	0.266	0.530
Cycle 7 BOC	0.464	0.500	0.373	0.451	0.226	0.415	0.345	0.562
Cycle 7 BMOC	0.313	0.352	0.259	0.363	0.147	0.343	0.268	0.534
Cycle 7 MOC	0.320	0.368	0.199	0.300	0.086	0.283	0.216	0.500
Cycle 7 AMOC	0.286	0.337	0.193	0.302	0.087	0.295	0.212	0.522
Cycle 7 NEOC	0.224	0.279	0.118	0.229	0.041	0.228	0.147	0.450

Table 2-4 Estimated Maximum Exposure to Shroud Welds.

Weld Identification	Location of Maximum			End of Cycle 7 Fast (E > 1 MeV) Fluence (n/cm^2)	End of Cycle 8 Fast (E > 1 MeV) Fluence (n/cm^2)
	ID Surface Radius (in)	Height Above BAF (in)	angle (degrees)		
Vertical Welds					
V24,V25[1]	98.38	-29.43	0	1.4E+19	1.7E+19
V18-V23[1]	101.56	-25.43	0, 30	9.2E+18	1.2E+19
V16,V17	101.56	7.07	45	3.64E+19	4.41E+19
V14,V15	101.56	80.69	0	7.47E+19	9.11E+19
V12,V13	101.56	111.00	45	1.51E+20	1.85E+20
V6,V9	101.56	143.57	0	3.27E+19	3.85E+19
V7,V8,V10, V11	101.56	143.57	30	1.31E+20	1.59E+20
V4,V5	101.56	146.07	5	2.89E+19	3.40E+19
V1-V3[1]	108.00	181.69	5, 25, 35	2.8E+19	3.4E+19
Horizontal Welds					
H7	98.38	-29.43	24.6	1.4E+19	1.7E+19
H6	101.56	-25.43	24.6	9.2E+18	1.2E+19
H5	101.56	7.07	24.6	1.26E+20	1.58E+20
H4	101.56	80.69	24.6	4.77E+20	6.04E+20
H3	101.56	143.57	24.6	2.06E+20	2.51E+20
H2	101.56	146.07	24.6	1.63E+20	1.97E+20
H1	108.00	181.69	24.6	2.8E+19	3.4E+19

[1] At elevations above and below the active fuel, the objective is to determine a bounding fluence for all welds at that elevation. Accordingly, the azimuthal position is not relevant for these welds. Vertical weld azimuthal locations were extracted from GE Report GE NE-B13-02047-00-17-01.

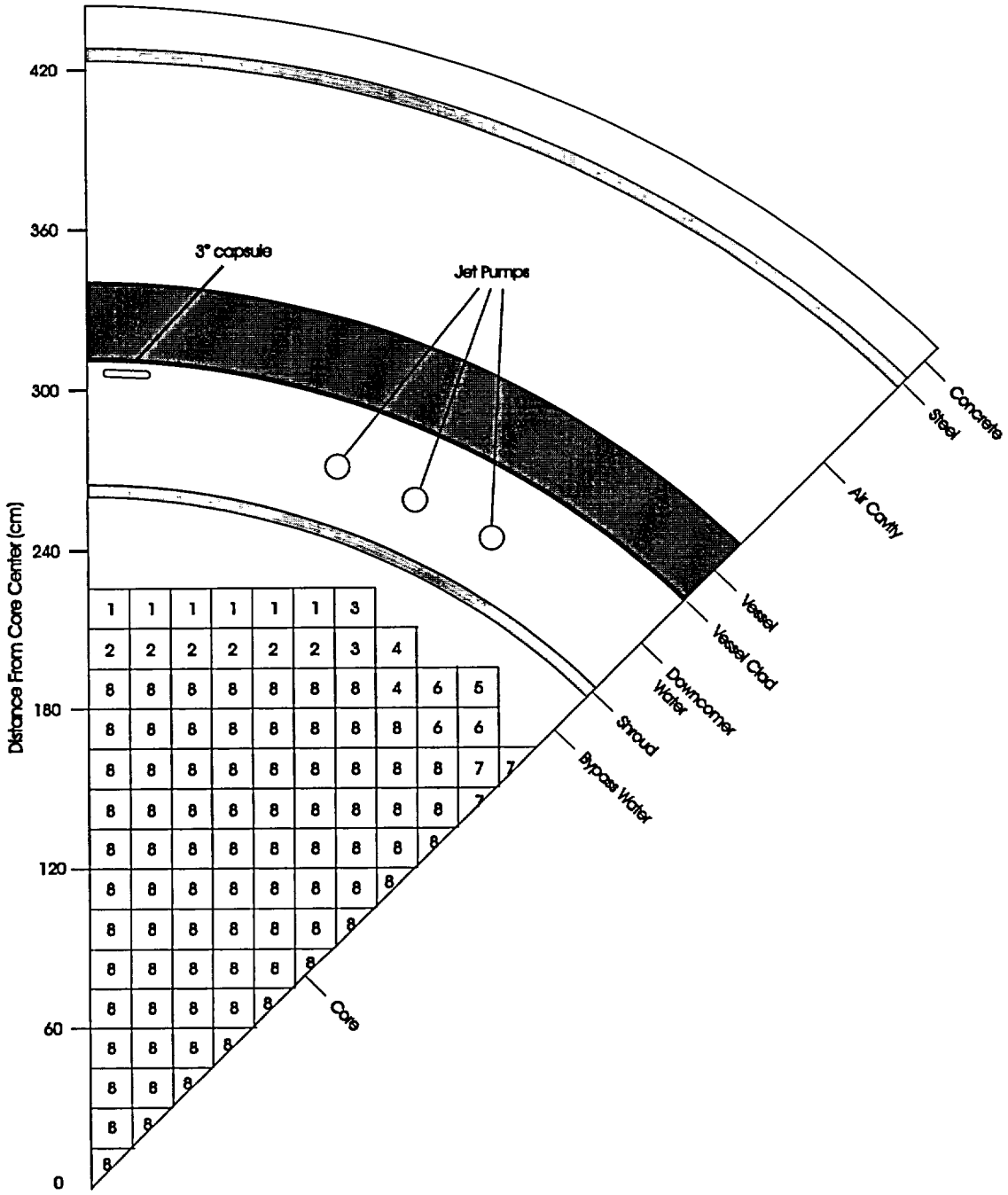

Figure 2-1 **Nine Mile Point Unit 2 R-θ Geometry Used in the DORT Calculations.**
(Note: jet pumps and capsule are not drawn to scale)

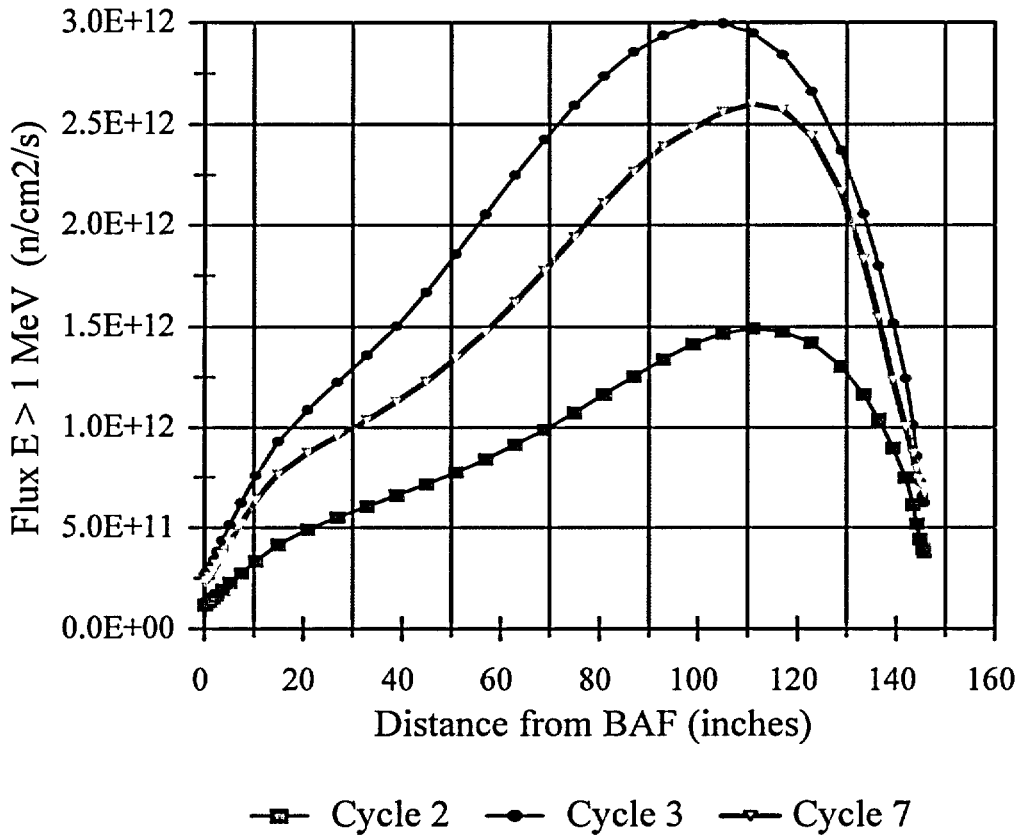

Figure 2-2 **Calculated Flux (E > 1 MeV) at the Inner Radius of the Shroud at the Maximum Azimuthal Position (24.6°) for Cycles 2, 3, and 7.**

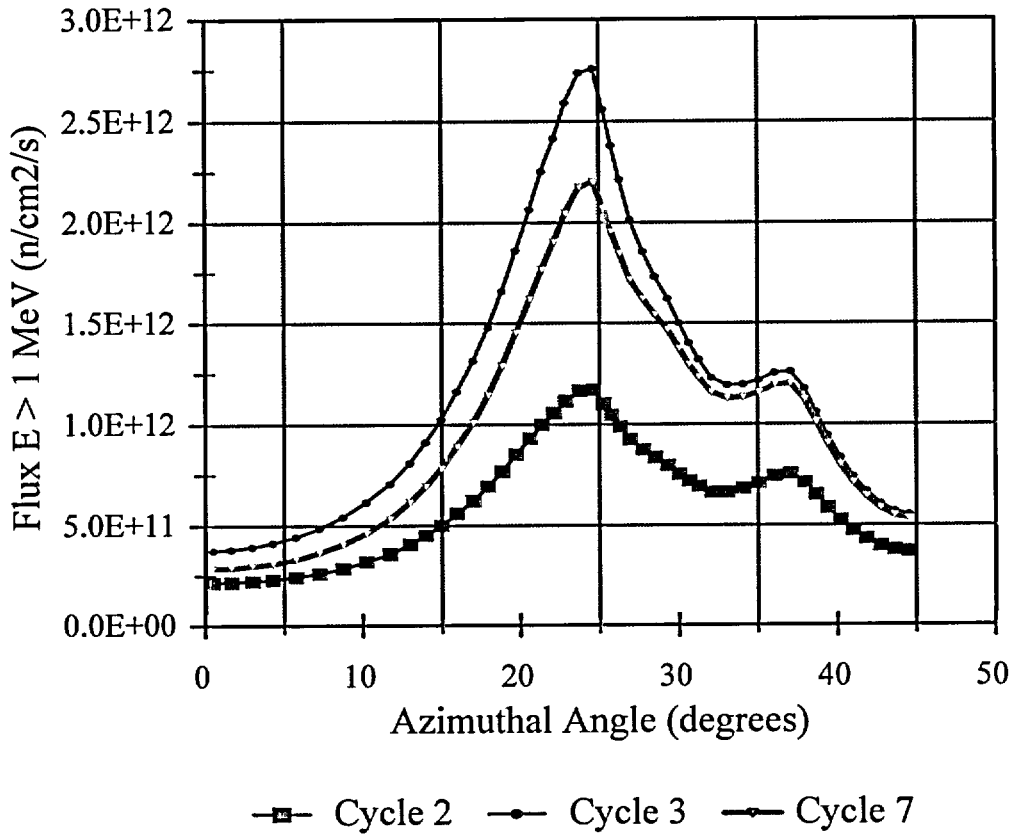

Figure 2-3 Calculated Flux (E > 1 MeV) at the Inner Radius of the Shroud for Weld H4 for Cycles 2, 3, and 7.

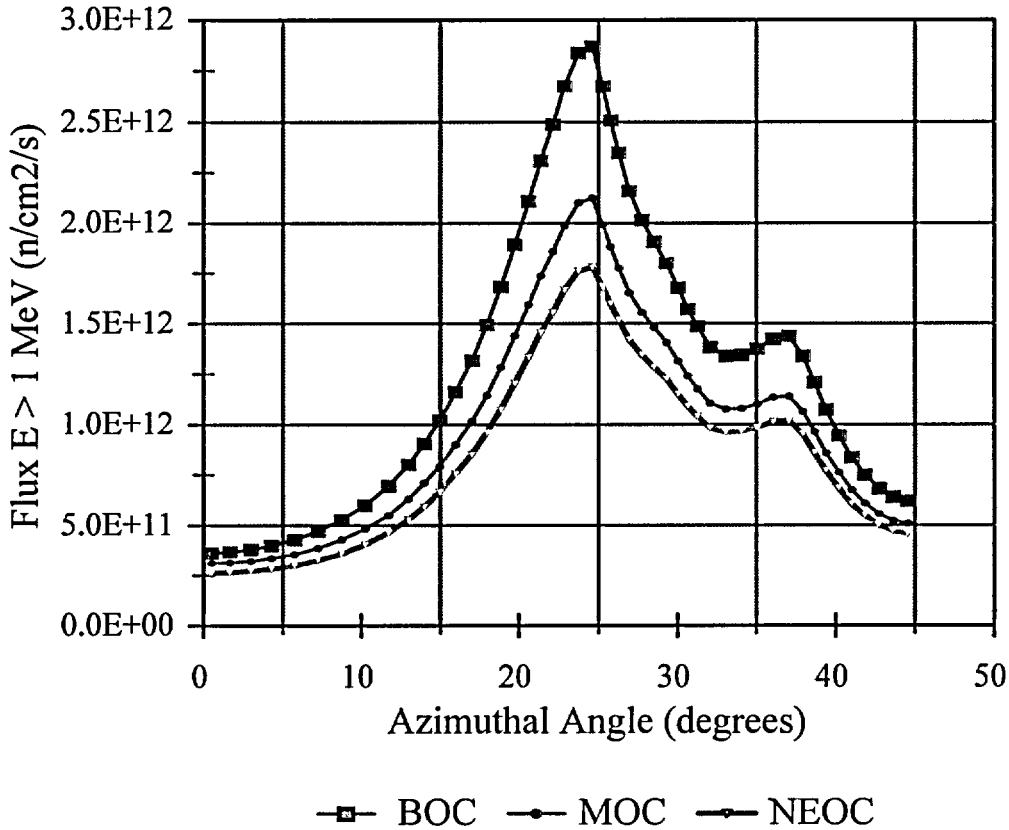

Figure 2-4 Calculated Flux (E > 1 MeV) at the Inner Radius of the Shroud for Weld H4 for Cycle7 BOC, MOC, and NEOC.

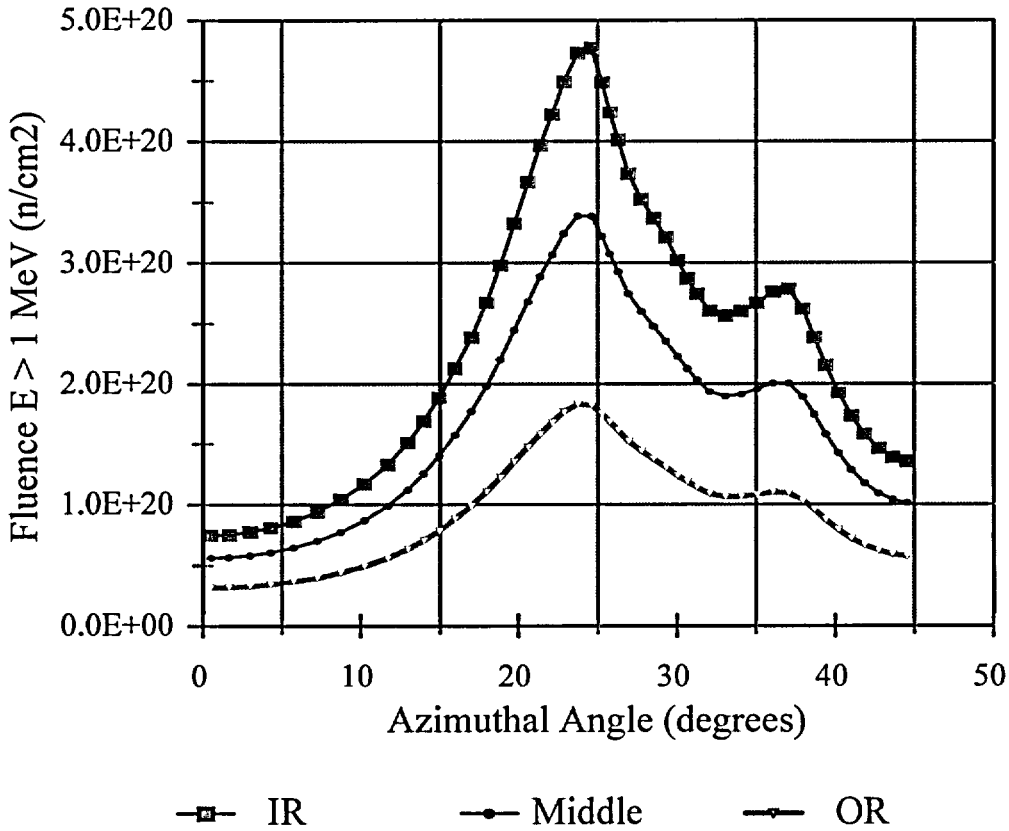

Figure 2-5 Calculated Fluence (E > 1 MeV) to Shroud Weld H4 at End of Cycle 7.

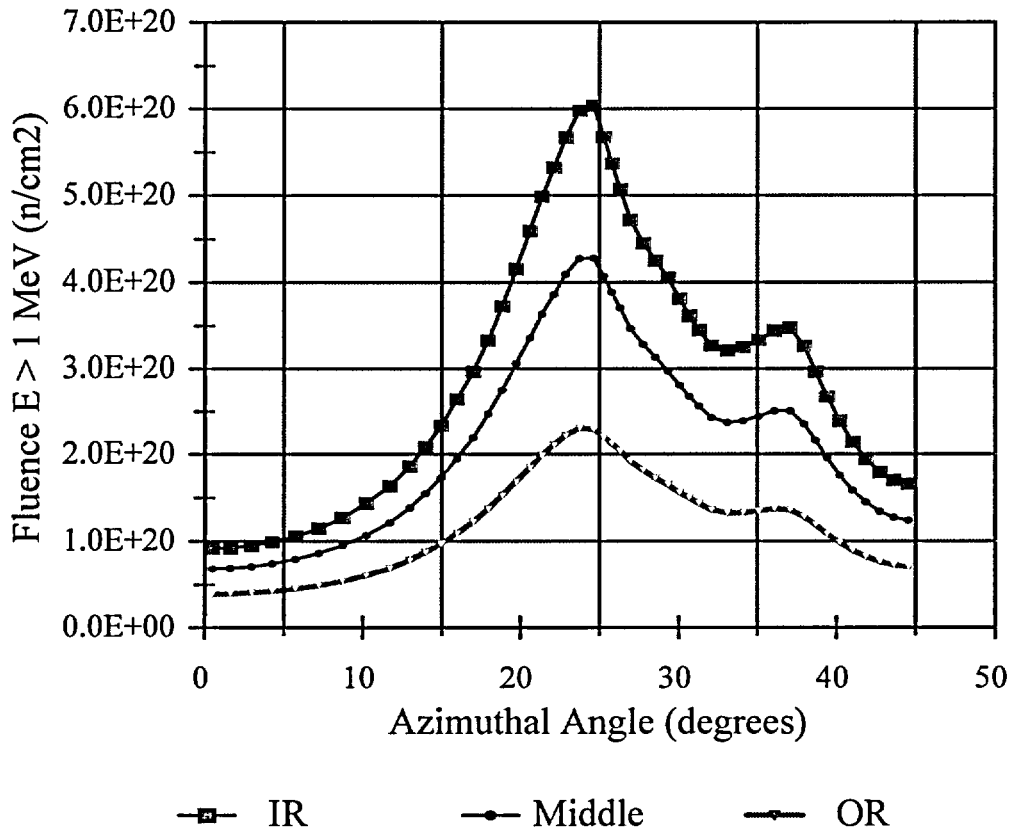

Figure 2-6 **Calculated Fluence (E > 1 MeV) to Shroud Weld H4 Projected to End of Cycle 8.**

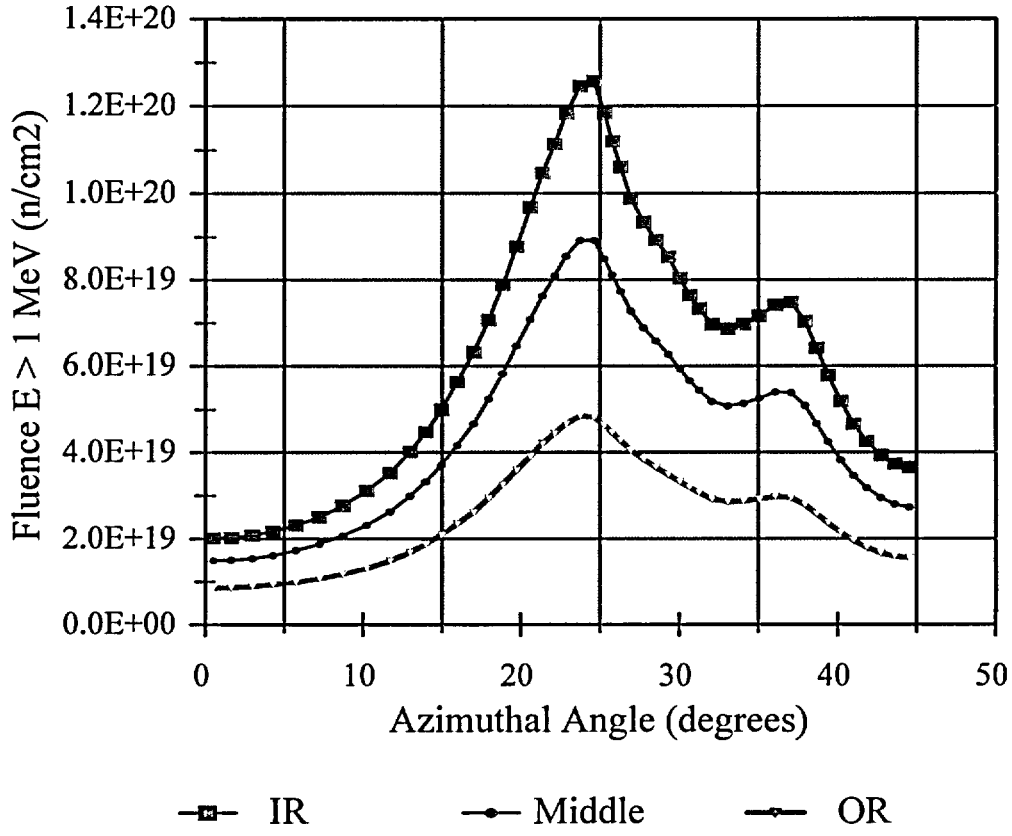

Figure 2-7 Calculated Fluence (E > 1 MeV) to Shroud Weld H5 at End of Cycle 7.

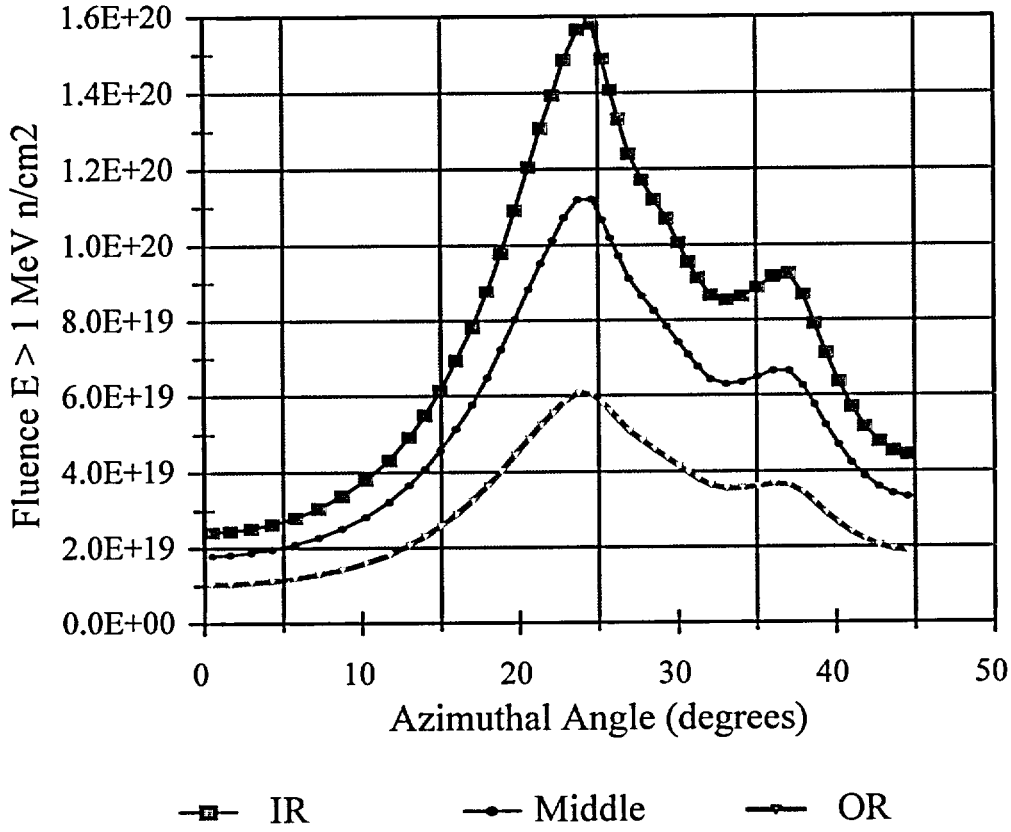

Figure 2-8 **Calculated Fluence (E > 1 MeV) to Shroud Weld H5 Projected to End of Cycle 8.**

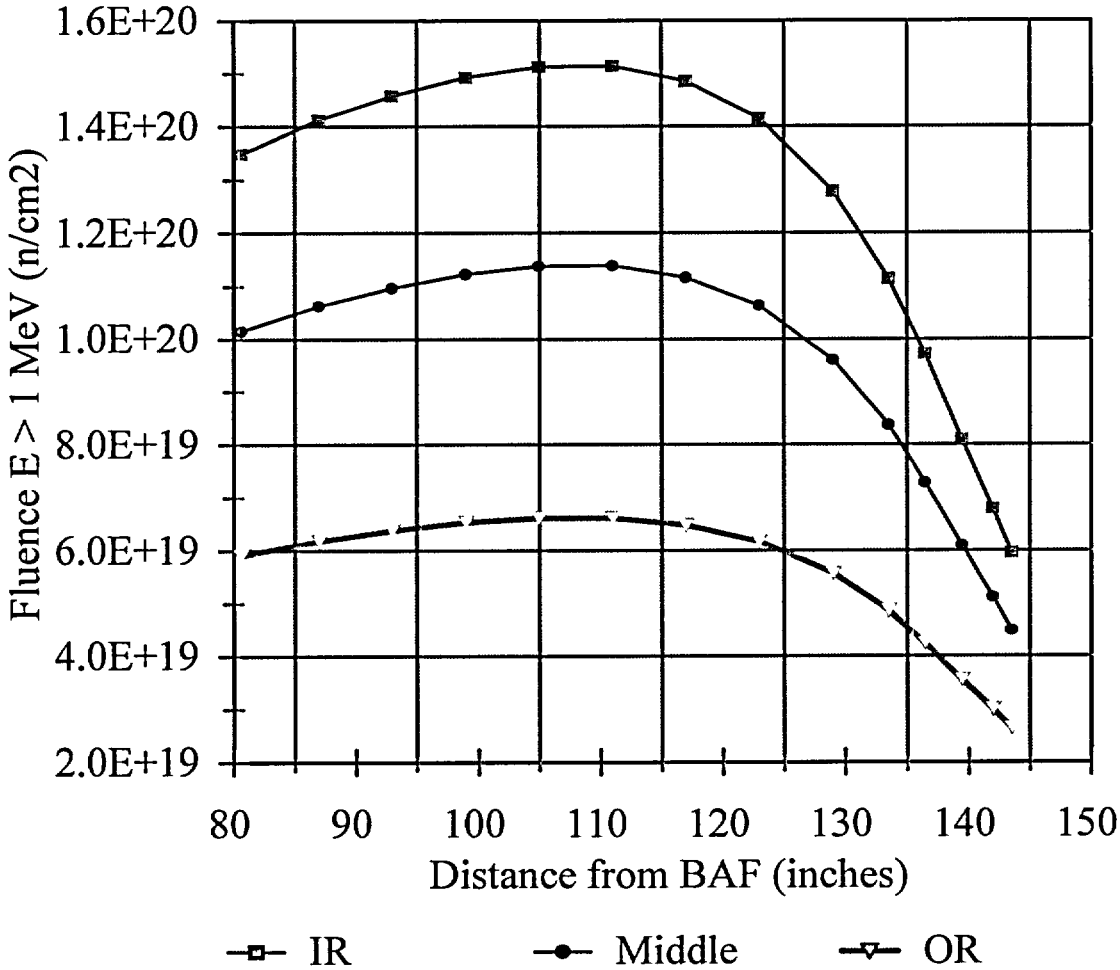

Figure 2-9 Calculated Fluence (E > 1 MeV) to Shroud Welds V12 and V13 at End of Cycle 7.

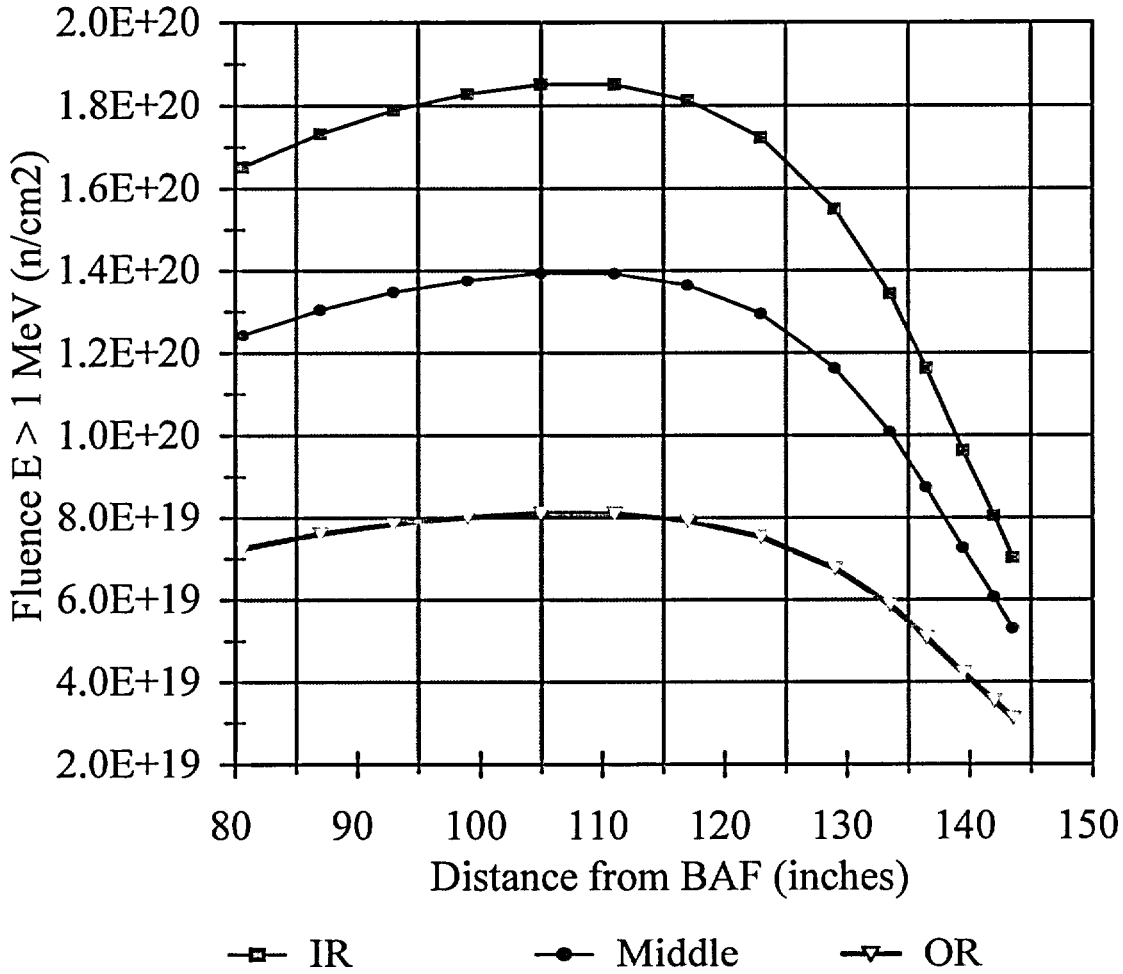

Figure 2-10 Calculated Fluence (E > 1 MeV) to Shroud Welds V12 and V13 Projected to End of Cycle 8.

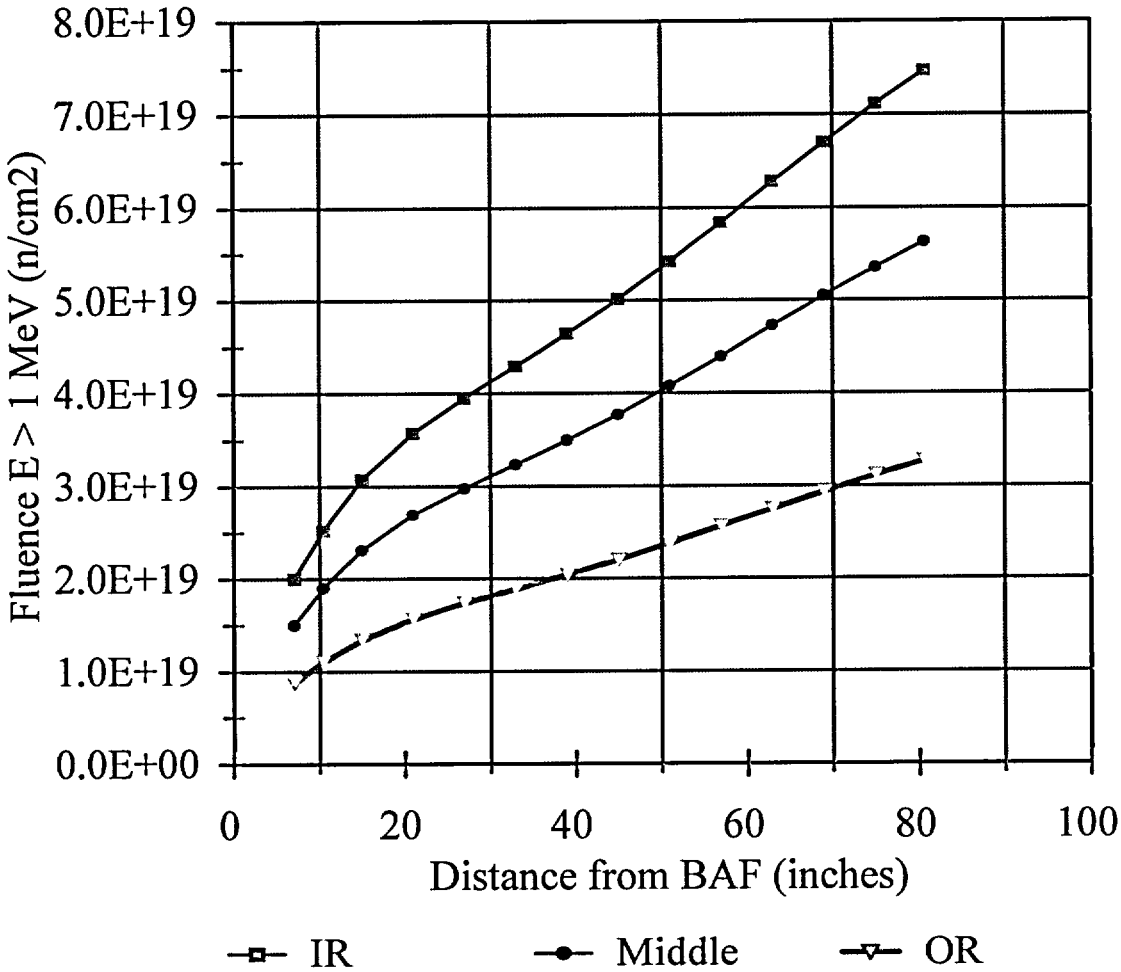

Figure 2-11 Calculated Fluence (E > 1 MeV) to Shroud Welds V14 and V15 at End of Cycle 7.

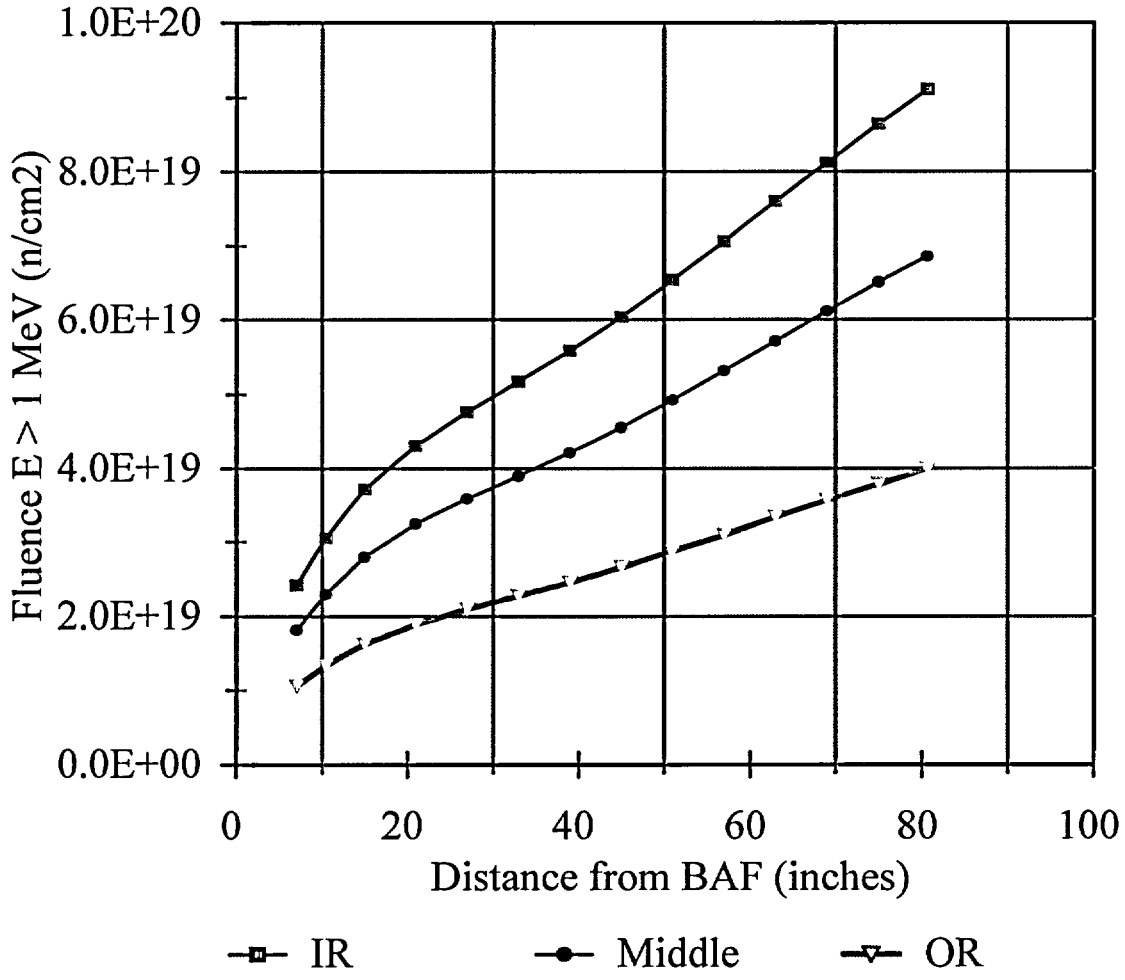

Figure 2-12 Calculated Fluence (E > 1 MeV) to Shroud Welds V14 and V15 Projected to End of Cycle 8.

3.0 Fluence to Capsule and Vessel

3.1 Surveillance Capsule Results

The calculated fluxes for each case for the 3° surveillance capsule are given in Table 3-1. These values are for the midpoint of the capsule at the axial midplane. As shown in Table 3-1, the five cases for cycle 7 are averaged, the average of the flux values for the seven cycles is also calculated (this is a straight average, not a weighted average), and the fractional standard deviation is determined. It is seen that variation between the cycles gives a standard deviation of 19%. For the five cycle 7 cases, the standard deviation is about 16%.

Table 3-2 gives fluence values for the capsule for each of the 7 cycles and the total fluence at the end of cycle 7. The fluence (E > 1 MeV) at the center of the capsule is slightly higher than that previously calculated [3-1]. The difference (about 6%) is due to a combination of small changes in model assumptions, the more detailed evaluation of the cycle 7 flux variation, and the inclusion of the calculations of cycles 1,2, 5, and 6.

Values for the flux may be compared to previous calculations. In reference [3-2], several results of other calculations are given, and the calculation by GE [3-3] was recommended. This calculation obtained a value for the capsule of 2.70 E8 for the flux E>1 MeV at the uprated power for cycle 5. The comparable value in the present calculation is 2.53 E8, which is a difference of 7%. This is considered very good agreement considering all the differences between the calculations, including differences in the fuel power distribution used, different models, and different cross section data (including the changes in the iron cross section that occurred with the change to the BUGLE-96 library). In reference [3-3], a lead factor for the vessel ID (ratio of capsule flux to maximum flux at the vessel surface) was calculated to be 0.30. The value in the present calculation for cycle 5 is 0.41. This difference can be partly explained by the omission of the jet pumps from the model used in the reference [3-3] calculation. A calculation with the jet pumps omitted indicated a flux increase at the maximum vessel point of about 10% [3-1]. The jet pump modeling does not affect the capsule flux because the capsule is located at a significantly different azimuthal position.

Uncertainty in the evaluation of the capsule fluence is evaluated in Section 4.

3.2 Reactor Vessel Results

The fluence to the reactor vessel was also determined from the calculations for each cycle using the flux synthesis. The flux shape was found to vary somewhat from cycle to cycle due to the differences in fuel loading pattern and due to differences in axial power shape and void fraction. Inspection of the azimuthal variation of the fast flux indicated that the maximum value in the vessel occurs at approximately 26°. This is shown in Figure 3-1 which is a plot of the fluence (E > 1 MeV) at the end of cycle 7 at core midplane. The fluence is shown for the vessel IR which is the clad-base metal interface, at 1/4 of the distance into the vessel (1/4 T), and at 3/4

of the distance through the vessel (3/4 T).

The peak fluence point varies axially, both during cycles and between cycles. Therefore, the maximum fluence point must be determined by integrating the flux at several axial heights to find the peak value. The maximum fluence point at the end of cycle 7 is at about 30 inches above midplane. This is shown in Figure 3-2 which plots the fluence (E > 1 MeV) at the end of cycle 7 versus axial distance from core midplane for the IR, 1/4 T, and 3/4 T positions. The fluence in this figure is at the maximum azimuth.

Values for the calculated maximum vessel fluence E > 1 Mev, fluence E > 0.1 MeV, and dpa are given in Table 3-3 for the inner radius of the vessel clad, the vessel base metal IR, the 1/4 T position and the 3/4 T position calculated at the end of cycle 7 (8.72 EFPY). Exposure values extrapolated to 22 EFPY are also given in Table 3-3. These have been extrapolated using cycle 7 average flux and dpa/s values since future cycles are projected to be similar to cycle 7. Since the maximum flux point for cycle 7 is slightly closer to axial midplane, the maximum vessel fluence at 22 EFPY was determined by integrating the flux at various axial points and taking the maximum value which was found to occur at 24 inches above midplane. The difference between the maximum value at 24 inches above midplane and 30 inches above midplane at 22 EFPY is only a small fraction of a percent (about 0.3% for fluence (E > 1 MeV) and this difference is not deemed to be significant. The values in Table 3-3 are the calculated maxima and thus the axial position of the fluence values in this table for 8.72 and 22 EFPY are not the same.

The dpa values in this report are calculated from the ASTM E693-94 Standard dpa cross-sections [3-4]. This evaluation of the dpa cross section is based on the ENDF-IV cross-section file. A new dpa cross-section evaluation based on ENDF-VI (consistent with the cross-sections in BUGLE-96) is expected to be used as the standard in the future. This change is not expected to have any significant impact on the results.

3.3 Capsule Measurement Results

Dosimetry from the capsule removed at the end of cycle 7 was measured and the results are documented in [3-5]. The capsule was irradiated from reactor start-up to March 3, 2000 for a total of 8.72 effective full power years. The dosimetry consisted of two sets of Cu and Fe wires. An additional measurement was made on a steel sample taken from a broken Charpy bar. The latter measurement was used to provide the data needed to calculate accurate calculated-to-measured (C/M) ratios.

The C/M ratios for each dosimeter measurement and the average are given in Table 3-4 (taken from [3-5]) . Assuming the dosimeter is located at the center of the capsule, the average C/M ratio (1.07) indicates good agreement between the calculation and the measurement. The Fe and Cu dosimetry results do show a difference, however, with the Fe showing a C/M over 20%. It should be noted that 95% of the iron response is from the last two irradiation cycles, while 48% of the copper response is from earlier cycles. In addition, copper has a much higher reaction threshold and so only responds to a small fraction of the fast neutrons, while the iron

responds to a larger fraction. In addition, the copper cross section is not as well known as the iron cross section. Since these observations are not expected to explain all of the discrepancy, additional measurements and analyses were made to better quantify the C/M ratio.

The location of the dosimeters in BWR capsules is uncertain. Unlike most PWR capsule designs, the BWR dosimeters are not placed in sealed containers inside the capsule. Instead, the bare wires are held by spring load near the top or bottom of the capsule for most BWR capsules. For NMP-2, the intended location is near the front top of the capsule at the right side as viewed from the core. This would place the dosimeters at about 0.48 cm towards the core from the capsule radial center and about 6 inches above core midplane. The radial correction would increase the calculated activity by 4.6% for copper and 7.4% for iron. The axial correction varies during the fuel cycle and between cycles, but the activities 6 inches above midplane average about 4% higher. The azimuthal difference is small, but the activity to the right (higher angles in the first octant) increases by about 1% from that at the center of the capsule. If all these factors are included, the calculated copper activity at the indicated dosimeter position is higher by about 10% compared to the capsule center and the iron by 13%. This results in average C/M ratios of 1.02 for copper and 1.37 for iron, and an average C/M of 1.19.

However, it may also be postulated that the copper dosimeter is positioned towards the core side of the capsule, while the iron is positioned towards the vessel side. This assumption is plausible since the capsule contained a cylindrical spacer which fits tightly inside the rectangular outer wrapper. If this assumption is made, then the iron average C/M ratio is 1.19 and the average of the two dosimeter types is 1.11. It is also possible to assume that the dosimeter wires dropped to the bottom of the capsule. This would lower the calculated activity by 4% compared to the capsule axial midplane (instead of increasing it as noted above for the correction to the top of the capsule). The average C/M ratio would then be about 1.02.

Since the bottom of the NMP-2 capsule was cut during capsule disassembly and the wires were located somewhere in the capsule above the cut location, it is not possible to determine the dosimeter wire locations during irradiation. Therefore, to reduce the dosimeter location uncertainty and to obtain a meaningful C/M ratio, an additional measurement was made using a sample cut from a Charpy bar. The sample was a complete slice across the specimen taken near the fracture surface and thus is radially centered and located very near the azimuthal center of the capsule. The sample was modeled at the radial center of the capsule because the counting geometry for the slice approximates a point source at the radial center. Unfortunately, the axial location within the capsule could not be determined because the specimens were not recorded for axial position during disassembly. This is not a serious problem because the axial uncertainty is only a few percent. The measurement result, adjusted to the reference time, is 30.62 dps/mg. The Charpy is not pure iron, but has been determined to have an iron fraction of 0.9694. Using this value, the dps/mg of iron is then 31.59. This result is 12% higher than the result from the iron dosimeters and gives a C/M ratio of 1.08. This indicates that the iron dosimeters are located towards the rear of the capsule, and most likely at the bottom. The results using this location for the iron dosimeter, and assuming the copper location towards the core, are shown in the last column of Table 3-4. The average C/M for copper is 0.95 and for iron is 1.09, for an overall

average of 1.02, indicating excellent agreement of the calculation with measurement.

Uncertainty in the activity measurements are given in Table 2-7 of Reference [3-5]. These values are regarded as precision estimates. The measurements also contain a bias (due primarily to calibration uncertainty) that is typically about 3% [3-6,3-7]. The uncertainty in the C/M ratio also contains the contribution from the dosimeter position uncertainty, dosimeter cross section uncertainty, and the flux history uncertainty. As discussed above, the dosimeter position uncertainty can be as large as 10-13%. However, using the Charpy measurement which has a better known position, reduces this uncertainty to about 5%. The dosimeter cross section uncertainty is limited by correlation with benchmark measurements. It can be assumed that typical iron and copper reaction integral cross sections are known to within 3% [3-8]. The flux history uncertainty will vary with the half-life, but can be conservatively assumed to be less than 8% (see discussion in Section 4). The total uncertainty in the measurement is then about 10%. The uncertainty in the calculated values may be taken from the calculated fluence uncertainty evaluated in Section 4 to be 15.3%.

It is seen that the Charpy bar C/M value of 1.08 is well within both the measurement uncertainty and the calculation uncertainty. It is concluded that the measurement provides an excellent validation of the adequacy of the calculation. Additional verification is provided by comparisons to dosimetry measurements from the NMP-1 reactor as described in Reference [3-9] which was calculated using identical methodology. These measurements are discussed further in Section 5. In accordance with RG 1.190 [3-10], the calculated fluence values are recommended for use in estimating vessel embrittlement and in heatup and cooldown curves.

3.4 Chapter 3 References

[3-1] "Nine Mile Point Unit 2 Shroud Neutron Transport and Uncertainty Analysis," Report MPM-200623, MPM Technologies, Inc., 2161 Sandy Drive, State College, PA 16803-2283, February 2000.

[3-2] "Nine Mile Point Unit 2 Reactor Pressure Vessel Surveillance Capsule Withdrawal Schedule Analysis", MPM-1197409, November, 1997.

[3-3] GE letter NMP2-95-21, D. R. Pankratz to A. D. Sassini, "RPV Fluence Lead Factor Analysis for NMP-2 Power Uprate (Cycle 5), May 8, 1995.

[3-4] ASTM Designation E693-94, *Standard Practice for Characterizing Neutron Exposures in Iron and Low Alloy Steels in Terms of Displacements Per Atom (DPA), E706(ID)*, in ASTM Standards, Section 12, American Society for Testing and Materials, Philadelphia, PA, 2000.

[3-5] "Nine Mile Point Unit 2 3-Degree Pressure Vessel Surveillance Capsule Report," Report MPM-1200676, MPM Technologies, Inc., 2161 Sandy Drive, State College, PA 16803-2283, December 2000.

[3-6] ASTM Designation E263-00, Standard Test Method for Measuring Fast-Neutron Reaction Rates by Radioactivation of Iron, in ASTM Standards, Section 12, American Society for Testing and Materials, Philadelphia, PA, 2000.

[3-7] ASTM Designation E523-92, *Standard Test Method for Measuring Fast-Neutron Reaction Rates by Radioactivation of Copper*, in ASTM Standards, Section 12, American Society for Testing and Materials, Philadelphia, PA, 2000.

[3-8] ASTM Designation E261-94, *Standard Practice for Determining Neutron Fluence, Fluence Rate, and Spectra by Radioactivation Techniques*, in ASTM Standards, Section 12, American Society for Testing and Materials, Philadelphia, PA, 2000.

[3-9] "Nine Mile Point Unit 1 Shroud Neutron Transport and Uncertainty Analysis," Report Number MPM-108679, MPM Technologies, Inc, 2161 Sandy Drive, State College, PA 16803-2283, October, 1998.

[3-10] Regulatory Guide 1.190, *Calculational and Dosimetry Methods for Determining Pressure Vessel Neutron Fluence*, U. S. Nuclear Regulatory Commission, March 2001.

Table 3-1 NMP-2 Surveillance Capsule Flux and dpa/s Results at the Capsule Center.

Case	Flux (E > 1 MeV) n/cm^2 /s	Flux (E > 0.1 MeV) n/cm^2 /s	dpa/s
Cycle 1	3.45E+08	5.90E+08	5.43E-13
Cycle 2	2.41E+08	4.12E+08	3.80E-13
Cycle 3	4.23E+08	7.28E+08	6.67E-13
Cycle 4	2.62E+08	4.52E+08	4.15E-13
Cycle 5	2.53E+08	4.34E+08	4.00E-13
Cycle 6	3.36E+08	5.73E+08	5.29E-13
Cycle 7 BOC	4.20E+08	7.22E+08	6.62E-13
Cycle 7 BMOC	3.19E+08	5.49E+08	5.04E-13
Cycle 7 MOC	3.48E+08	5.96E+08	5.49E-13
Cycle 7 AMOC	2.78E+08	4.77E+08	4.39E-13
Cycle 7 NEOC	3.10E+08	5.32E+08	4.89E-13
Cycle 7 average	3.28E+08	5.63E+08	5.18E-13
Average (all cycles)	3.13E+08	5.36E+08	4.93E-13
Fractional std. dev. (all cycles)	0.19192787368	0.19274680344	0.19120324701

Note: For comparison purposes, all the values in the above table are normalized to a full power of 3467 MWth. Cycles 1 through 4 actually operated at 3323 MWth.

Table 3-2 Surveillance Capsule Fluence and dpa Results for NMP-2 Capsule Center.

Cycle	Effective Full-Power Seconds	Fluence (E>1 MeV) n/cm^2	Fluence (E > 0.1 MeV) n/cm^2	dpa
1	4.41E+07	1.46E+16	2.49E+16	2.29E-05
2	2.69E+07	6.20E+15	1.06E+16	9.78E-06
3	3.64E+07	1.48E+16	2.54E+16	2.33E-05
4	3.87E+07	9.73E+15	1.68E+16	1.54E-05
5	3.95E+07	1.00E+16	1.72E+16	1.58E-05
6	4.24E+07	1.42E+16	2.43E+16	2.24E-05
7	4.69E+07	1.54E+16	2.64E+16	2.43E-05
Total (end of cycle 7)	5.86E+08	8.49E+16	1.46E+17	1.34E-04

Note: The effective full-power seconds are calculated using a full power of 3323 MWth for cycles 1 to 4 and 3467 MWth for cycles 5 to 7. The flux values in Table 3-1 were adjusted down by 3323/3467 before multiplying by the efps in this table to get the correct fluence.

Table 3-3 NMP-2 Calculated Maximum Vessel Fluence and dpa at End of Cycle 7 (8.72 EFPY) and at 22 EFPY.

Position	Fluence (E > 1 MeV) n/cm^2	Fluence (E > 0.1 MeV) n/cm^2	dpa
End of Cycle 7 (8.72 EFPY)			
Clad IR	1.98E+17	3.60E+17	3.09E-04
Vessel IR	1.95E+17	3.67E+17	3.04E-04
Vessel 1/4 T	1.31E+17	3.24E+17	2.12E-04
Vessel 3/4 T	4.34E+16	1.72E+17	8.34E-05
After 22 EFPY[a]			
Clad IR	5.71E+17	1.03E+18	8.90E-04
Vessel IR	5.62E+17	1.06E+18	8.74E-04
Vessel 1/4 T	3.76E+17	9.29E+17	6.08E-04
Vessel 3/4 T	1.25E+17	4.86E+17	2.37E-04

a. Extrapolated using maximum values of flux (E > 1 MeV), flux (E > 0.1 MeV), and dpa/s averaged over cycle 7. At the vessel IR these values are 8.78E8 n/cm^2/s, 1.64E9 n/cm^2/s, and 1.36E-12 s^{-1}, respectively. Note that due to a slight shift in the axial position of the maximum flux point, the difference in maximum fluence values between 8.72 and 22 EFPY is not directly proportional to these maximum values but the differences are a small fraction of a percent.

Table 3-4 Tabulation of NMP-2 Dosimetry Results [3-5].

Dosimeter	Measured Activity (dps/mg)	Calculated Activity (dps/mg) [a]	Ratio (C/M) [a]	Ratio (C/M) [b]
Cu-1	4.97	4.50	0.91	0.92
Cu-2	4.62	4.50	0.97	0.99
Avg Cu	4.80	4.50	0.94	0.95
Fe-1	27.84	34.10	1.22	1.10
Fe-2	28.49	34.10	1.20	1.08
Avg Fe	28.16	34.10	1.21	1.09
Capsule Average			1.07	1.02
Charpy Bar	31.59[c]	34.10	1.08[c]	N/A

Notes: a. There is uncertainty in the NMP-2 capsule dosimetry location. The results in this column are based on the assumption that the dosimetry is at the capsule center.

b. The results in this column are based on the assumption that the dosimetry is at the best estimate positions. Dosimetry results from the Charpy bar indicate that the dosimetry wires may have moved from their intended locations within the capsule.

c. The Charpy bar dosimetry results have been corrected for iron composition. A slice was taken from the Charpy bar parallel to and near fracture surface. This approach resulted in an approximate point source near the radial and azimuthal center of the capsule.

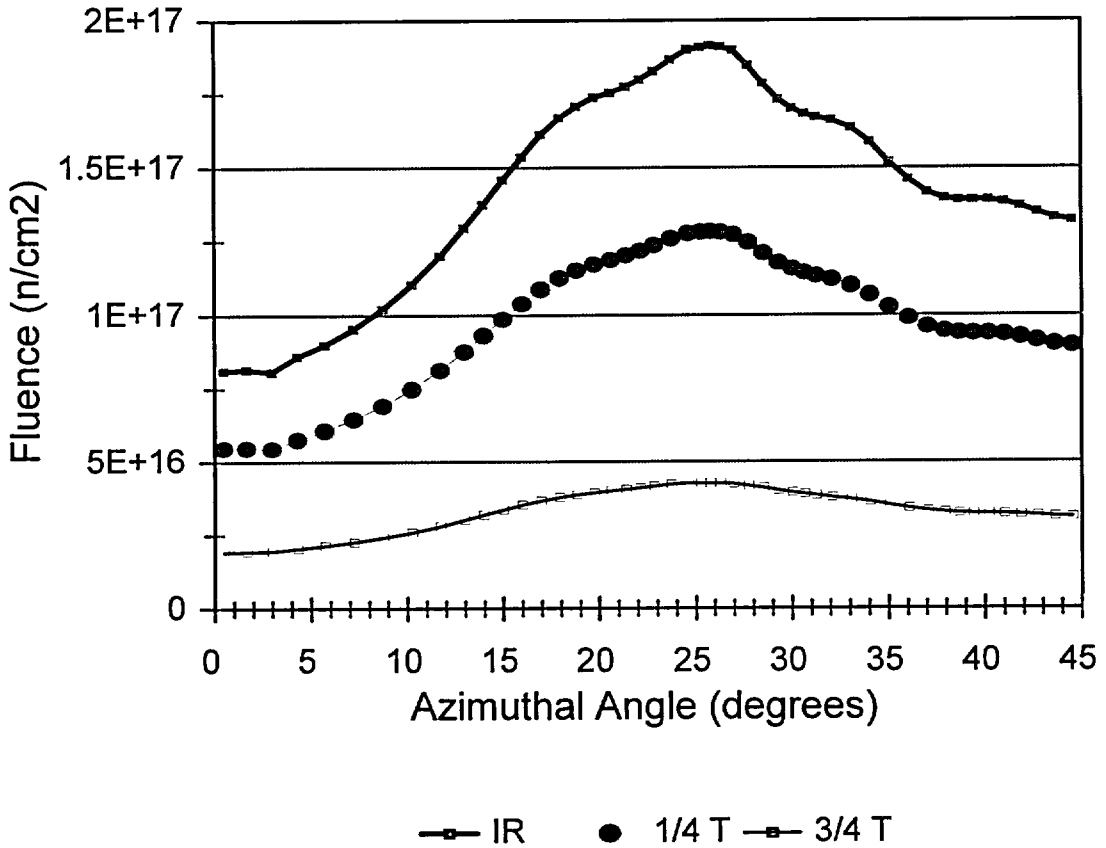

Figure 3-1 Reactor Vessel Fluence at the End of Cycle 7 at Core Midplane.

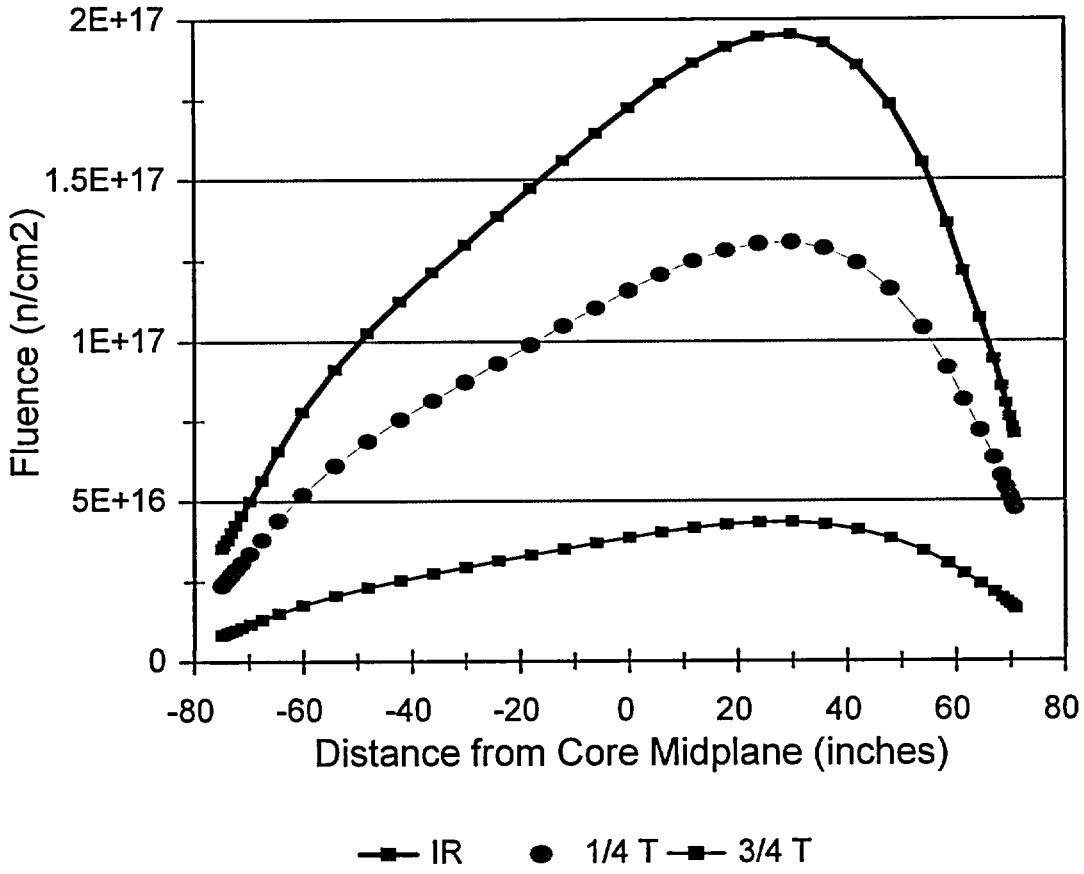

Figure 3-2 Reactor Vessel Fluence at the End of Cycle 7 at Azimuthal Maximum .

4.0 Uncertainty Analysis

A detailed uncertainty analysis was performed to estimate each source of uncertainty in the calculated fluence values. This analysis made use of defined uncertainties and tolerances where possible, but some of the uncertainty estimates had to be based on data variation. The latter uncertainty estimates include such contributors as the detailed power distribution and void fraction variations within a single cycle. These are based in part on estimates derived for the uncertainty analysis previously performed for the NMP-1 shroud [4-1]. The geometry uncertainty assignments are from Reference [4-2] and are the same as those used for the previous shroud calculation [4-3]. The uncertainty estimates for parameters based on data variation are similar to those in Reference [4-3] except for increasing the power history uncertainty based on the new analysis of the variations in capsule flux level by cycle for NMP-2. Discussion of each uncertainty assumption is given below. The final uncertainty values for each parameter are given in Table 4-1. Based on these uncertainty values, detailed uncertainty evaluations were performed for the shroud and critical shroud welds, surveillance capsule, and reactor vessel. The uncertainty evaluations for reactor beltline locations are summarized in Table 4-2 and the uncertainty evaluations for welds H4 and H5 are given in Table 4-3.

In the uncertainty evaluations, uncertainties were treated as normally distributed and all uncertainties were valued in terms of 1 standard deviation (1σ). The individual uncertainties were assumed to be randomly distributed and independent except where correlations occur (for example, an increase in steel thickness will result in a decreased water thickness). The total uncertainty is then determined by quadrature (square root of the sum of the squares of the contributing uncertainty components given as 1σ values).

4.1 Uncertainty Assumptions

Nuclear Data

Nuclear data input to the transport calculations includes the multigroup cross sections and neutron spectrum. Uncertainties in the cross sections are complicated because of the large number of cross section values and the correlations between these values. Although the uncertainties in individual cross section values may be relatively large, the total effect of cross section uncertainties is limited by adjustments made by cross section evaluators to agree with benchmark data. The approach taken here is to limit the cross section uncertainty effects to just the total cross section and to evaluate this by varying the material densities (see below).

Uncertainty in the multigroup fission source arises from uncertainty in the fission spectra for each fissioning isotope, the distribution of fission among the fissioning isotopes, the energy release per fission (κ), and the number of neutrons produced per fission (υ). Uncertainty in the fission spectrum is mainly at the higher energies, which has little effect on the fluence above 1 MeV except for very deep penetrations. The uncertainty was represented as an uncertainty in burnup, which was taken as 10,000 MWd/MTU (megawatt days per metric ton of uranium). The

uncertainty is assumed to be fairly large to encompass the use of average burnup of the outer fuel bundles rather than attempting to include explicitly the detailed radial and axial burnup variation in the models. The uncertainty is assumed to be fairly large to encompass the use of average burnup of the outer fuel bundles rather than including explicitly the detailed radial and axial burnup variation. Thus the uncertainty of 10,000 MWd/MTU is a conservative estimate of the burnup variation that affects the fuel bundles important for fluence to the shroud and vessel. A 1-D calculation was performed [4-1] to determine the spectral effect and it was found to vary between 0.2% in the core to 1.8% at the outside of the vessel.

The parameters υ and κ both increase with burnup, but the source normalization is proportional to the ratio υ / κ. Thus, the variation with burnup is small. For an uncertainty of 10,000 MWd/MTU, the normalization uncertainty is 1.1%. Since this is in the same direction as the spectrum uncertainty, it is added to the spectrum contribution to give the values in Tables 4-2 and 4-3.

Normalization

In addition to the normalization uncertainty due to υ / κ, there is an overall normalization uncertainty in reactor power as measured by the heat balance. This uncertainty is estimated by the plant to be 2%.

Geometry

Geometry uncertainties are taken from Reference [4-2]. The vessel inner radius uncertainty was taken to be a typical value [4-1]. The uncertainty in the shroud inner radius was based on as-built measurements of the inner diameter. These measurements indicate a range of 203.062 to 203.250 inches. The radius will then have a maximum to minimum range of 101.531 to 101.625 inches (a range of 0.094 inches). The important distance is, however, the distance from the core edge to the shroud and if the shroud is slightly off-center, then this uncertainty could be larger. To be conservative, an uncertainty of 0.188 inches was used and assumed to be 1 standard deviation. The shroud radius used in the calculation was actually not the center of the range, but was the design radius of 101.56 inches which is only 0.029 inches from the minimum as-built value. Thus, the true uncertainty is more in the direction of lower fluence than higher fluence, an additional conservatism. The tolerance on the shroud thickness of 0.042 is a conservative value taken from [4-1]. The shroud thickness uncertainty has no impact on the inside of the shroud, but has a 0.5% effect on the outside.

Jet Pumps

The jet pumps could not be exactly modeled in the calculations. The steel from the jet pumps was approximately included as slabs of steel placed appropriately in the downcomer region in the R,θ calculation. The jet pumps were not included in the R,Z calculation. To estimate the uncertainty introduced by the crude jet pump model, a separate R,θ calculation was made with the jet pumps omitted. This had no effect on the shroud or surveillance capsule

fluence, but the maximum fluence at the vessel inner radius increased up to 16.4%. For fluence at the maximum fluence points, a reasonable estimate of the 1-σ uncertainty from the imperfect modeling of the jet pumps is 25% of this value, or 4.1%.

Material Densities

The material density uncertainty was treated differently for the water density and the steel density. The water density in the core decreases with height as the void fraction increases. Based on the variation in the void fraction at NMP-1 [4-1], on a comparison of the Unit 2 data for the various cycles, and on the necessity for the heat generation in the core to produce a certain rate of steam, the void fraction uncertainty was estimated to be 5%. The bypass water is not thought to have any void volume, but the temperature may vary from the value that was assumed. The uncertainty was estimated by taking one half of the difference between the estimated bypass water density at the bottom and top. This indicates an uncertainty of 1.3%. This is consistent with the value of 1.4% in Reference [4-1] which was estimated using a slightly different method. The slightly higher value of 1.4% was adopted. The uncertainty in the downcomer water density was calculated from a temperature uncertainty of 5 °F [4-1].

The effect of each of the water density uncertainties on the fluence was calculated separately. Because of the relatively large azimuthal variation in shroud and vessel fluence, the effect of the core water density uncertainty and the bypass water density uncertainty were calculated using 2-dimensional R,θ calculations. The azimuthal variation of the bypass water is particularly pronounced and is lowest at the highest flux point where the distance from the core to the shroud is the smallest. The uncertainty due to the downcomer water density does not affect the shroud fluence and was determined by a 1-dimensional calculation.

The uncertainty in steel density is less than about 1%. However, as noted above, the cross section uncertainty was included as an addition to the steel density uncertainty. An estimate for this uncertainty was derived by considering vessel mockup benchmark results [4-4], comparisons of reactor cavity and surveillance capsule measurements [4-5, 4-6, 4-7, 4-8], and comparisons of cross section evaluations [4-9]. It was concluded that uncertainties due to the iron cross section contributes a 10% effect on fluence through a reactor vessel. This translates into a cross section uncertainty of 3.5%. This value was adopted as the density variation and uncertainties were calculated based on this uncertainty estimate. In addition, the core cross sections for the fuel and cladding were also assumed to have this uncertainty. This estimate includes effects due to the core homogenization.

Source Uncertainty

Source uncertainties were estimated in [4-1] based on the variation of the calculated power distributions at points within a single cycle. This produced estimated uncertainties of 6% radially and 3.7% axially. Larger differences were observed between cycles and these uncertainties were included in the flux history uncertainty (see below). These estimates were compared with differences between the Unit 2 cycle 4 and cycle 7 power distributions and it was

felt that the cycle differences were bounded by these uncertainty estimates.

Methods Uncertainty

The neutron transport was calculated using a model of the reactor and S_N code. This is only an approximation to the solution of the Boltzmann transport equation and thus also contributes uncertainty. Two components of this uncertainty were considered. First, the uncertainty of the fuel model was considered. From the VENUS benchmark measurements, it was found that a typical range of C/M results was about 10% [4-10]. Thus the standard deviation was about 5% and this value was used here. The second component was the adequacy of the S_8 calculation. To test this, S_{16} calculations were performed to indicate the accuracy [4-1]. Differences of 1.4% were observed in the shroud and as high as 3% at the outside of the vessel. The differences were added in quadrature to the 5% from the fuel model effect.

Additional uncertainty is introduced by the 3-D synthesis procedure in regions near the edge of the core where the modeling is less precise. Uncertainty contributions due to these effects only are significant for fluences well below the maxima. In particular, the welds at the very top of the core will have increased uncertainty due to the synthesis and also due to the changes in fuel height from 150 inches to 146 inches that have occurred during the transition of fuel designs. the synthesis uncertainty in the capsule and vessel is considered to already be included in the 5% modeling uncertainty except for points more than 60 inches from axial midplane. Thus no additional fluence uncertainty is added to either the dosimetry position in the capsule or the vessel maximum fluence position.

Flux History

In Reference [4-1], an estimate of the impact of flux history uncertainty on the fluence was made. It was estimated that a conservative value for this uncertainty contributor was 7% based on cycle-to-cycle variation. This value was adopted for the previous NMP-2 shroud fluence uncertainty evaluation [4-3]. For the present series of calculations, it was found that the flux at the surveillance capsule had a standard deviation of about 19% over the seven cycles and about 16% within cycle 7. Moreover, while the cycle 7 MOC calculation fell near the middle, it was about 6% different at the capsule compared to a cycle average over the 5 calculated points in time. Most of the effects of the cycle variation are included in the MOC representations, but this variation within the cycle remains as an uncertainty. This uncertainty was estimated by taking one-half of the 16% cycle standard deviation to provide a reasonable estimate of the MOC variation from the cycle average. Thus this uncertainty contribution was increased from 7% used in previous calculations [4-3]to 8%.

4.2 Uncertainty Evaluation

4.2.1 Shroud and Vessel Fluence Uncertainty

The results for the uncertainty evaluation are summarized in Table 4-2 which is applicable to the shroud and vessel in the beltline region and to the surveillance capsule. In this table, some of the uncertainty results are given as ranges that are derived from the 2-dimensional calculations. The uncertainty contributions due to the void fraction uncertainty and the shroud inner radius uncertainty peak at the azimuthal maximum fluence point, whereas the uncertainty contribution from the bypass water density is a minimum at this point. A range for the steel density uncertainty is also given for the shroud but the maximum value occurs at the outside of the shroud and the uncertainty from this source at the IR is negligible. For the vessel, the jet pump uncertainty is a maximum at the maximum fluence point.

A total uncertainty was derived by combining the independent individual contributors in quadrature. This gave an uncertainty for the maximum shroud fluence of 16.0%. The uncertainty at other points in the shroud vary slightly from this value but fall within the range of 15.5% to 16.5%. The uncertainty in the maximum vessel fluence is evaluated to be 15.0% and the variation with position of the fluence uncertainty at the vessel IR is small also. The uncertainty in the shroud fluence is slightly greater than that for the vessel because of the greater uncertainty in the shroud diameter.

4.2.2 Shroud Weld Fluence Uncertainty

The uncertainty in the fluence to the shroud welds will contain an additional component due to uncertainty in the weld location. For the horizontal welds, this uncertainty is in the axial position relative to the BAF. For the vertical welds, the uncertainty is in the exact azimuthal location.

For the most important horizontal welds, H4 and H5, the uncertainty analysis is summarized in Table 4-3. The axial location uncertainty has been added to the elements in Table 4-2. Based on engineering judgement, the axial location uncertainty was assumed to be 1 inch. Using this value, the location uncertainty is only 1.2% for weld H4, but is 8.0% for weld H5 which is located near the core bottom in a much steeper flux gradient. In order to obtain a conservative uncertainty for the entire shroud, the maximum uncertainty values for each contributor has been used in Table 4-2. Using these conservative values, the total uncertainty then becomes 16.6% for H4 and 18.4% for H5.

In reality, since the azimuthal variation in shroud fluence uncertainty is relatively small (again about $\pm$ 0.5%), the uncertainty in the shroud falls between 15.6% and 16.6% for weld H4 and between 17.4% and 18.4% for weld H5. Within the accuracy of the uncertainty estimates, it is recommended that the maximum values be used as the uncertainty estimate for all points on the horizontal welds. This is illustrated in Figures 4-1 through 4-4. Figure 4-1 shows the

calculated fluence for weld H4 at the end of cycle 7 with the 1σ uncertainty bounds shown by dashed lines. Similarly, the fluence with uncertainty at the end of cycle 8 is shown in Figure 4-2. Similar plots for weld H5 are shown in Figures 4-3 and 4-4.

Typical vertical weld uncertainties in location are 5° [4-1]. The impact of this uncertainty is very different for each weld. For welds located at nominal positions of 0° and 45°, any location error will result in a higher fluence. At 0°, a 5° shift will raise the fluence by 14% and at 45° (which is in a steeper gradient) the fluence will increase by 44%. At 30°, the bounds are +46% and -10%. For vertical welds that have their maximum fluence location near the top and bottom of the core, there is also a contribution from axial uncertainty in the peak location, but the dominant uncertainty is due to the azimuthal location uncertainty.

4.2.3 Surveillance Capsule Fluence Uncertainty

The uncertainty in the surveillance capsule fluence is similar to that for the reactor vessel inner radius with only minor differences. The assumption is made that the accuracy of the capsule location is the same as the accuracy of the vessel IR. The jet pumps are not near the capsule so no error is contributed from the jet pump model. It may also be assumed that the axial and azimuthal location of the capsule is well known. For a 1 inch error in axial height for the capsule, the fluence uncertainty averages about 0.8% and for a 1 degree uncertainty in azimuth, the uncertainty averages about 2.5%. These two uncertainties combined are 2.6%. The capsule radial location uncertainty is taken to be the same as for the vessel IR. The total uncertainty in capsule fluence (summing in quadrature all the components from Table 4-2) is 15.3%.

4.3 Chapter 4 References

[4-1] "Nine Mile Point Unit 1 Shroud Neutron Transport and Uncertainty Analysis," Report Number MPM-108679, MPM Technologies, Inc, 2161 Sandy Drive, State College, PA 16803-2283, October, 1998.

[4-2] Letter, Shashi K. Dhar to M. P. Manahan, "Input Data for NMP-2 Fluence/Transport Calculations - Final," File Code ESB2-M99058, October 26, 1999.

[4-3] "Nine Mile Point Unit 2 Shroud Neutron Transport and Uncertainty Analysis," Report MPM-200623, MPM Technologies, Inc., 2161 Sandy Drive, State College, PA 16803-2283, February 2000.

[4-4] McElroy, W.N., Ed., "LWR-PV-SDIP: PCA Experiments and Blind Test", NUREG/CR-1861, 1981.

[4-5] Lippincott, E.P., "Consumers Power Company Palisades Nuclear Plant Reactor Vessel Fluence Analysis", WCAP-13348, May 1992.

[4-6] Maerker, R.E., et.al., "Application of LEPRICON Methodology to LWR Pressure Vessel Dosimetry", *Reactor Dosimetry: Methods, Applications, and Standardization, ASTM STP 1001*, 1989, pp 405-414.

[4-7] Anderson, S.L., "Westinghouse Fast Neutron Exposure Methodology for Pressure Vessel Fluence Determination and Dosimetry Evaluation", WCAP-13362, May 1992.

[4-8] Lippincott, E.P., et.al., "Evaluation of Surveillance Capsule and Reactor Cavity Dosimetry from H. B. Robinson Unit 2, Cycle 9", WCAP-11104, NUREG/CR-4576, February 1987.

[4-9] Haghighat, A. and Veerasingam, "Comparison of the Different Cross Section Libraries used for Reactor Pressure Vessel Fluence Calculations", *Trans. Amer. Nuclear Society*, 64, p. 357, 1991.

[4-10] Fero, A.H., "Neutron and Gamma Ray Flux Calculations for the Venus PWR Engineering Mockup," NUREG/CR-4827 (WCAP-11173), January, 1987.

Table 4-1 Nine Mile Point Unit 2 Uncertainty Contributors.

Uncertainty Contributor	Assigned Uncertainty
Fission Spectrum and ν/κ	10000 MWd/MTU
Heat Balance	2%
Shroud IR	0.188 inches[a]
Shroud Thickness	0.042 inches
Vessel IR	0.125 inches
Core Void Fractions	5%
Bypass Water Density	1.4%
Downcomer Water Temperature	5 °F
Steel Density (total cross section)	3.5%
Core Fuel Density	3.5%
Radial Source Dist.	6.0%
Axial Source Dist.	3.7%
Methods Uncertainty	5%
Flux History	8.0%

Note: a. The assigned uncertainty is based on maximum/minimum shroud diameter for location R3 (Beltline Region) (Reference VPF-3735-139-2).

Table 4-2 Nine Mile Point Unit 2 Fluence Calculational Uncertainty for Reactor Beltline Locations.

Uncertainty Contributor	Assigned Uncertainty	Shroud Fluence Uncertainty % (1σ)	Vessel IR Fluence Uncertainty % (1σ)	Capsule Fluence Uncertainty % (1σ)
Fission Spectrum and nu/kappa	10000 MWd/MTU	2.1	2.9	2.9
Heat Balance	2%	2.0	2.0	2.0
Shroud IR	0.188 inches	5.6 - 7.5	0.0	0.0
Shroud Thickness	0.042 inches	0.0	1.0	1.0
Vessel IR	0.125 inches	0.0	3.2	3.2
Core Void Fractions	5%	6.1 - 6.4	4.4	4.4
Bypass Water Density	1.4%	1.6 - 4.4	1.6 - 3.2	2.9
Downcomer Water Temperature	5 °F	0.0	3.9	3.9
Steel Density (total cross section)	3.5%	0.0 - 1.4	2.3	2.3
Core Fuel Density	3.5%	2.7	3.0	3.0
Radial Source Dist.	6.0%	6.0	6.0	6.0
Axial Source Dist.	3.7%	3.7	3.7	3.7
Methods Uncertainty	5%+	5.2	5.8	5.8
Flux History	8.0%	8.0	8.0	8.0
Jet Pump Model	25% of steel	0	0.0 - 4.1	0.0
Capsule Location	1° azimuth, 1 inch axial	0	0	2.6
Total		16.0	15.5	15.3

Table 4-3 Nine Mile Point Unit 2 Fluence Uncertainty for Welds H4 and H5.

Uncertainty Contributor	Assigned Uncertainty	Weld H4 Uncertainty % (1σ)	Weld H5 Uncertainty % (1σ)
Fission Spectrum and nu/kappa	10000 MWd/MTU	2.1	2.1
Heat Balance	2%	2.0	2.0
Shroud IR	0.188 inches	7.5	7.5
Shroud Thickness	0.042 inches	0.0	0.0
Vessel IR	0.125 inches	0.0	0.0
Core Void Fractions	5%	6.4	6.4
Bypass Water Density	1.4%	4.4	4.4
Downcomer Water Temperature	5 °F	0.0	0.0
Steel Density (total cross section)	3.5%	1.4	1.4
Core Fuel Density	3.5%	2.7	2.7
Radial Source Dist.	6.0%	6.0	6.0
Axial Source Dist.	3.7%	3.7	3.7
Methods Uncertainty	5%+	5.2	5.2
Flux History	8.0%	8.0	8.0
Axial Location	1 inch (assumed)	1.2	8.0
Total		16.6	18.4

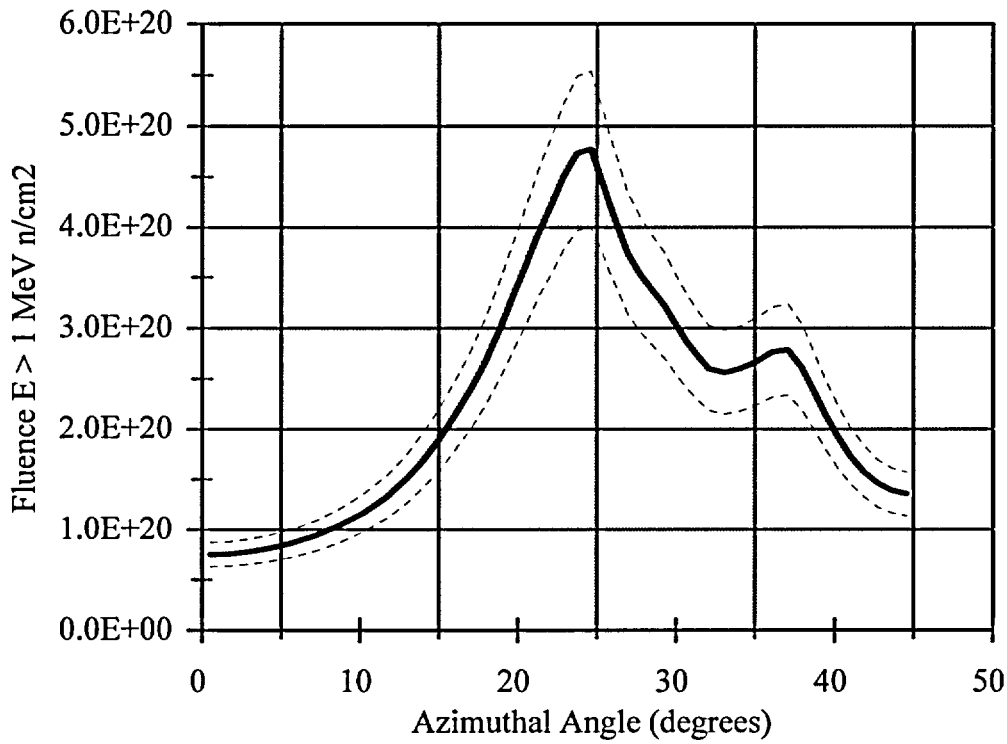

Figure 4-1 **Calculated Fluence (E > 1 MeV) to the Inner Radius of Shroud Weld H4 at End of Cycle 7 Showing 1σ Uncertainty Bands.**

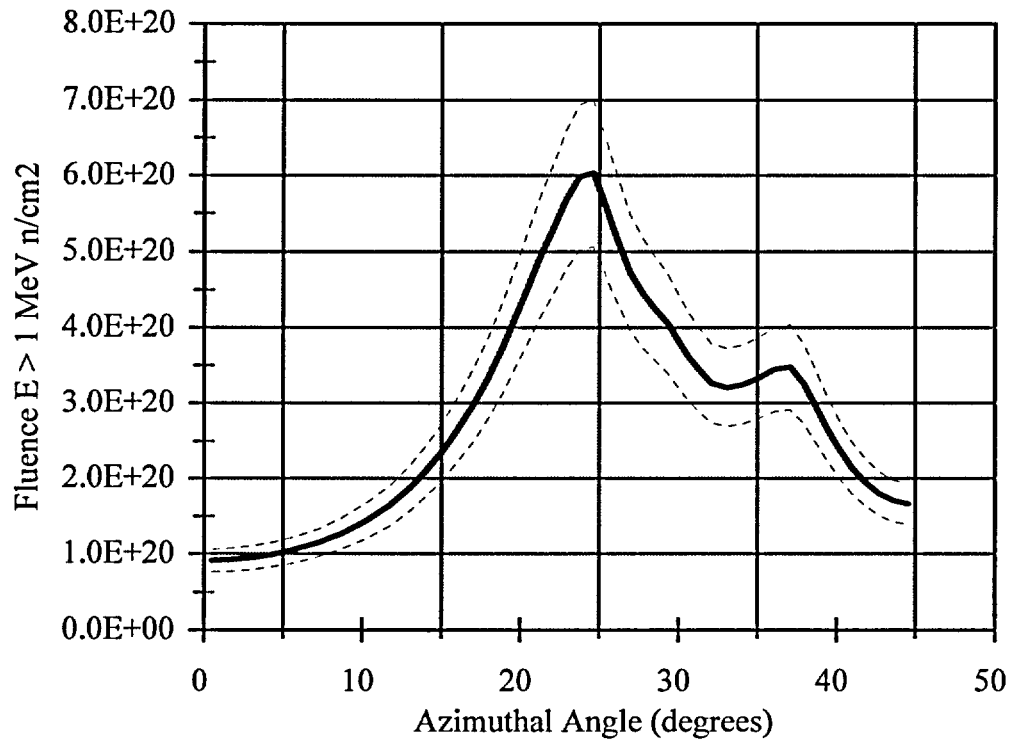

Figure 4-2 Calculated Fluence (E > 1 MeV) to the Inner Radius of Shroud Weld H4 Projected to End of Cycle 8 Showing 1σ Uncertainty Bands.

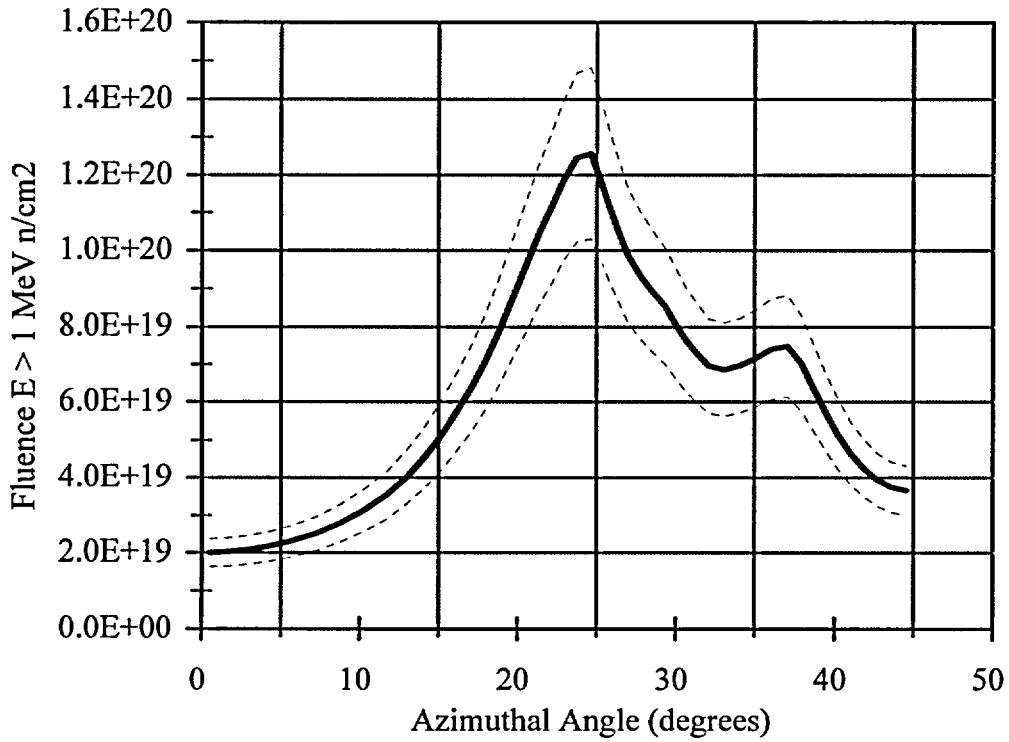

Figure 4-3 **Calculated Fluence (E > 1 MeV) to the Inner Radius of Shroud Weld H5 at End of Cycle 7 Showing 1σ Uncertainty Bands.**

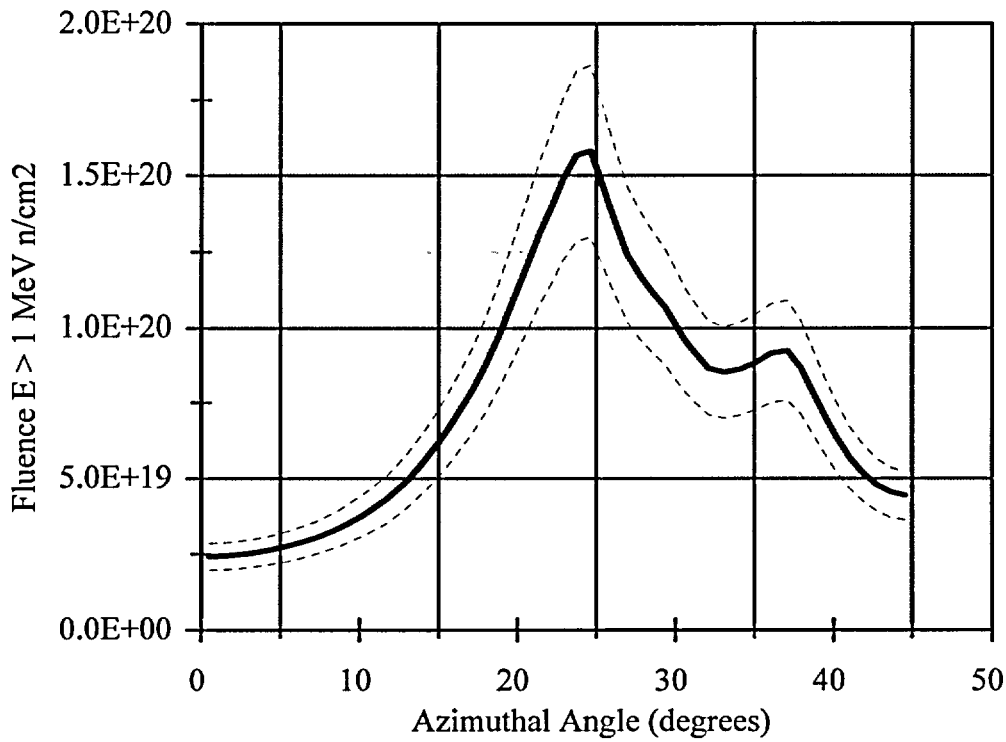

Figure 4-4 Calculated Fluence (E > 1 MeV) to the Inner Radius of Shroud Weld H5 Projected to End of Cycle 8 Showing 1σ Uncertainty Bands.

5.0 Methodology Validation

5.1 Compliance With RG 1.190

The United States Nuclear Regulatory Commission has issued RG 1.190 on Calculational and Dosimetry Methods for Determining Pressure Vessel Neutron Fluence [5-1]. This guide covers recommended practices for neutron transport calculations and applies to other reactor components in addition to the primary emphasis on the pressure vessel. The regulatory positions in the guide that pertain to calculational methodology are summarized in Table 5-1 which is taken directly from RG 1.190. The table references paragraphs in the guide that give more detailed information on each position.

The compliance of the NMP-2 shroud fluence calculations with the guide is summarized below.

Fluence Determination: This calculation was performed using an absolute fluence calculation.
Meets guide requirement.

Modeling Data: All the data used in the models are documented and verified.
Meets guide requirement.

Nuclear Data: The calculations use the BUGLE-96 cross section set which is based on the latest version (VI) of the Evaluated Nuclear Data File (ENDF/B). The BUGLE-96 set has undergone extensive testing and benchmarking to ensure its validity for LWR calculations.
Meets guide requirement.

Cross-Section Angular Representation: The calculations use a P3 angular expansion in accordance with the guide.
Meets guide requirement.

Cross-Section Group Collapsing: The calculations use the BUGLE-96 library without additional collapsing. Benchmarking has shown that the 47 group structure is adequate for LWR neutron transport calculations.
Meets guide requirement.

Neutron Source: Isotopic variation is accounted for in the neutron spectrum, neutrons per fission, and energy per fission within the modeling limitations. Moderator density is included in detail.
Meets guide requirement.

End-of-Life Predictions: Fluence projections are made based on the best estimate that future fuel cycles will be similar to cycle 7.
Meets guide requirement.

Spatial Representation: The model uses an azimuthal mesh with 48 angular intervals in an octant. Radial intervals are generally about 1 cm except near boundaries where a finer mesh is used. Inside the core, where flux changes are small, larger radial intervals are used. The quadrature used was S8.
Meets guide requirement.

Multiple Transport Calculations: It was not necessary to use bootstrapping for these calculations so this requirement does not apply.

Point Estimates: This requirement only applies to Monte Carlo calculations which are not used here.

Statistical Tests: This requirement only applies to Monte Carlo calculations which are not used here.

Variance Reduction: This requirement only applies to Monte Carlo calculations which are not used here.

Spectral Effects on RT_{NDT}: This requirement only applies to extrapolation through the vessel and has been applied to the vessel calculation as discussed in Reference [5-2].
Meets guide requirement.

Cavity Calculations: Cavity flux calculations have not been performed for this plant and do not have any impact on the results of this analysis.

Methods Qualification: Methods qualification for these calculations is discussed in detail in the next section which deals with benchmarking of the methodology. A complete analytical uncertainty analysis (described in Section 4) was carried out in accordance with the guide.
Meets guide requirement.

Fluence Calculational Uncertainty: An extensive evaluation of all contributors to the uncertainty in the calculated fluence was made. This evaluation indicated that the uncertainty in calculated fluences in the reactor beltline region is below 20% as specified in the guide. In addition, the comparisons with measurements indicate agreement well within the 20% limit.
Meets guide requirement.

5.2 Benchmarking of Methodology

The qualification of the methods used for the reactor transport calculations can be divided into two parts. The first step is the qualification of the cross-section library and calculational methods that are used to calculate the neutron transport. The second step is the validation of the plant specific application to the NMP-2 plant. Details of the extensive benchmarking effort are contained in a separate document [5-3]. The benchmarking results are briefly summarized here.

The qualification of the cross-section library and calculational methods is particularly important for vessel fluence calculations because of the large amount of neutron attenuation between the source in the core and the vessel. The cross-sections are first developed as an evaluated file that details all the reactions as a continuous function of energy. The ENDF/B evaluators take into account various measurements, including integral measurements (such as criticality and dosimetry measurements) that provide a test of the adequacy of the evaluation. For transport calculations using discrete ordinates, the ENDF/B cross-section files must be collapsed to multigroup files. This is done in two steps. First, fine-group cross-sections are calculated (Vitamin B6 library). To produce the 47-group BUGLE-96 library, the Vitamin B6 library is further collapsed using spectra typical of LWR environments. The BUGLE-96 file contains cross-sections collapsed using a BWR core spectrum, a PWR core spectrum, a PWR downcomer spectrum, a PWR vessel spectrum, and a concrete shield spectrum. These various cross-section libraries are then tested against various benchmarks and compared with measured results and results calculated using the fine-group cross-sections [5-4]. The BUGLE-96 library was concluded to give good accuracy for LWR calculations [5-4].

Calculations of LWR benchmarks have indicated that the BUGLE-96 library produces very good agreement with measurements. A particularly appropriate benchmark for geometry outside the core to the vessel is the PCA benchmark [5-5]. This benchmark provides validation of the transport through typical reactor structures and the simulated reactor vessel in a simple geometry. The PCA has high-accuracy measurement results extending from inside a simulated thermal shield through to the outside of a simulated vessel. The PCA benchmark was calculated using the MPM methodology and results are in [5-3]. The calculational results show a slight consistent bias (less than 10%) with respect to the measurements, but no significant change in bias is observed with change in irradiation position. This indicates that the transport methodology is calculating the flux attenuation outside the core region with high accuracy. The observed bias is consistent with that obtained by other synthesis calculations that have been reported [5-5,5-6].

In addition to comparison with measurement results, another benchmarking requirement of RG 1.190 is to compare with a suitable calculational benchmark. The calculational benchmarks to satisfy this requirement are documented in Reference [5-7]. The benchmark problems include 3 different PWR geometries and a single BWR problem. It is intended that the analyst select the benchmark problem or problems appropriate to the plant being analyzed. Accordingly, the BWR problem has been calculated since this problem is the one particularly appropriate for NMP-2 as well as other BWRs. The BWR vessel fluence benchmark problem is for a typical BWR geometry and is very similar to NMP-2. The core has 800 fuel bundles that have an axial height of 381 cm. Structures between the core and vessel that are included are the shroud, jet pumps and risers, and surveillance capsule. The model extends outside the vessel into an outer concrete biological shield. The core power distribution and burnup are for a typical equilibrium cycle. The problem specification includes the dimensions of all components, material compositions by region, and the core neutron source.

The BWR benchmark problem was calculated using the MPM methodology. Although the

model used for the benchmark DORT calculations was included with the description, an independent model was constructed using the same considerations that defined the NMP-2 models. Comparisons were made between the MPM calculations and the benchmark calculational results which indicated very good agreement [5-3]. In the capsule the average results were about 3% low and at the vessel IR and within the vessel the average results were about 2-3% high. All compared results fell within ±10%.

The second part of benchmarking is to compare calculations with measurement in a geometry as close as possible to that which is to be used. In the case of NMP-2, it has been demonstrated that the capsule measurements (see Section 3.3) are very well reproduced by the calculations. In addition, measurements from NMP-1 are reported in Reference [5-8] for both the shroud and a surveillance capsule. The shroud measurements provide a unique benchmarking of the methodology used here in a very similar geometry. The measurements were made on boat samples removed from the shroud and counted for nickel and iron activities. Comparisons of calculations with fast flux values derived from these measurements are shown in Table 5-2 which is taken from [5-8]. Samples were taken at two axial locations and at three radial positions in the shroud. All the samples were taken from a nominal azimuthal angle of 20°, and within 2 vertical welds fairly close to the axial midplane of the fuel. The calculations average 15.7% (with a standard deviation of 3.1%) higher than the measurements, but are consistent through the shroud. One cause of the ~16% bias may be error in the exact azimuthal location of the samples. Since the samples were taken from an angle that has the peak flux, any deviation would result in a lower measured value than predicted.

The latest NMP-1capsule measurement is also described in detail in [5-8]. This exposure measurement is based on measurements from copper, nickel, and iron dosimeters located in a capsule just inside the reactor vessel. There were 3 of each dosimeter contained in the capsule. An average of the flux derived from the 9 dosimeters gave a value of 1.70E9 n/cm^2/s (E > 1 MeV) with a standard deviation of 8.4%. The calculated average capsule flux was 1.44E9 n/cm^2/s (E > 1 MeV) which results in a C/M ratio of 0.847. Thus the bias here is about the same magnitude as for the shroud samples but is in the opposite direction.

All the measurements in both NMP-1 and NMP-2, as well as the other benchmark calculations (Reference [5-3]), support the adequacy of the BWR calculations using the present methodology to determine fluence within the beltline region with uncertainty below 20%. The BWR measurements go beyond the other benchmarks in that they validate the entire methodology procedure as applied to these specific cases for both exposure through the shroud and at the inside of the vessel. The C/M comparisons test not only the cross-sections and the computer codes, but also the plant-specific modeling including the geometrical dimensions and fuel data. It is concluded that these measurements provide a good verification of the calculational results.

5.3 Chapter 5 References

[5-1] Regulatory Guide 1.190, *Calculational and Dosimetry Methods for Determining Pressure Vessel Neutron Fluence*, U. S. Nuclear Regulatory Commission, March 2001.

[5-2] "Nine Mile Point Unit 2 3-Degree Pressure Vessel Surveillance Capsule Report," Report MPM-1200676, MPM Technologies, Inc., 2161 Sandy Drive, State College, PA 16803-2283, December 2000.

[5-3] "Benchmarking of Nine Mile Point Unit 1 and Unit 2 Neutron Transport Calculations," Report Number MPM-402781, MPM Technologies, Inc., 2161 Sandy Drive, State College, PA 16803-2283, January, 2003.

[5-4] RSICC Data Library Collection, DLC-185, BUGLE-96, Coupled 47 Neutron, 20 Gamma Ray Group Cross Section Library Derived from ENDF/B-VI for LWR Shielding and Pressure Vessel Dosimetry Applications, available from the Radiation Safety Information Computational Center, Oak Ridge National Laboratory, Oak Ridge, TN, March 1996.

[5-5] Remec, I. and Kam, F.B.K., *Pool Critical Assembly Pressure Vessel Facility Benchmark*, NUREG/CR-6454, (ORNL/TM-13205), USNRC, July 1997.

[5-6] Fero, A.H., Anderson, S.L. and Roberts, G.K., "Analysis of the ORNL PCA Benchmark Using TORT and BUGLE-96," Reactor Dosimetry: Radiation Metrology and Assessment, ASTM STP 1398, John G. Williams, David W. Vehar, Frank H. Ruddy, and David Gilliam, Eds., American Society for Testing and Materials, West Conshohocken, PA, 2001.

[5-7] Carew, J. F., Hu, K., Aronson, A., Prince, A., and Zamonsky, G., PWR and BWR Pressure Vessel Fluence Calculational Benchmark Problems and Solutions, NUREG/CR-6115 (BNL-NUREG-52395), Draft completed May 20, 1997.

[5-8] "Nine Mile Point Unit 1 Shroud Neutron Transport and Uncertainty Analysis," Report Number MPM-108679, MPM Technologies, Inc, 2161 Sandy Drive, State College, PA 16803-2283, October, 1998.

Table 5-1 Summary of Regulatory Positions on Fluence Calculation Methods.

	Regulatory Position
Fluence Determination. Absolute fluence calculations, rather than extrapolated fluence measurements, must be used for the fluence determination.	1.3
Modeling Data. The calculation modeling (geometry, materials, etc.) should be based on documented and verified plant-specific data.	1.1.1
Nuclear Data. The latest version of the Evaluated Nuclear Data File (ENDF/B) should be used for determining nuclear cross- sections. Cross-section sets based on earlier or equivalent nuclear-data sets that have been thoroughly benchmarked are also acceptable. When the recommended cross-section data change, the effect of these changes on the licensee-specific methodology must be evaluated and the fluence estimates updated when the effects are significant.	1.1.2
Cross-Section Angular Representation. In discrete ordinates transport calculations, a P_3 angular decomposition of the scattering cross-sections (at a minimum) must be employed.	1.1.2
Cross-Section Group Collapsing. The adequacy of the collapsed job library must be demonstrated by comparing calculations for a representative configuration performed with both the master library and the job library.	1.1.2
Neutron Source. The core neutron source should account for local fuel isotopics and, where appropriate, moderator density. The neutron source normalization and energy dependence must account for the fuel exposure dependence of the fission spectra, the number of neutrons produced per fission, and the energy released per fission.	1.2
End-of-Life Predictions. Predictions of the vessel end-of-life fluence should be made with a best-estimate or conservative generic power distribution. If a best estimate is used, the power distribution must be updated if changes in core loadings, surveillance measurements, or other information indicate a significant change in projected fluence values.	1.2
Spatial Representation. Discrete ordinates neutron transport calculations should incorporate a detailed radial- and azimuthal-spatial mesh of ~2 intervals per inch radially. The discrete ordinates calculations must employ (at a minimum) an S_8 quadrature and (at least) 40-80 intervals per octant.	1.3.1
Multiple Transport Calculations. If the calculation is performed using two or more "bootstrap" calculations, the adequacy of the overlap regions must be demonstrated.	1.3.1

Table 5-1 Summary of Regulatory Positions on Fluence Calculation Methods (Continued).

	Regulatory Position
Point Estimates. If the dimensions of the tally region or the definition of the average-flux region introduce a bias in the talley edit, the Monte Carlo prediction should be adjusted to eliminate the calculational bias. The average-flux region surrounding the point location should not include material boundaries or be located near reflecting, periodic or white boundaries.	1.3.2
Statistical Tests. The Monte Carlo estimated mean and relative error should be tested and satisfy all statistical criteria.	1.3.2
Variance Reduction. All variance reduction methods should be qualified by comparison with calculations performed without variance reduction.	1.3.2
Capsule Modeling. The capsule fluence is extremely sensitive to the geometrical representation of the capsule geometry and internal water region, and the adequacy of the capsule representation and mesh must be demonstrated	1.3.3
Spectral Effects on RT_{NDT}. In order to account for the neutron spectrum dependence of RT_{NDT}, when it is extrapolated from the inside surface of the pressure vessel to the T/4 and 3T/4 vessel locations using the > 1-MeV fluence, a spectral lead factor must be applied to the fluence for the calculation of ΔRT_{NDT}.	1.3.3
Cavity Calculations. In discrete ordinates transport-calculations, the adequacy of the S_8 angular quadrature used in cavity transport calculations must be demonstrated.	1.3.5
Methods Qualification. The calculational methodology must be qualified by both (1) comparisons to measurement and calculational benchmarks and (2) an analytic uncertainty analysis. The methods used to calculate the benchmarks must be consistent (to the extent possible) with the methods used to calculate the vessel fluence. The overall calculational bias and uncertainty must be determined by an appropriate combination of the analytic uncertainty analysis and the uncertainty analysis based on the comparisons to the benchmarks.	1.4.1, 1.4.2, 1.4.3
Fluence Calculational Uncertainty. The vessel fluence (1 sigma) calculational uncertainty must be demonstrated to be 20% for RT_{PTS} and RT_{NDT} determination. In these applications, if the benchmark comparisons indicate differences greater than ~20%, the calculational model must be adjusted or a correction must be applied to reduce the difference between the fluence prediction and the upper 1-sigma limit to within 20%. For other applications, the accuracy should be determined using the approach described in Regulatory Position 1.4, and an uncertainty allowance should be included in the fluence estimate as appropriate in the specific application.	1, 1.4.3

Table 5-2 Measured and Calculated Boat Sample Flux Values from Nine Mile Point Unit 1.

Radial Location[a] (in)	Axial Location[b] (in)	Flux (E > 1 MeV) n/cm²/s		C/M Ratio
		Measured[c] (M)	Calculated (C)	
Vertical Weld V9				
0.000	26.4	6.59E+11	7.55E+11	1.14567526555
0.337	26.4	6.02E+11	6.86E+11	1.13953488372
0.850	26.4	5.01E+11	5.62E+11	1.12175648703
Average C/M				1.136
Vertical Weld V10				
0.882	-8.3	3.78E+11	4.61E+11	1.21957671958
1.062	-8.3	3.36E+11	3.88E+11	1.15476190476
1.500	-8.3	2.68E+11	3.11E+11	1.16044776119
Average C/M				1.179

[a] Measured from shroud ID surface.
[b] Measured from fuel axial midplane.
[c] Average of flux derived from 2 iron and 2 nickel measurements at each location. The flux is determined from the measurements by dividing the average reaction rate (calculated from the measured decay rate per mg. of sample using the reactor power history as adjusted by the relative flux calculation) by the spectrum average cross section.

6.0 Summary and Conclusions

A new detailed calculation of the fluence for NMP-2 has been completed to define the shroud exposure. Comparisons of capsule flux values with previous calculations indicate that the new calculations produced consistent results. Detailed tables of fluence to all the shroud welds within the beltline region were produced. Application of the transport calculation results to the shroud structural assessment shows that the peak fluence to the beltline welds will not exceed 5.0E+20 n/cm^2 at the end of cycle 7. However, weld H4 is projected to exceed 5.0E+20 n/cm^2 during cycle 8.

Comparisons of calculations with NMP-2 capsule dosimetry measurements indicate excellent agreement. These comparisons are supplemented by NMP-1 capsule and shroud measurements that support the analytic uncertainty analysis which indicates that the shroud fluence is determined within about 16% (1σ). The MPM calculational methodology has been validated by comparison with measurement and calculational benchmarks. This calculation meets all the requirements of RG 1.190.

7.0 Nomenclature

AMOC	after middle of cycle
BAF	bottom of active fuel
BMOC	before middle of cycle
BOC	beginning of cycle
C/M	calculated to measured ratio
dpa	displacements per atom
EFPS	effective full-power seconds
EFPY	effective full-power years
ID	inner diameter
IR	inner radius
MOC	middle of cycle
MPM	MPM Technologies, Inc.
NEOC	near end of cycle
NMPC	Niagara Mohawk Power Corporation
NMP-1	Nine Mile Point Unit 1
NMP-2	Nine Mile Point Unit 2
OD	outer diameter
OR	outer radius
RG	Regulatory Guide
RPV	reactor pressure vessel
T	vessel wall thickness

ATTACHMENT 3

REPORT NO. MPM-301624A

NINE MILE POINT UNIT 2
SHROUD NEUTRON TRANSPORT AND UNCERTAINTY ANALYSIS: ADDENDUM

Nine Mile Point Unit 2 Shroud Neutron Transport and Uncertainty Analysis: Addendum

© Copyright 2003 MPM Technologies, Inc..
All Rights Reserved

MPM Technologies, Inc.

...serving client needs through advanced technology ..

Report Number MPM-301624A
Revision 1

January, 2003

Report Number MPM-301624A
Revision 1

Final Report

entitled

Nine Mile Point Unit 2 Shroud Neutron Transport and Uncertainty Analysis: Addendum

prepared for
Niagara Mohawk Power Corporation
Nine Mile Point Unit 2
Lake Road
Lycoming, NY 13093

by
MPM Technologies, Inc.
2161 Sandy Drive
State College, PA 16803-2283

January, 2003

Preparer	**Checker**
1/7/03	**1/7/03**
Date	**Date**

MPM Approval

1/7/03

Date

© Copyright 2002 MPM Technologies, Inc.
All Rights Reserved

Nuclear Quality Assurance Certification

This document certifies that MPM has performed all work under NMPC Purchase Order Number 00-30028 in accordance with the requirements of the Purchase Order. All work has been performed under the MPM Nuclear Quality Assurance Program.

M P Manahan, Sr.

M. P. Manahan, Sr.
President
1/7/03

Date

S. Clinger

S. Clinger
QA Manager
1/7/03

Date

Contents

Calculated Shroud Results ..... Page Number 1

Calculated Fluence for Shroud Horizontal Welds at End of Cycle 7 ..... Page Number 2

Calculated Average Cycle 7 Fluence Rates for Shroud Horizontal Welds ..... Page Number 10

Calculated Fluence for Shroud Horizontal Welds at End of Cycle 8 ..... Page Number 18

Calculated Fluence for Shroud Vertical Welds at End of Cycle 7 ..... Page Number 26

Calculated Average Cycle 7 Fluence Rates for Shroud Vertical Welds ..... Page Number 30

Calculated Fluence for Shroud Vertical Welds at End of Cycle 8 ..... Page Number 34

Calculated Shroud Results

This addendum to MPM Report No. MPM-301624 contains tabulations of calculated flux and fluence data for the welds in the Nine Mile Point Unit 2 shroud beltline region. Data are given for the evaluated fluence at the end of Cycle 7 (8.72 EFPY). This evaluation uses neutron transport calculations for each fuel cycle. For cycles 1 through 6, analyses showed that the fuel power distribution calculated near the middle of the cycle was a good representation of the cycle average, and therefore calculations were performed near middle-of-cycle. For cycle 7 a more detailed evaluation was done using fuel power distributions at 5 representative points during the cycle to calculate a more accurate integral of the flux for dosimetry analysis for the 3-degree surveillance capsule which was withdrawn at the end of cycle 7.

Tables are also given for the average fluence rate during cycle 7. This was calculated by taking the cycle 7 fluence determined by sum of the 5 cycle parts and dividing by the total cycle length for cycle 7. Assuming that future cycles are similar to cycle 7 (the current plan), these values may be used to project the fluence to future times. Tables of the fluence projected to the end of fuel cycle 8 are also given. These tables use an estimated length of cycle 8 of 1.82 EFPY (5.75E7 s) at a power of 3467 MWth.

Tables 1 through 4 give the calculated neutron fluence values (E > 1 MeV) at the end of cycle 7 for the horizontal shroud welds within the beltline region. The fluence is tabulated at 48 azimuthal angles and at 7 radial points from the inner surface to the outer surface of the shroud. Tables 5 through 8 give fluence rate values for these same welds averaged over cycle 7. Tables 9 through 12 give the horizontal weld fluence values projected to the end of cycle 8.

Fluence values for the end of cycle 7 for vertical welds within the beltline region are given in Tables 13 through 16. Values are tabulated for axial heights from the bottom to top of each weld for points within the beltline region. Tables 17 through 20 give fluence rate values for these same welds averaged over cycle 7. Tables 21 through 24 give fluence values for the vertical welds projected to the end of cycle 8.

Table 1 Tabulation of Calculated Fluence (n/cm^2 above 1 MeV) for Weld H5 at End of Cycle 7

Azimuthal Angle (Deg)	Distance Into Shroud from Inner Surface (inches)						
	0.00	0.333	0.667	1.00	1.333	1.667	2.00
0.50	2.01E+19	1.86E+19	1.70E+19	1.50E+19	1.30E+19	1.10E+19	8.58E+18
1.68	2.03E+19	1.88E+19	1.71E+19	1.52E+19	1.32E+19	1.11E+19	8.65E+18
3.00	2.09E+19	1.93E+19	1.76E+19	1.56E+19	1.35E+19	1.14E+19	8.89E+18
4.32	2.18E+19	2.02E+19	1.83E+19	1.63E+19	1.41E+19	1.19E+19	9.27E+18
5.75	2 32E+19	2.15E+19	1.95E+19	1.73E+19	1.50E+19	1.26E+19	9.86E+18
7.25	2.51E+19	2.33E+19	2.12E+19	1.88E+19	1.63E+19	1.37E+19	1.07E+19
8.75	2.78E+19	2.57E+19	2.34E+19	2.07E+19	1.80E+19	1.51E+19	1.18E+19
10.25	3.12E+19	2.88E+19	2.62E+19	2.32E+19	2.01E+19	1.69E+19	1.32E+19
11.75	3.53E+19	3.27E+19	2.97E+19	2.63E+19	2.28E+19	1.91E+19	1.49E+19
13.00	4.01E+19	3.71E+19	3.37E+19	2.99E+19	2.59E+19	2.17E+19	1.69E+19
14.00	4.48E+19	4.14E+19	3.76E+19	3.33E+19	2.88E+19	2.41E+19	1.88E+19
15.00	5.00E+19	4.63E+19	4.20E+19	3.72E+19	3.21E+19	2.70E+19	2.10E+19
16 00	5.63E+19	5.20E+19	4.71E+19	4.17E+19	3.60E+19	3.02E+19	2.35E+19
17.00	6.32E+19	5.83E+19	5.29E+19	4.68E+19	4.04E+19	3.38E+19	2.63E+19
17.97	7.07E+19	6 54E+19	5.93E+19	5.24E+19	4.52E+19	3.79E+19	2.94E+19
18.84	7.88E+19	7.27E+19	6.59E+19	5.82E+19	5.02E+19	4.20E+19	3.26E+19
19.75	8.78E+19	8 09E+19	7.32E+19	6.46E+19	5.56E+19	4.64E+19	3.60E+19
20.62	9.67E+19	8.90E+19	8.04E+19	7.08E+19	6.09E+19	5.07E+19	3.92E+19
21.40	1.05E+20	9.61E+19	8.67E+19	7.62E+19	6.54E+19	5.45E+19	4.21E+19
22.15	1.11E+20	1.02E+20	9.21E+19	8.09E+19	6.95E+19	5.78E+19	4.45E+19
22.88	1.18E+20	1.08E+20	9.75E+19	8.55E+19	7.32E+19	6.08E+19	4.68E+19
23.75	1.25E+20	1.14E+20	1.02E+20	8.92E+19	7.62E+19	6.32E+19	4.85E+19
24.63	1.26E+20	1.14E+20	1.02E+20	8.92E+19	7.61E+19	6.30E+19	4.83E+19
25.28	1.18E+20	1.08E+20	9.71E+19	8.49E+19	7.27E+19	6.03E+19	4.64E+19

Table 1 (cont) Tabulation of Calculated Fluence (n/cm^2 above 1 MeV) for Weld H5 At End of Cycle 7

Azimuthal Angle (Deg)	Distance Into Shroud from Inner Surface (inches)						
	0.00	0.333	0.667	1.00	1.333	1.667	2.00
25.79	1.12E+20	1.03E+20	9.24E+19	8.12E+19	6.96E+19	5.80E+19	4.47E+19
26.31	1.06E+20	9.75E+19	8.80E+19	7.74E+19	6.66E+19	5.55E+19	4.29E+19
26.96	9.88E+19	9.11E+19	8.25E+19	7.27E+19	6.27E+19	5.23E+19	4.05E+19
27.76	9.34E+19	8.62E+19	7.81E+19	6.89E+19	5.94E+19	4.96E+19	3.85E+19
28.55	8.93E+19	8.24E+19	7.46E+19	6.58E+19	5.67E+19	4.74E+19	3.67E+19
29.35	8.54E+19	7.86E+19	7.11E+19	6.27E+19	5.40E+19	4.51E+19	3.50E+19
30.06	8.04E+19	7.42E+19	6.72E+19	5.93E+19	5.12E+19	4.28E+19	3.32E+19
30.68	7.65E+19	7.07E+19	6.41E+19	5.67E+19	4.90E+19	4.10E+19	3.19E+19
31.30	7.33E+19	6.77E+19	6.14E+19	5.44E+19	4.70E+19	3.94E+19	3.07E+19
32.10	6.96E+19	6 44E+19	5.85E+19	5.18E+19	4.48E+19	3.76E+19	2.93E+19
33.10	6 87E+19	6.34E+19	5.75E+19	5.08E+19	4.39E+19	3.68E+19	2.86E+19
34.09	6.97E+19	6.42E+19	5.81E+19	5.13E+19	4.43E+19	3.70E+19	2.87E+19
35.09	7.16E+19	6.59E+19	5.96E+19	5.25E+19	4.52E+19	3.78E+19	2.92E+19
36.08	7.40E+19	6.80E+19	6.13E+19	5.39E+19	4.63E+19	3.86E+19	2.97E+19
37.07	7.48E+19	6.84E+19	6.15E+19	5.39E+19	4.62E+19	3.84E+19	2.95E+19
37.94	7.03E+19	6.44E+19	5.80E+19	5.08E+19	4.36E+19	3.63E+19	2.79E+19
38.69	6.42E+19	5.90E+19	5.32E+19	4.68E+19	4.03E+19	3.36E+19	2.59E+19
39.43	5.79E+19	5.33E+19	4.83E+19	4.26E+19	3.67E+19	3.06E+19	2.37E+19
40.22	5.19E+19	4.79E+19	4.34E+19	3.84E+19	3.31E+19	2.77E+19	2.15E+19
41.04	4.67E+19	4.32E+19	3.92E+19	3.47E+19	3.00E+19	2.52E+19	1.96E+19
41.86	4.26E+19	3.95E+19	3.59E+19	3.18E+19	2.76E+19	2.31E+19	1.81E+19
42.73	3.94E+19	3.66E+19	3.33E+19	2.95E+19	2.56E+19	2.15E+19	1.68E+19
43.64	3.75E+19	3.47E+19	3.16E+19	2.81E+19	2.43E+19	2.05E+19	1.60E+19
44.55	3.66E+19	3.39E+19	3.09E+19	2.74E+19	2.37E+19	1.99E+19	1.56E+19

Table 2 Tabulation of Calculated Fluence (n/cm^2 above 1 MeV) for Weld H4 At End of Cycle 7

Azimuthal Angle (Deg)	Distance Into Shroud from Inner Surface (inches)						
	0.00	0.333	0.667	1.00	1.333	1.667	2.00
0.50	7.52E+19	6.97E+19	6.34E+19	5.62E+19	4.87E+19	4.09E+19	3.19E+19
1.68	7.58E+19	7.03E+19	6.40E+19	5.67E+19	4.91E+19	4.12E+19	3.22E+19
3.00	7.80E+19	7.23E+19	6.58E+19	5.83E+19	5.05E+19	4.24E+19	3.31E+19
4.32	8.14E+19	7.55E+19	6.87E+19	6.09E+19	5.27E+19	4.43E+19	3.45E+19
5.75	8.67E+19	8.04E+19	7.31E+19	6.48E+19	5.61E+19	4.71E+19	3.67E+19
7.25	9.41E+19	8.72E+19	7.94E+19	7.03E+19	6.09E+19	5.11E+19	3.99E+19
8.75	1.04E+20	9.67E+19	8.79E+19	7.79E+19	6.74E+19	5.66E+19	4.40E+19
10.25	1.17E+20	1.08E+20	9.86E+19	8.74E+19	7.56E+19	6.34E+19	4.94E+19
11.75	1.33E+20	1.23E+20	1.12E+20	9.92E+19	8.58E+19	7.19E+19	5.59E+19
13.00	1.51E+20	1.40E+20	1.27E+20	1.13E+20	9.74E+19	8.16E+19	6.34E+19
14.00	1.69E+20	1.56E+20	1.42E+20	1.26E+20	1.08E+20	9.09E+19	7.06E+19
15.00	1.89E+20	1.75E+20	1.59E+20	1.40E+20	1.21E+20	1.02E+20	7.89E+19
16.00	2.13E+20	1.96E+20	1.78E+20	1.58E+20	1.36E+20	1.14E+20	8.84E+19
17.00	2.39E+20	2.20E+20	2.00E+20	1.77E+20	1.53E+20	1.28E+20	9.90E+19
17.97	2.67E+20	2.47E+20	2.24E+20	1.98E+20	1.71E+20	1.43E+20	1.11E+20
18.84	2.98E+20	2.75E+20	2.49E+20	2.20E+20	1.90E+20	1.59E+20	1.23E+20
19.75	3.32E+20	3.07E+20	2.78E+20	2.45E+20	2.10E+20	1.75E+20	1.35E+20
20.62	3.67E+20	3.37E+20	3.05E+20	2.68E+20	2.30E+20	1.92E+20	1.48E+20
21.40	3.97E+20	3.65E+20	3.29E+20	2.89E+20	2.48E+20	2.06E+20	1.59E+20
22.15	4.22E+20	3.88E+20	3.50E+20	3.07E+20	2.63E+20	2.19E+20	1.68E+20
22.88	4.49E+20	4.12E+20	3.70E+20	3.24E+20	2.78E+20	2.30E+20	1.76E+20
23.75	4.73E+20	4.32E+20	3.87E+20	3.38E+20	2.89E+20	2.39E+20	1.83E+20
24.63	4.77E+20	4.34E+20	3.88E+20	3.38E+20	2.89E+20	2.39E+20	1.82E+20
25.28	4.49E+20	4.10E+20	3.68E+20	3.22E+20	2.75E+20	2.28E+20	1.75E+20

Table 2 (cont) Tabulation of Calculated Fluence (n/cm² above 1 MeV) for Weld H4 At End of Cycle 7

Azimuthal Angle (Deg)	Distance Into Shroud from Inner Surface (inches)						
	0.00	0 333	0.667	1.00	1.333	1.667	2.00
25.79	4.24E+20	3.89E+20	3.50E+20	3.08E+20	2.64E+20	2.19E+20	1.68E+20
26.31	4.01E+20	3.69E+20	3.33E+20	2.93E+20	2.52E+20	2.10E+20	1.62E+20
26.96	3.73E+20	3.45E+20	3.12E+20	2.75E+20	2.37E+20	1.97E+20	1.52E+20
27.76	3.53E+20	3.25E+20	2.95E+20	2.60E+20	2.24E+20	1.87E+20	1.44E+20
28.55	3.37E+20	3.11E+20	2.81E+20	2.48E+20	2.14E+20	1.78E+20	1.38E+20
29.35	3.21E+20	2.96E+20	2.68E+20	2.36E+20	2.03E+20	1.69E+20	1.31E+20
30.06	3.02E+20	2.79E+20	2.53E+20	2.23E+20	1.92E+20	1.61E+20	1.24E+20
30.68	2.87E+20	2.65E+20	2.41E+20	2.13E+20	1.84E+20	1.54E+20	1.19E+20
31.30	2.75E+20	2.54E+20	2.30E+20	2.04E+20	1.76E+20	1.47E+20	1.14E+20
32.10	2.61E+20	2.41E+20	2.19E+20	1.94E+20	1.68E+20	1.40E+20	1.09E+20
33.10	2.57E+20	2.37E+20	2.15E+20	1.90E+20	1.64E+20	1.37E+20	1.06E+20
34.09	2.60E+20	2.40E+20	2.17E+20	1.91E+20	1.65E+20	1.38E+20	1.07E+20
35.09	2.67E+20	2.46E+20	2.22E+20	1.96E+20	1.69E+20	1.41E+20	1.08E+20
36.08	2.76E+20	2.54E+20	2.29E+20	2.01E+20	1.72E+20	1.43E+20	1.10E+20
37.07	2.79E+20	2.55E+20	2.29E+20	2.01E+20	1.72E+20	1.43E+20	1.10E+20
37.94	2.62E+20	2.40E+20	2.16E+20	1.89E+20	1.62E+20	1.35E+20	1.03E+20
38.69	2.39E+20	2.20E+20	1.98E+20	1.74E+20	1.50E+20	1.25E+20	9.61E+19
39.43	2.16E+20	1.99E+20	1.80E+20	1.58E+20	1.36E+20	1.14E+20	8.79E+19
40 22	1.93E+20	1.78E+20	1.62E+20	1.43E+20	1.23E+20	1.03E+20	7.97E+19
41.04	1.73E+20	1.61E+20	1.46E+20	1.29E+20	1.11E+20	9.33E+19	7.25E+19
41.86	1.58E+20	1.47E+20	1.33E+20	1.18E+20	1.02E+20	8.58E+19	6.68E+19
42.73	1.46E+20	1.36E+20	1.24E+20	1.10E+20	9.50E+19	7.98E+19	6.22E+19
43.64	1.39E+20	1.29E+20	1.17E+20	1.04E+20	9.02E+19	7.58E+19	5.91E+19
44.55	1.36E+20	1.26E+20	1.15E+20	1.02E+20	8.80E+19	7.39E+19	5.76E+19

Table 3 Tabulation of Calculated Fluence (n/cm^2 above 1 MeV) for Weld H3 At End of Cycle 7

Azimuthal Angle (Deg)	Distance Into Shroud from Inner Surface (inches)						
	0.00	0.333	0.667	1.00	1.333	1.667	2.00
0.50	3.29E+19	3.05E+19	2.78E+19	2.46E+19	2.14E+19	1.80E+19	1.41E+19
1.68	3.32E+19	3.08E+19	2.80E+19	2.48E+19	2.16E+19	1.81E+19	1.42E+19
3.00	3.41E+19	3.16E+19	2.88E+19	2.55E+19	2.22E+19	1.86E+19	1.46E+19
4.32	3.56E+19	3.30E+19	3.00E+19	2.67E+19	2.31E+19	1.94E+19	1.52E+19
5.75	3.79E+19	3.52E+19	3.20E+19	2.84E+19	2.46E+19	2.07E+19	1.62E+19
7.25	4.11E+19	3.81E+19	3.47E+19	3.08E+19	2.67E+19	2.24E+19	1.76E+19
8.75	4.56E+19	4.22E+19	3.84E+19	3.40E+19	2.95E+19	2.48E+19	1.94E+19
10.25	5.11E+19	4.73E+19	4.30E+19	3.82E+19	3.31E+19	2.78E+19	2.17E+19
11.75	5.79E+19	5.37E+19	4.88E+19	4.33E+19	3.75E+19	3.15E+19	2.46E+19
13.00	6.59E+19	6.10E+19	5.54E+19	4.91E+19	4.25E+19	3.57E+19	2.79E+19
14.00	7.35E+19	6.79E+19	6.17E+19	5.47E+19	4.73E+19	3.97E+19	3.10E+19
15.00	8 20E+19	7.60E+19	6.90E+19	6.11E+19	5.29E+19	4.44E+19	3.46E+19
16 00	9.24E+19	8.53E+19	7.74E+19	6.85E+19	5.93E+19	4.97E+19	3.87E+19
17.00	1.04E+20	9.57E+19	8.68E+19	7.68E+19	6.64E+19	5.57E+19	4.33E+19
17.97	1.16E+20	1.07E+20	9.74E+19	8.61E+19	7.44E+19	6 23E+19	4.84E+19
18.84	1.29E+20	1.19E+20	1.08E+20	9.56E+19	8.26E+19	6.91E+19	5.36E+19
19.75	1.44E+20	1.33E+20	1.20E+20	1.06E+20	9.15E+19	7.64E+19	5.92E+19
20.62	1.59E+20	1.46E+20	1.32E+20	1.16E+20	1.00E+20	8.35E+19	6.45E+19
21.40	1.72E+20	1.58E+20	1.42E+20	1.25E+20	1.08E+20	8.96E+19	6 92E+19
22.15	1.83E+20	1.68E+20	1.51E+20	1.33E+20	1.14E+20	9.51E+19	7.33E+19
22.88	1.94E+20	1.78E+20	1.60E+20	1.40E+20	1.20E+20	1.00E+20	7.70E+19
23.75	2.04E+20	1.87E+20	1.67E+20	1.47E+20	1.25E+20	1.04E+20	7.98E+19
24.63	2.06E+20	1.88E+20	1.68E+20	1.47E+20	1.25E+20	1.04E+20	7.94E+19
25.28	1.94E+20	1.77E+20	1.59E+20	1.40E+20	1.19E+20	9.92E+19	7.63E+19

Table 3 (cont) Tabulation of Calculated Fluence (n/cm^2 above 1 MeV) for Weld H3 At End of Cycle 7

Azimuthal Angle (Deg)	Distance Into Shroud from Inner Surface (inches)						
	0.00	0.333	0.667	1.00	1.333	1.667	2.00
25.79	1.84E+20	1.68E+20	1.52E+20	1.33E+20	1.14E+20	9.53E+19	7.36E+19
26 31	1.74E+20	1.60E+20	1.44E+20	1.27E+20	1.09E+20	9.13E+19	7.06E+19
26.96	1.62E+20	1.49E+20	1.35E+20	1.19E+20	1.03E+20	8.61E+19	6.67E+19
27.76	1.53E+20	1.41E+20	1.28E+20	1.13E+20	9.75E+19	8.15E+19	6.33E+19
28.55	1.46E+20	1.35E+20	1.22E+20	1.08E+20	9.31E+19	7.78E+19	6.03E+19
29.35	1.40E+20	1.29E+20	1.17E+20	1.03E+20	8.87E+19	7.41E+19	5.75E+19
30.06	1.32E+20	1.21E+20	1.10E+20	9.73E+19	8.40E+19	7.03E+19	5.47E+19
30.68	1.25E+20	1.16E+20	1.05E+20	9.30E+19	8.04E+19	6.74E+19	5.24E+19
31.30	1.20E+20	1.11E+20	1.01E+20	8.92E+19	7.71E+19	6.47E+19	5.05E+19
32.10	1.14E+20	1.05E+20	9.58E+19	8.49E+19	7.35E+19	6.17E+19	4.81E+19
33.10	1.13E+20	1.04E+20	9.42E+19	8.34E+19	7.21E+19	6.05E+19	4.71E+19
34.09	1.14E+20	1.05E+20	9.54E+19	8.42E+19	7.27E+19	6.09E+19	4.73E+19
35.09	1.17E+20	1.08E+20	9.78E+19	8.63E+19	7.43E+19	6.21E+19	4.81E+19
36 08	1.21E+20	1.12E+20	1.01E+20	8.86E+19	7.61E+19	6.34E+19	4.90E+19
37.07	1.23E+20	1.12E+20	1.01E+20	8.86E+19	7.59E+19	6.32E+19	4.87E+19
37.94	1.15E+20	1.06E+20	9.52E+19	8.36E+19	7.17E+19	5.97E+19	4.60E+19
38.69	1.05E+20	9.68E+19	8.74E+19	7.70E+19	6.62E+19	5.52E+19	4.27E+19
39.43	9.50E+19	8.76E+19	7.93E+19	7.00E+19	6.03E+19	5.04E+19	3.91E+19
40.22	8.52E+19	7.86E+19	7.13E+19	6.30E+19	5.45E+19	4.56E+19	3.55E+19
41.04	7.66E+19	7.08E+19	6.44E+19	5.70E+19	4.93E+19	4.14E+19	3.23E+19
41.86	6.99E+19	6.48E+19	5.89E+19	5.23E+19	4.53E+19	3.81E+19	2.98E+19
42.73	6.46E+19	6 00E+19	5.46E+19	4.85E+19	4.21E+19	3.54E+19	2.77E+19
43.64	6.15E+19	5.70E+19	5.19E+19	4.61E+19	4.00E+19	3.37E+19	2.64E+19
44.55	6 01E+19	5.57E+19	5.07E+19	4.50E+19	3.90E+19	3.28E+19	2.57E+19

Table 4 Tabulation of Calculated Fluence (n/cm^2 above 1 MeV) for Weld H2 At End of Cycle 7

Azimuthal Angle (Deg)	Distance Into Shroud from Inner Surface (inches)						
	0.00	0.333	0.667	1.00	1.333	1.667	2.00
0.50	2.61E+19	2.42E+19	2.20E+19	1.96E+19	1.70E+19	1.43E+19	1.13E+19
1.68	2.63E+19	2.44E+19	2.22E+19	1.97E+19	1.71E+19	1.44E+19	1.13E+19
3.00	2.71E+19	2.51E+19	2.28E+19	2.03E+19	1.76E+19	1.48E+19	1.17E+19
4.32	2.82E+19	2.62E+19	2.38E+19	2.12E+19	1.84E+19	1.55E+19	1.22E+19
5.75	3.01E+19	2.79E+19	2.54E+19	2.26E+19	1.96E+19	1.65E+19	1.30E+19
7.25	3.26E+19	3.03E+19	2.75E+19	2.45E+19	2.12E+19	1.79E+19	1.40E+19
8.75	3.61E+19	3.35E+19	3.05E+19	2.71E+19	2.35E+19	1.98E+19	1.55E+19
10.25	4.05E+19	3.76E+19	3.42E+19	3.03E+19	2.63E+19	2.21E+19	1.74E+19
11.75	4.59E+19	4.26E+19	3.88E+19	3.44E+19	2.98E+19	2.51E+19	1.97E+19
13.00	5.22E+19	4.84E+19	4.40E+19	3.90E+19	3.38E+19	2.84E+19	2.23E+19
14.00	5.83E+19	5.39E+19	4.90E+19	4.34E+19	3.76E+19	3.16E+19	2.48E+19
15.00	6.50E+19	6.03E+19	5.48E+19	4.85E+19	4.20E+19	3.53E+19	2.77E+19
16.00	7.32E+19	6.77E+19	6.14E+19	5.44E+19	4.71E+19	3.96E+19	3.10E+19
17.00	8.22E+19	7.59E+19	6.89E+19	6.10E+19	5.28E+19	4.43E+19	3.46E+19
17.97	9.19E+19	8.52E+19	7.73E+19	6.84E+19	5.92E+19	4.96E+19	3.87E+19
18.84	1.02E+20	9.47E+19	8.58E+19	7.60E+19	6.56E+19	5.50E+19	4.29E+19
19.75	1.14E+20	1.05E+20	9.54E+19	8.43E+19	7.27E+19	6.08E+19	4.73E+19
20.62	1.26E+20	1.16E+20	1.05E+20	9.24E+19	7.96E+19	6.65E+19	5.15E+19
21.40	1.36E+20	1.25E+20	1.13E+20	9.94E+19	8.55E+19	7.14E+19	5.53E+19
22.15	1.45E+20	1.33E+20	1.20E+20	1.06E+20	9.08E+19	7.57E+19	5.86E+19
22.88	1.54E+20	1.41E+20	1.27E+20	1.12E+20	9.57E+19	7.96E+19	6 15E+19
23.75	1.62E+20	1.48E+20	1.33E+20	1.16E+20	9.96E+19	8.27E+19	6 38E+19
24.63	1.63E+20	1.49E+20	1.33E+20	1.16E+20	9.94E+19	8.25E+19	6 35E+19
25 28	1.54E+20	1.41E+20	1.26E+20	1.11E+20	9.49E+19	7.89E+19	6.10E+19

Table 4 (cont) Tabulation of Calculated Fluence (n/cm^2 above 1 MeV) for Weld H2 At End of Cycle 7

Azimuthal Angle (Deg)	Distance Into Shroud from Inner Surface (inches)						
	0.00	0.333	0.667	1.00	1.333	1.667	2.00
25.79	1.45E+20	1.34E+20	1.20E+20	1.06E+20	9.09E+19	7.59E+19	5.88E+19
26.31	1.38E+20	1.27E+20	1.14E+20	1.01E+20	8.69E+19	7.26E+19	5.64E+19
26.96	1.28E+20	1.18E+20	1.07E+20	9.48E+19	8.18E+19	6.85E+19	5.33E+19
27.76	1.21E+20	1.12E+20	1.01E+20	8.97E+19	7.75E+19	6.49E+19	5.05E+19
28.55	1.16E+20	1.07E+20	9.70E+19	8.56E+19	7.39E+19	6.19E+19	4.82E+19
29.35	1.11E+20	1.02E+20	9.24E+19	8.16E+19	7.04E+19	5.90E+19	4.59E+19
30 06	1.04E+20	9.63E+19	8.73E+19	7.72E+19	6.67E+19	5.59E+19	4.36E+19
30.68	9.91E+19	9.17E+19	8.32E+19	7.37E+19	6.38E+19	5.36E+19	4.19E+19
31.30	9.49E+19	8.78E+19	7.98E+19	7.07E+19	6.12E+19	5.15E+19	4.03E+19
32.10	9.02E+19	8.35E+19	7.59E+19	6.74E+19	5.84E+19	4.91E+19	3.84E+19
33.10	8.90E+19	8.23E+19	7.47E+19	6 61E+19	5.72E+19	4.81E+19	3.76E+19
34.09	9.03E+19	8.34E+19	7.55E+19	6.68E+19	5.77E+19	4.84E+19	3.77E+19
35.09	9.29E+19	8.56E+19	7.75E+19	6.84E+19	5.90E+19	4.94E+19	3.84E+19
36.08	9.61E+19	8.84E+19	7.98E+19	7.02E+19	6.04E+19	5.04E+19	3.91E+19
37.07	9.71E+19	8.89E+19	8.00E+19	7.02E+19	6.03E+19	5.02E+19	3.88E+19
37.94	9.12E+19	8.37E+19	7.54E+19	6.63E+19	5.69E+19	4.75E+19	3.67E+19
38.69	8.33E+19	7.67E+19	6.92E+19	6.10E+19	5.26E+19	4.39E+19	3.41E+19
39.43	7.52E+19	6.94E+19	6.28E+19	5.55E+19	4.79E+19	4.01E+19	3.12E+19
40.22	6.74E+19	6.23E+19	5.65E+19	5 00E+19	4.32E+19	3.63E+19	2.83E+19
41.04	6.06E+19	5.61E+19	5.10E+19	4 52E+19	3.92E+19	3.29E+19	2.58E+19
41.86	5.53E+19	5.13E+19	4.67E+19	4 15E+19	3.60E+19	3.03E+19	2.38E+19
42.73	5.12E+19	4.75E+19	4.33E+19	3.85E+19	3.34E+19	2.82E+19	2.21E+19
43.64	4.87E+19	4.52E+19	4.11E+19	3.66E+19	3.18E+19	2.68E+19	2.11E+19
44 55	4.75E+19	4.41E+19	4.02E+19	3.57E+19	3.10E+19	2.61E+19	2.05E+19

Table 5 Tabulation of Calculated Fluence Rate (n/cm²/s above 1 MeV) for Weld H5 Averaged over Cycle 7

Azimuthal Angle (Deg)	Distance Into Shroud from Inner Surface (inches)						
	0.00	0.333	0.667	1.00	1.333	1.667	2.00
0.50	7.36E+10	6.81E+10	6.20E+10	5.50E+10	4.76E+10	4.00E+10	3.11E+10
1.68	7.43E+10	6.87E+10	6.25E+10	5.55E+10	4.81E+10	4.04E+10	3.14E+10
3.00	7.66E+10	7.08E+10	6.44E+10	5.71E+10	4.95E+10	4.16E+10	3.23E+10
4.32	8.01E+10	7.41E+10	6.74E+10	5.98E+10	5.18E+10	4.35E+10	3.38E+10
5.75	8.57E+10	7.92E+10	7.20E+10	6.39E+10	5.54E+10	4.65E+10	3.62E+10
7.25	9.35E+10	8.65E+10	7.87E+10	6.98E+10	6.05E+10	5.08E+10	3.95E+10
8.75	1.05E+11	9.66E+10	8.79E+10	7.79E+10	6.75E+10	5.67E+10	4.41E+10
10.25	1.19E+11	1.10E+11	9.98E+10	8.85E+10	7.67E+10	6.44E+10	5.00E+10
11.75	1.37E+11	1.27E+11	1.15E+11	1.02E+11	8.84E+10	7.42E+10	5.75E+10
13.00	1.58E+11	1.46E+11	1.33E+11	1.17E+11	1.02E+11	8.53E+10	6.62E+10
14.00	1.79E+11	1.65E+11	1.50E+11	1.32E+11	1.14E+11	9.61E+10	7.44E+10
15.00	2.01E+11	1.86E+11	1.69E+11	1.50E+11	1.29E+11	1.08E+11	8.40E+10
16.00	2.29E+11	2.11E+11	1.92E+11	1.70E+11	1.47E+11	1.23E+11	9.51E+10
17.00	2.60E+11	2.39E+11	2.17E+11	1.92E+11	1.66E+11	1.39E+11	1.08E+11
17.97	2.94E+11	2.72E+11	2.46E+11	2.18E+11	1.88E+11	1.57E+11	1.22E+11
18.84	3.31E+11	3.05E+11	2.76E+11	2.44E+11	2.11E+11	1.76E+11	1.36E+11
19.75	3.73E+11	3.43E+11	3.10E+11	2.74E+11	2.36E+11	1.97E+11	1.52E+11
20.62	4.15E+11	3.81E+11	3.45E+11	3.03E+11	2.61E+11	2.17E+11	1.67E+11
21.40	4.54E+11	4.16E+11	3.75E+11	3.30E+11	2.83E+11	2.36E+11	1.81E+11
22.15	4.89E+11	4.48E+11	4 03E+11	3.54E+11	3.04E+11	2.53E+11	1.94E+11
22.88	5.25E+11	4.80E+11	4.31E+11	3.78E+11	3.24E+11	2.69E+11	2.05E+11
23.75	5.58E+11	5.08E+11	4.55E+11	3.97E+11	3.40E+11	2.81E+11	2.14E+11
24.63	5.65E+11	5.12E+11	4.58E+11	3.99E+11	3.40E+11	2.81E+11	2.14E+11
25.28	5.31E+11	4.84E+11	4.34E+11	3.80E+11	3.25E+11	2.69E+11	2.05E+11

Table 5 (cont) Tabulation of Calculated Fluence Rate (n/cm²/s above 1 MeV) for Weld H5 Averaged over Cycle 7

Azimuthal Angle (Deg)	Distance Into Shroud from Inner Surface (inches)						
	0.00	0.333	0.667	1.00	1.333	1.667	2.00
25.79	5.01E+11	4.58E+11	4.13E+11	3.62E+11	3.11E+11	2.58E+11	1.98E+11
26.31	4.73E+11	4.34E+11	3.92E+11	3.45E+11	2.97E+11	2.47E+11	1.90E+11
26.96	4.40E+11	4.05E+11	3.66E+11	3.23E+11	2.78E+11	2.32E+11	1.79E+11
27.76	4.14E+11	3.82E+11	3.46E+11	3.05E+11	2.63E+11	2.20E+11	1.69E+11
28.55	3.95E+11	3.64E+11	3.29E+11	2.90E+11	2.50E+11	2.09E+11	1.61E+11
29.35	3.76E+11	3.45E+11	3.12E+11	2.75E+11	2.37E+11	1.98E+11	1.52E+11
30.06	3.51E+11	3.23E+11	2.93E+11	2.59E+11	2.23E+11	1.86E+11	1.44E+11
30.68	3.32E+11	3.06E+11	2.77E+11	2.45E+11	2.12E+11	1.77E+11	1.37E+11
31.30	3.15E+11	2.91E+11	2.64E+11	2.33E+11	2.02E+11	1.69E+11	1.31E+11
32.10	2.96E+11	2.73E+11	2.48E+11	2.20E+11	1.90E+11	1.59E+11	1.23E+11
33.10	2.88E+11	2.66E+11	2.41E+11	2.13E+11	1.84E+11	1.54E+11	1.19E+11
34.09	2.90E+11	2.66E+11	2.41E+11	2.13E+11	1.84E+11	1.54E+11	1.19E+11
35.09	2.96E+11	2.72E+11	2.46E+11	2.17E+11	1.87E+11	1.56E+11	1.20E+11
36 08	3.05E+11	2.79E+11	2.52E+11	2.21E+11	1.90E+11	1.58E+11	1.21E+11
37.07	3.07E+11	2.80E+11	2.52E+11	2.21E+11	1.89E+11	1.57E+11	1.20E+11
37.94	2.87E+11	2.62E+11	2.36E+11	2.07E+11	1.77E+11	1.47E+11	1.13E+11
38.69	2.59E+11	2.38E+11	2.15E+11	1.89E+11	1.62E+11	1.35E+11	1.04E+11
39.43	2.31E+11	2.13E+11	1.92E+11	1.70E+11	1.46E+11	1.22E+11	9.41E+10
40.22	2.05E+11	1.89E+11	1.71E+11	1.51E+11	1.31E+11	1.09E+11	8.44E+10
41.04	1.82E+11	1.68E+11	1.52E+11	1.35E+11	1.17E+11	9.79E+10	7.58E+10
41.86	1.64E+11	1.51E+11	1.38E+11	1.22E+11	1.06E+11	8.88E+10	6.90E+10
42.73	1.49E+11	1.38E+11	1.26E+11	1.12E+11	9.70E+10	8.16E+10	6.35E+10
43.64	1.41E+11	1.30E+11	1.18E+11	1.05E+11	9.12E+10	7.67E+10	5.98E+10
44.55	1.36E+11	1.26E+11	1.15E+11	1.02E+11	8.84E+10	7.44E+10	5.79E+10

Table 6 Tabulation of Calculated Fluence Rate (n/cm²/s above 1 MeV) for Weld H4 Averaged over Cycle 7

Azimuthal Angle (Deg)	Distance Into Shroud from Inner Surface (inches)						
	0.00	0.333	0.667	1.00	1.333	1.667	2.00
0.50	2.87E+11	2.66E+11	2.42E+11	2.15E+11	1.86E+11	1.56E+11	1.21E+11
1.68	2.90E+11	2.68E+11	2.44E+11	2.16E+11	1.87E+11	1.57E+11	1.22E+11
3.00	2.99E+11	2.76E+11	2.51E+11	2.23E+11	1.93E+11	1.62E+11	1.26E+11
4.32	3.12E+11	2.89E+11	2.63E+11	2.33E+11	2.02E+11	1.69E+11	1.31E+11
5.75	3.34E+11	3.09E+11	2.81E+11	2.49E+11	2.16E+11	1.81E+11	1.40E+11
7.25	3.64E+11	3.37E+11	3.06E+11	2.72E+11	2.35E+11	1.97E+11	1.53E+11
8.75	4.07E+11	3.76E+11	3.42E+11	3.03E+11	2.63E+11	2.20E+11	1.71E+11
10.25	4.62E+11	4.27E+11	3.89E+11	3.44E+11	2.98E+11	2.50E+11	1.94E+11
11.75	5.33E+11	4.93E+11	4.48E+11	3.97E+11	3.43E+11	2.88E+11	2.23E+11
13.00	6.15E+11	5.69E+11	5.16E+11	4.57E+11	3.95E+11	3.31E+11	2.56E+11
14.00	6.95E+11	6 41E+11	5.82E+11	5.15E+11	4.45E+11	3.73E+11	2.88E+11
15.00	7.84E+11	7.25E+11	6.58E+11	5.82E+11	5.03E+11	4.21E+11	3.26E+11
16.00	8.92E+11	8.23E+11	7.46E+11	6.60E+11	5.70E+11	4.77E+11	3.69E+11
17.00	1.01E+12	9.33E+11	8.46E+11	7.48E+11	6.46E+11	5.41E+11	4.17E+11
17.97	1.14E+12	1.06E+12	9.60E+11	8.48E+11	7.32E+11	6.12E+11	4.71E+11
18.84	1.29E+12	1.19E+12	1.08E+12	9.52E+11	8.20E+11	6.85E+11	5.27E+11
19.75	1.45E+12	1.34E+12	1.21E+12	1.07E+12	9.18E+11	7.66E+11	5.88E+11
20.62	1.62E+12	1.49E+12	1.34E+12	1.18E+12	1.02E+12	8.46E+11	6.48E+11
21.40	1.77E+12	1.62E+12	1.46E+12	1.29E+12	1.10E+12	9.18E+11	7.02E+11
22.15	1.91E+12	1.75E+12	1.57E+12	1.38E+12	1.18E+12	9.84E+11	7.51E+11
22.88	2.05E+12	1.87E+12	1.68E+12	1.47E+12	1.26E+12	1.05E+12	7.96E+11
23.75	2.17E+12	1.98E+12	1.78E+12	1.55E+12	1.32E+12	1.10E+12	8 32E+11
24.63	2.20E+12	2.00E+12	1.79E+12	1.56E+12	1.33E+12	1.10E+12	8 31E+11
25.28	2.07E+12	1.89E+12	1.69E+12	1.48E+12	1.27E+12	1.05E+12	7.98E+11

Table 6 (cont) Tabulation of Calculated Fluence Rate (n/cm²/s above 1 MeV) for Weld H4 Averaged over Cycle 7

Azimuthal Angle (Deg)	Distance Into Shroud from Inner Surface (inches)						
	0.00	0.333	0.667	1.00	1.333	1.667	2.00
25.79	1.96E+12	1.79E+12	1.61E+12	1.41E+12	1.21E+12	1.01E+12	7.70E+11
26.31	1.85E+12	1.70E+12	1.53E+12	1.35E+12	1.16E+12	9.62E+11	7.38E+11
26.96	1.72E+12	1.58E+12	1.43E+12	1.26E+12	1.09E+12	9.05E+11	6.95E+11
27.76	1.62E+12	1.49E+12	1.35E+12	1.19E+12	1.03E+12	8.55E+11	6.58E+11
28.55	1.54E+12	1.42E+12	1.29E+12	1.13E+12	9.75E+11	8.14E+11	6.25E+11
29.35	1.47E+12	1.35E+12	1.22E+12	1.07E+12	9.24E+11	7.71E+11	5.92E+11
30.06	1.37E+12	1.26E+12	1.14E+12	1.01E+12	8.70E+11	7.27E+11	5.59E+11
30.68	1.29E+12	1.20E+12	1.08E+12	9.58E+11	8.27E+11	6.92E+11	5.33E+11
31.30	1.23E+12	1.14E+12	1.03E+12	9.11E+11	7.87E+11	6.59E+11	5 09E+11
32.10	1.16E+12	1.07E+12	9.70E+11	8.59E+11	7.42E+11	6.22E+11	4.80E+11
33.10	1.13E+12	1.04E+12	9.42E+11	8.32E+11	7.19E+11	6.02E+11	4.65E+11
34.09	1.13E+12	1.04E+12	9.43E+11	8.32E+11	7.18E+11	6.00E+11	4.62E+11
35.09	1.16E+12	1.06E+12	9.61E+11	8.47E+11	7.29E+11	6.08E+11	4.67E+11
36.08	1.19E+12	1.09E+12	9.86E+11	8.66E+11	7.43E+11	6.18E+11	4.73E+11
37.07	1.20E+12	1.10E+12	9.85E+11	8.62E+11	7.38E+11	6.12E+11	4.67E+11
37.94	1.12E+12	1.02E+12	9.22E+11	8.08E+11	6.92E+11	5.75E+11	4.39E+11
38.69	1.01E+12	9.30E+11	8.39E+11	7.38E+11	6.34E+11	5.27E+11	4.04E+11
39.43	9.05E+11	8.32E+11	7.53E+11	6.64E+11	5.71E+11	4.77E+11	3.66E+11
40.22	8.01E+11	7.38E+11	6.69E+11	5.91E+11	5.10E+11	4.26E+11	3.29E+11
41.04	7.10E+11	6.56E+11	5.96E+11	5.27E+11	4.56E+11	3.82E+11	2.95E+11
41.86	6 40E+11	5.92E+11	5.38E+11	4.77E+11	4.13E+11	3.47E+11	2.68E+11
42.73	5 84E+11	5.41E+11	4.93E+11	4.37E+11	3.79E+11	3.18E+11	2.47E+11
43.64	5 49E+11	5.08E+11	4.63E+11	4.11E+11	3.56E+11	2.99E+11	2.33E+11
44.55	5 33E+11	4.93E+11	4.49E+11	3.98E+11	3.45E+11	2.90E+11	2.25E+11

Table 7 Tabulation of Calculated Fluence Rate (n/cm²/s above 1 MeV) for Weld H3 Averaged over Cycle 7

Azimuthal Angle (Deg)	Distance Into Shroud from Inner Surface (inches)						
	0.00	0.333	0.667	1.00	1.333	1.667	2.00
0 50	1.03E+11	9.52E+10	8.67E+10	7.70E+10	6.69E+10	5.64E+10	4.41E+10
1.68	1.04E+11	9.60E+10	8.75E+10	7.77E+10	6.75E+10	5.68E+10	4.44E+10
3.00	1.07E+11	9.89E+10	9.00E+10	7.99E+10	6.94E+10	5.85E+10	4.57E+10
4.32	1.12E+11	1.03E+11	9.41E+10	8.35E+10	7.26E+10	6.11E+10	4.78E+10
5.75	1.19E+11	1.10E+11	1.00E+11	8.92E+10	7.75E+10	6.52E+10	5.10E+10
7.25	1.30E+11	1.20E+11	1.09E+11	9.72E+10	8.44E+10	7.11E+10	5.56E+10
8.75	1.45E+11	1.34E+11	1.22E+11	1.08E+11	9.41E+10	7.92E+10	6.18E+10
10.25	1.64E+11	1.52E+11	1.38E+11	1.23E+11	1.07E+11	8.97E+10	7.01E+10
11.75	1.89E+11	1.75E+11	1.59E+11	1.41E+11	1.23E+11	1.03E+11	8.05E+10
13.00	2.18E+11	2.02E+11	1.83E+11	1.63E+11	1.41E+11	1.19E+11	9.24E+10
14.00	2.46E+11	2.27E+11	2.06E+11	1.83E+11	1.59E+11	1.33E+11	1.04E+11
15.00	2.77E+11	2.56E+11	2.33E+11	2.06E+11	1.79E+11	1.50E+11	1.17E+11
16.00	3.15E+11	2.91E+11	2.64E+11	2.34E+11	2.03E+11	1.70E+11	1.32E+11
17.00	3.57E+11	3.29E+11	2.99E+11	2.65E+11	2.29E+11	1.93E+11	1.50E+11
17.97	4.04E+11	3.73E+11	3.39E+11	3.00E+11	2.60E+11	2.18E+11	1.69E+11
18.84	4.54E+11	4.19E+11	3.80E+11	3.36E+11	2.91E+11	2.44E+11	1.89E+11
19.75	5.11E+11	4.71E+11	4.26E+11	3.77E+11	3.25E+11	2.72E+11	2.10E+11
20.62	5.69E+11	5.23E+11	4.73E+11	4.17E+11	3.59E+11	3.00E+11	2.32E+11
21.40	6.21E+11	5.70E+11	5.15E+11	4.53E+11	3.90E+11	3.25E+11	2.51E+11
22.15	6.68E+11	6.13E+11	5.53E+11	4.86E+11	4.18E+11	3.48E+11	2.68E+11
22 88	7.17E+11	6.56E+11	5.90E+11	5.18E+11	4 45E+11	3.70E+11	2.84E+11
23.75	7.61E+11	6.94E+11	6.22E+11	5.45E+11	4.66E+11	3.87E+11	2.97E+11
24.63	7.71E+11	7.00E+11	6.26E+11	5.47E+11	4 67E+11	3.87E+11	2.96E+11
25.28	7.25E+11	6.61E+11	5.94E+11	5.21E+11	4 46E+11	3.71E+11	2.85E+11

Table 7 (cont) Tabulation of Calculated Fluence Rate (n/cm²/s above 1 MeV) for Weld H3 Averaged over Cycle 7

Azimuthal Angle (Deg)	Distance Into Shroud from Inner Surface (inches)						
	0.00	0.333	0.667	1.00	1.333	1.667	2.00
25.79	6.86E+11	6.28E+11	5.66E+11	4.97E+11	4.27E+11	3.56E+11	2.75E+11
26.31	6.48E+11	5.95E+11	5.38E+11	4.74E+11	4.08E+11	3.41E+11	2.63E+11
26.96	6.03E+11	5.55E+11	5.03E+11	4.44E+11	3.84E+11	3.21E+11	2.48E+11
27.76	5.69E+11	5.24E+11	4.75E+11	4.20E+11	3.63E+11	3.04E+11	2.35E+11
28.55	5.42E+11	5.00E+11	4.53E+11	4.00E+11	3.45E+11	2.89E+11	2.24E+11
29.35	5.16E+11	4.75E+11	4.30E+11	3.79E+11	3.27E+11	2.74E+11	2.12E+11
30.06	4.83E+11	4.45E+11	4.04E+11	3.57E+11	3.09E+11	2.59E+11	2.01E+11
30.68	4.57E+11	4.22E+11	3.83E+11	3.39E+11	2.93E+11	2.46E+11	1.91E+11
31.30	4.34E+11	4.01E+11	3.64E+11	3.23E+11	2.80E+11	2.35E+11	1.83E+11
32.10	4.08E+11	3.77E+11	3.43E+11	3.04E+11	2.64E+11	2.22E+11	1.73E+11
33.10	3.98E+11	3.67E+11	3.33E+11	2.95E+11	2.56E+11	2.15E+11	1.67E+11
34.09	4.00E+11	3.68E+11	3.34E+11	2.95E+11	2.55E+11	2.14E+11	1.66E+11
35.09	4.08E+11	3.76E+11	3.40E+11	3.00E+11	2.59E+11	2.17E+11	1.68E+11
36.08	4.21E+11	3.86E+11	3.48E+11	3.07E+11	2.64E+11	2.20E+11	1.70E+11
37.07	4.23E+11	3.87E+11	3.48E+11	3.05E+11	2.62E+11	2.18E+11	1.68E+11
37.94	3.95E+11	3.62E+11	3.26E+11	2.86E+11	2.46E+11	2.05E+11	1.57E+11
38.69	3.57E+11	3.28E+11	2.96E+11	2.61E+11	2.25E+11	1.88E+11	1.45E+11
39.43	3.19E+11	2.94E+11	2.66E+11	2.35E+11	2.03E+11	1.70E+11	1.32E+11
40.22	2.83E+11	2.61E+11	2.37E+11	2.09E+11	1.81E+11	1.52E+11	1.18E+11
41.04	2.51E+11	2 32E+11	2.11E+11	1.87E+11	1.62E+11	1.36E+11	1.06E+11
41.86	2.26E+11	2.09E+11	1.91E+11	1.69E+11	1.47E+11	1.24E+11	9.66E+10
42.73	2.07E+11	1.91E+11	1.75E+11	1.55E+11	1.35E+11	1.14E+11	8.89E+10
43.64	1.94E+11	1.80E+11	1.64E+11	1.46E+11	1.27E+11	1.07E+11	8.37E+10
44.55	1.88E+11	1.75E+11	1.59E+11	1.41E+11	1.23E+11	1.04E+11	8.11E+10

Table 8 Tabulation of Calculated Fluence Rate (n/cm²/s above 1 MeV) for Weld H2 Averaged over Cycle 7

Azimuthal Angle (Deg)	Distance Into Shroud from Inner Surface (inches)						
	0.00	0.333	0.667	1.00	1.333	1.667	2.00
0.50	7.85E+10	7.28E+10	6.63E+10	5.89E+10	5.12E+10	4.32E+10	3.39E+10
1.68	7.92E+10	7.34E+10	6.68E+10	5.94E+10	5.16E+10	4.36E+10	3.42E+10
3.00	8.15E+10	7.56E+10	6.87E+10	6.11E+10	5.31E+10	4.48E+10	3.52E+10
4.32	8.52E+10	7.90E+10	7.19E+10	6.39E+10	5.55E+10	4.69E+10	3.68E+10
5.75	9.09E+10	8.43E+10	7.67E+10	6.82E+10	5.93E+10	5.00E+10	3.93E+10
7.25	9.91E+10	9.18E+10	8.36E+10	7.43E+10	6.46E+10	5.45E+10	4.28E+10
8.75	1.11E+11	1.02E+11	9.32E+10	8.28E+10	7.20E+10	6.07E+10	4.76E+10
10.25	1.25E+11	1.16E+11	1.06E+11	9.39E+10	8.16E+10	6.88E+10	5.40E+10
11.75	1.44E+11	1.34E+11	1.22E+11	1.08E+11	9.39E+10	7.92E+10	6.20E+10
13.00	1.66E+11	1.54E+11	1.40E+11	1.24E+11	1.08E+11	9.09E+10	7.12E+10
14.00	1.88E+11	1.73E+11	1.58E+11	1.40E+11	1.21E+11	1.02E+11	8.00E+10
15.00	2.11E+11	1.96E+11	1.78E+11	1.58E+11	1.37E+11	1.15E+11	9.02E+10
16.00	2.41E+11	2.22E+11	2.02E+11	1.79E+11	1.55E+11	1.31E+11	1.02E+11
17.00	2.73E+11	2.52E+11	2.28E+11	2.03E+11	1.75E+11	1.48E+11	1.15E+11
17.97	3.08E+11	2.85E+11	2.59E+11	2.29E+11	1.99E+11	1.67E+11	1.30E+11
18.84	3.47E+11	3.20E+11	2.90E+11	2.57E+11	2.22E+11	1.87E+11	1.45E+11
19.75	3.90E+11	3.60E+11	3.26E+11	2.88E+11	2.49E+11	2.08E+11	1.62E+11
20.62	4.34E+11	4.00E+11	3.61E+11	3.19E+11	2.75E+11	2.30E+11	1.78E+11
21.40	4.74E+11	4.36E+11	3.93E+11	3.46E+11	2.98E+11	2 49E+11	1.93E+11
22.15	5.10E+11	4.68E+11	4.22E+11	3.72E+11	3.20E+11	2.67E+11	2.06E+11
22.88	5.47E+11	5.01E+11	4.51E+11	3.96E+11	3.40E+11	2.84E+11	2.19E+11
23.75	5.81E+11	5.30E+11	4.75E+11	4.16E+11	3.57E+11	2.97E+11	2.28E+11
24.63	5.88E+11	5.35E+11	4.78E+11	4.18E+11	3.57E+11	2.97E+11	2.28E+11
25.28	5.53E+11	5.05E+11	4.54E+11	3.98E+11	3.41E+11	2.84E+11	2.19E+11

Table 8 (cont) Tabulation of Calculated Fluence Rate (n/cm²/s above 1 MeV) for Weld H2 Averaged over Cycle 7

Azimuthal Angle (Deg)	Distance Into Shroud from Inner Surface (inches)						
	0.00	0.333	0.667	1.00	1.333	1.667	2.00
25.79	5.23E+11	4.80E+11	4.32E+11	3.80E+11	3.27E+11	2.73E+11	2.11E+11
26.31	4.95E+11	4.55E+11	4.11E+11	3.62E+11	3.12E+11	2.61E+11	2.03E+11
26.96	4.60E+11	4.24E+11	3.84E+11	3.40E+11	2.94E+11	2.46E+11	1.91E+11
27.76	4.34E+11	4.01E+11	3.63E+11	3.21E+11	2.77E+11	2.33E+11	1.81E+11
28.55	4.14E+11	3.82E+11	3.46E+11	3.06E+11	2.64E+11	2.22E+11	1.72E+11
29.35	3.94E+11	3.63E+11	3.28E+11	2.90E+11	2.50E+11	2.10E+11	1.63E+11
30.06	3.69E+11	3.40E+11	3.08E+11	2.73E+11	2.36E+11	1.98E+11	1.54E+11
30.68	3.48E+11	3.22E+11	2.92E+11	2.59E+11	2.24E+11	1.89E+11	1.47E+11
31.30	3.31E+11	3.06E+11	2.78E+11	2.47E+11	2.14E+11	1.80E+11	1.41E+11
32.10	3.11E+11	2.88E+11	2.62E+11	2.33E+11	2.02E+11	1.70E+11	1.33E+11
33.10	3.04E+11	2.80E+11	2.54E+11	2.26E+11	1.95E+11	1.65E+11	1.29E+11
34.09	3.05E+11	2.81E+11	2.55E+11	2.26E+11	1.95E+11	1.64E+11	1.28E+11
35.09	3.11E+11	2.87E+11	2.60E+11	2.29E+11	1.98E+11	1.66E+11	1.29E+11
36.08	3.21E+11	2.95E+11	2.66E+11	2.35E+11	2.02E+11	1.69E+11	1.31E+11
37.07	3.23E+11	2.96E+11	2.66E+11	2.33E+11	2.00E+11	1.67E+11	1.29E+11
37.94	3.01E+11	2.76E+11	2.49E+11	2.19E+11	1.88E+11	1.57E+11	1.21E+11
38 69	2.73E+11	2.51E+11	2.26E+11	2.00E+11	1.72E+11	1.44E+11	1.12E+11
39.43	2.44E+11	2.25E+11	2.03E+11	1.80E+11	1.55E+11	1.30E+11	1.01E+11
40.22	2.16E+11	1.99E+11	1.81E+11	1.60E+11	1.39E+11	1.17E+11	9.10E+10
41.04	1.92E+11	1.77E+11	1.61E+11	1.43E+11	1.24E+11	1.04E+11	8.18E+10
41.86	1.73E+11	1.60E+11	1.46E+11	1.29E+11	1.12E+11	9.49E+10	7.44E+10
42.73	1.58E+11	1.46E+11	1.33E+11	1.19E+11	1.03E+11	8.72E+10	6 85E+10
43.64	1.48E+11	1.37E+11	1.25E+11	1.12E+11	9.70E+10	8.20E+10	6 45E+10
44.55	1.44E+11	1.33E+11	1.21E+11	1.08E+11	9.40E+10	7.95E+10	6.25E+10

Table 9 Tabulation of Calculated Fluence (n/cm^2 above 1 MeV) for Weld H5 Projected to End of Cycle 8

Azimuthal Angle (Deg)	Distance Into Shroud from Inner Surface (inches)						
	0.00	0.333	0.667	1.00	1.333	1.667	2.00
0.50	2.44E+19	2.26E+19	2.05E+19	1.82E+19	1.58E+19	1.33E+19	1.04E+19
1.68	2.46E+19	2.27E+19	2.07E+19	1.84E+19	1.59E+19	1.34E+19	1.05E+19
3.00	2.53E+19	2.34E+19	2.13E+19	1.89E+19	1.64E+19	1.37E+19	1.07E+19
4.32	2.64E+19	2.44E+19	2.22E+19	1.97E+19	1.71E+19	1.44E+19	1.12E+19
5.75	2.81E+19	2.60E+19	2.37E+19	2.10E+19	1.82E+19	1.53E+19	1.19E+19
7.25	3.05E+19	2.82E+19	2.57E+19	2.28E+19	1.97E+19	1.66E+19	1.30E+19
8.75	3.38E+19	3.13E+19	2.85E+19	2.52E+19	2.19E+19	1.84E+19	1.43E+19
10.25	3.80E+19	3.51E+19	3.19E+19	2.83E+19	2.45E+19	2.06E+19	1.61E+19
11.75	4 32E+19	4.00E+19	3.64E+19	3.22E+19	2.79E+19	2.34E+19	1.82E+19
13.00	4.92E+19	4.55E+19	4.13E+19	3.66E+19	3.17E+19	2.66E+19	2.07E+19
14.00	5.51E+19	5.08E+19	4.62E+19	4.09E+19	3.53E+19	2.97E+19	2.31E+19
15.00	6 15E+19	5.70E+19	5.17E+19	4.58E+19	3.96E+19	3.32E+19	2.58E+19
16.00	6 95E+19	6.41E+19	5.81E+19	5.14E+19	4.45E+19	3.73E+19	2.90E+19
17.00	7.81E+19	7.20E+19	6.53E+19	5.78E+19	4.99E+19	4.18E+19	3.25E+19
17.97	8 76E+19	8.10E+19	7.34E+19	6.49E+19	5.60E+19	4.69E+19	3.64E+19
18.84	9.78E+19	9.02E+19	8.18E+19	7.22E+19	6.23E+19	5.21E+19	4.04E+19
19.75	1.09E+20	1.01E+20	9.11E+19	8.03E+19	6.92E+19	5.77E+19	4.47E+19
20.62	1.21E+20	1.11E+20	1.00E+20	8.82E+19	7.59E+19	6.32E+19	4.88E+19
21.40	1.31E+20	1.20E+20	1.08E+20	9.52E+19	8.17E+19	6.80E+19	5.25E+19
22.15	1.39E+20	1.28E+20	1.15E+20	1.01E+20	8.69E+19	7.23E+19	5.56E+19
22.88	1.49E+20	1.36E+20	1.22E+20	1.07E+20	9.18E+19	7.62E+19	5.85E+19
23.75	1.57E+20	1.43E+20	1.28E+20	1.12E+20	9.57E+19	7.93E+19	6.08E+19
24.63	1.58E+20	1.44E+20	1.29E+20	1.12E+20	9.56E+19	7.92E+19	6.05E+19
25.28	1.49E+20	1.36E+20	1.22E+20	1.07E+20	9.13E+19	7.57E+19	5.82E+19

Table 9 (cont) Tabulation of Calculated Fluence (n/cm^2 above 1 MeV) for Weld H5 Projected to End of Cycle 8

Azimuthal Angle (Deg)	Distance Into Shroud from Inner Surface (inches)						
	0.00	0.333	0.667	1.00	1.333	1.667	2.00
25.79	1.41E+20	1.29E+20	1.16E+20	1.02E+20	8.75E+19	7.28E+19	5.61E+19
26.31	1.33E+20	1.22E+20	1.11E+20	9.72E+19	8.36E+19	6.97E+19	5.38E+19
26.96	1.24E+20	1.14E+20	1.04E+20	9.13E+19	7.87E+19	6.57E+19	5.08E+19
27.76	1.17E+20	1.08E+20	9.79E+19	8 64E+19	7.45E+19	6 22E+19	4.82E+19
28.55	1.12E+20	1.03E+20	9.35E+19	8.25E+19	7.11E+19	5.94E+19	4.59E+19
29.35	1.07E+20	9.85E+19	8.90E+19	7.85E+19	6.76E+19	5.65E+19	4.37E+19
30.06	1.01E+20	9.28E+19	8.40E+19	7.42E+19	6.40E+19	5.35E+19	4.15E+19
30.68	9.55E+19	8.82E+19	8.01E+19	7.08E+19	6.12E+19	5.12E+19	3.98E+19
31.30	9.14E+19	8.44E+19	7.66E+19	6.78E+19	5.86E+19	4.91E+19	3.82E+19
32.10	8.66E+19	8.01E+19	7.27E+19	6.44E+19	5.57E+19	4.67E+19	3.64E+19
33.10	8 52E+19	7.87E+19	7.13E+19	6.31E+19	5.45E+19	4.57E+19	3.55E+19
34.09	8 63E+19	7.95E+19	7.20E+19	6.35E+19	5.48E+19	4.59E+19	3.56E+19
35.09	8 86E+19	8.15E+19	7.37E+19	6.50E+19	5.59E+19	4.67E+19	3.61E+19
36 08	9.16E+19	8.41E+19	7.58E+19	6.66E+19	5.72E+19	4.77E+19	3.67E+19
37.07	9.24E+19	8.45E+19	7.60E+19	6.66E+19	5.70E+19	4.74E+19	3.64E+19
37.94	8 68E+19	7.94E+19	7.15E+19	6.27E+19	5.38E+19	4.47E+19	3 44E+19
38.69	7.90E+19	7.26E+19	6.55E+19	5.77E+19	4.96E+19	4.13E+19	3.19E+19
39.43	7.12E+19	6.56E+19	5.93E+19	5.23E+19	4.51E+19	3.77E+19	2.92E+19
40.22	6.37E+19	5.87E+19	5.33E+19	4.70E+19	4.06E+19	3.40E+19	2.64E+19
41.04	5.71E+19	5.28E+19	4.79E+19	4.24E+19	3.67E+19	3.08E+19	2.40E+19
41.86	5.20E+19	4.82E+19	4.38E+19	3.88E+19	3.36E+19	2.82E+19	2.20E+19
42.73	4.80E+19	4.45E+19	4.05E+19	3.60E+19	3.12E+19	2.62E+19	2.05E+19
43.64	4.56E+19	4.22E+19	3.84E+19	3.41E+19	2.96E+19	2.49E+19	1.94E+19
44.55	4.44E+19	4.12E+19	3.75E+19	3.32E+19	2.88E+19	2 42E+19	1.89E+19

Table 10 Tabulation of Calculated Fluence (n/cm^2 above 1 MeV) for Weld H4 Projected to End of Cycle 8

Azimuthal Angle (Deg)	Distance Into Shroud from Inner Surface (inches)						
	0.00	0.333	0.667	1.00	1.333	1.667	2.00
0.50	9.17E+19	8.50E+19	7.74E+19	6.86E+19	5.94E+19	4.99E+19	3.89E+19
1.68	9.25E+19	8.57E+19	7.80E+19	6.91E+19	5.99E+19	5.03E+19	3.92E+19
3.00	9.52E+19	8.82E+19	8.02E+19	7.11E+19	6.16E+19	5.17E+19	4 03E+19
4.32	9.94E+19	9.21E+19	8.38E+19	7.42E+19	6.43E+19	5.40E+19	4.21E+19
5.75	1.06E+20	9.81E+19	8.93E+19	7.91E+19	6.85E+19	5.75E+19	4.48E+19
7.25	1.15E+20	1.07E+20	9.70E+19	8.59E+19	7.44E+19	6.25E+19	4.87E+19
8.75	1.28E+20	1.18E+20	1.08E+20	9.53E+19	8.25E+19	6.92E+19	5.38E+19
10.25	1.44E+20	1.33E+20	1.21E+20	1.07E+20	9.27E+19	7.77E+19	6.05E+19
11.75	1.64E+20	1.51E+20	1.38E+20	1.22E+20	1.06E+20	8.85E+19	6.87E+19
13.00	1.87E+20	1.73E+20	1.57E+20	1.39E+20	1.20E+20	1.01E+20	7.82E+19
14.00	2.09E+20	1.93E+20	1.75E+20	1.55E+20	1.34E+20	1.12E+20	8.72E+19
15.00	2.34E+20	2.16E+20	1.97E+20	1.74E+20	1.50E+20	1.26E+20	9.76E+19
16.00	2.64E+20	2.44E+20	2.21E+20	1.95E+20	1.69E+20	1.41E+20	1.10E+20
17.00	2.97E+20	2.74E+20	2.49E+20	2.20E+20	1.90E+20	1.59E+20	1.23E+20
17.97	3.33E+20	3.08E+20	2.80E+20	2.47E+20	2.13E+20	1.78E+20	1.38E+20
18.84	3.72E+20	3.44E+20	3.11E+20	2.75E+20	2.37E+20	1.98E+20	1.53E+20
19.75	4.16E+20	3.83E+20	3.47E+20	3.06E+20	2.63E+20	2.19E+20	1.69E+20
20.62	4.59E+20	4.23E+20	3.82E+20	3.36E+20	2.89E+20	2.40E+20	1.85E+20
21.40	4.99E+20	4.58E+20	4.13E+20	3.63E+20	3.11E+20	2.59E+20	1.99E+20
22.15	5.32E+20	4.88E+20	4.40E+20	3.86E+20	3.31E+20	2.75E+20	2.11E+20
22.88	5.67E+20	5.19E+20	4.67E+20	4.09E+20	3.50E+20	2.90E+20	2.22E+20
23.75	5 98E+20	5.46E+20	4 89E+20	4.28E+20	3.65E+20	3.02E+20	2.31E+20
24.63	6.04E+20	5.49E+20	4.91E+20	4.28E+20	3.65E+20	3.01E+20	2.30E+20
25.28	5.68E+20	5.19E+20	4.66E+20	4.07E+20	3.48E+20	2.88E+20	2.21E+20

Table 10 (cont) Tabulation of Calculated Fluence (n/cm^2 above 1 MeV) for Weld H4 Projected to End of Cycle 8

Azimuthal Angle (Deg)	Distance Into Shroud from Inner Surface (inches)						
	0.00	0.333	0.667	1.00	1.333	1.667	2.00
25.79	5.37E+20	4.92E+20	4.43E+20	3.89E+20	3.33E+20	2.77E+20	2.13E+20
26.31	5.07E+20	4 67E+20	4.21E+20	3.70E+20	3.18E+20	2.65E+20	2.04E+20
26.96	4.72E+20	4.35E+20	3.94E+20	3.47E+20	2.99E+20	2.49E+20	1.92E+20
27.76	4.46E+20	4.11E+20	3.72E+20	3.28E+20	2.83E+20	2.36E+20	1.82E+20
28.55	4.25E+20	3.92E+20	3.55E+20	3.13E+20	2.70E+20	2.25E+20	1.73E+20
29.35	4.05E+20	3.73E+20	3.38E+20	2.98E+20	2.56E+20	2.14E+20	1.65E+20
30.06	3.81E+20	3.51E+20	3.18E+20	2.81E+20	2.42E+20	2.02E+20	1.56E+20
30.68	3.61E+20	3.34E+20	3.03E+20	2.68E+20	2.31E+20	1.93E+20	1.50E+20
31.30	3.45E+20	3.19E+20	2.90E+20	2.56E+20	2.21E+20	1.85E+20	1.44E+20
32.10	3.27E+20	3.02E+20	2.75E+20	2.43E+20	2.10E+20	1.76E+20	1.37E+20
33.10	3.21E+20	2.97E+20	2.69E+20	2.38E+20	2.05E+20	1.72E+20	1.33E+20
34.09	3.25E+20	3.00E+20	2.71E+20	2.39E+20	2.06E+20	1.72E+20	1.33E+20
35.09	3.33E+20	3.07E+20	2.78E+20	2.45E+20	2.10E+20	1.75E+20	1.35E+20
36.08	3.45E+20	3.16E+20	2.85E+20	2.51E+20	2.15E+20	1.79E+20	1.37E+20
37.07	3.48E+20	3.18E+20	2.86E+20	2.50E+20	2.14E+20	1.78E+20	1.36E+20
37.94	3.26E+20	2.99E+20	2.69E+20	2.36E+20	2.02E+20	1.68E+20	1.29E+20
38.69	2.97E+20	2.73E+20	2.46E+20	2.17E+20	1.86E+20	1.55E+20	1.19E+20
39.43	2.68E+20	2.46E+20	2.23E+20	1.97E+20	1.69E+20	1.41E+20	1.09E+20
40.22	2.39E+20	2.21E+20	2.00E+20	1.77E+20	1.52E+20	1.27E+20	9.86E+19
41.04	2.14E+20	1.98E+20	1.80E+20	1.59E+20	1.38E+20	1.15E+20	8.95E+19
41.86	1.95E+20	1.81E+20	1.64E+20	1.46E+20	1.26E+20	1.06E+20	8.22E+19
42.73	1.80E+20	1.67E+20	1.52E+20	1.35E+20	1.17E+20	9.81E+19	7.64E+19
43.64	1.71E+20	1.58E+20	1.44E+20	1.28E+20	1.11E+20	9.30E+19	7.25E+19
44.55	1.66E+20	1.54E+20	1.40E+20	1.24E+20	1.08E+20	9.05E+19	7.06E+19

Table 11 Tabulation of Calculated Fluence (n/cm^2 above 1 MeV) for Weld H3 Projected to End of Cycle 8

Azimuthal Angle (Deg)	Distance Into Shroud from Inner Surface (inches)						
	0.00	0.333	0.667	1.00	1.333	1.667	2.00
0.50	3.88E+19	3.60E+19	3.28E+19	2.91E+19	2.52E+19	2.12E+19	1.66E+19
1.68	3.91E+19	3.63E+19	3.30E+19	2.93E+19	2.54E+19	2.14E+19	1.67E+19
3.00	4.03E+19	3.73E+19	3.40E+19	3.01E+19	2.61E+19	2.20E+19	1.72E+19
4.32	4.20E+19	3.89E+19	3.54E+19	3.15E+19	2.73E+19	2.30E+19	1.80E+19
5.75	4.48E+19	4.15E+19	3.78E+19	3.35E+19	2.91E+19	2.44E+19	1.91E+19
7.25	4.86E+19	4.50E+19	4.10E+19	3.64E+19	3.15E+19	2.65E+19	2.08E+19
8.75	5.39E+19	4.99E+19	4.54E+19	4.03E+19	3.49E+19	2.94E+19	2.30E+19
10.25	6.05E+19	5.60E+19	5.10E+19	4.52E+19	3.92E+19	3.29E+19	2.58E+19
11.75	6.88E+19	6.37E+19	5.80E+19	5.14E+19	4.45E+19	3.74E+19	2.92E+19
13.00	7.84E+19	7.26E+19	6.59E+19	5 84E+19	5.06E+19	4.25E+19	3.32E+19
14.00	8.77E+19	8.09E+19	7.36E+19	6 52E+19	5.64E+19	4.74E+19	3.70E+19
15.00	9.79E+19	9.07E+19	8.24E+19	7.29E+19	6.32E+19	5.30E+19	4.13E+19
16 00	1.10E+20	1.02E+20	9.26E+19	8.20E+19	7.09E+19	5.95E+19	4.63E+19
17.00	1.24E+20	1.15E+20	1.04E+20	9.21E+19	7.96E+19	6.67E+19	5.19E+19
17.97	1.39E+20	1.29E+20	1.17E+20	1.03E+20	8.93E+19	7.48E+19	5.81E+19
18.84	1.55E+20	1.43E+20	1.30E+20	1.15E+20	9.93E+19	8.31E+19	6.45E+19
19.75	1.73E+20	1.60E+20	1.45E+20	1.28E+20	1.10E+20	9.20E+19	7.13E+19
20.62	1.91E+20	1.76E+20	1.59E+20	1.40E+20	1.21E+20	1.01E+20	7.78E+19
21.40	2.07E+20	1.91E+20	1.72E+20	1.51E+20	1.30E+20	1.08E+20	8.37E+19
22.15	2.21E+20	2.03E+20	1.83E+20	1.61E+20	1.38E+20	1.15E+20	8.87E+19
22 88	2.36E+20	2.16E+20	1.94E+20	1.70E+20	1.46E+20	1.21E+20	9.33E+19
23.75	2 48E+20	2.27E+20	2.03E+20	1.78E+20	1.52E+20	1.26E+20	9.69E+19
24 63	2.51E+20	2.28E+20	2.04E+20	1.78E+20	1.52E+20	1.26E+20	9.64E+19
25.28	2 36E+20	2.15E+20	1.94E+20	1.69E+20	1.45E+20	1.20E+20	9.27E+19

Table 11 (cont) Tabulation of Calculated Fluence (n/cm^2 above 1 MeV) for Weld H3 Projected to End of Cycle 8

Azimuthal Angle (Deg)	Distance Into Shroud from Inner Surface (inches)						
	0.00	0.333	0 667	1.00	1.333	1.667	2.00
25.79	2.23E+20	2.04E+20	1.84E+20	1.62E+20	1.39E+20	1.16E+20	8.94E+19
26.31	2.11E+20	1.94E+20	1.75E+20	1.54E+20	1.33E+20	1.11E+20	8.58E+19
26.96	1.97E+20	1.81E+20	1.64E+20	1.45E+20	1.25E+20	1.04E+20	8.10E+19
27.76	1.86E+20	1.71E+20	1.55E+20	1.37E+20	1.18E+20	9.90E+19	7.68E+19
28.55	1.78E+20	1.64E+20	1.48E+20	1.31E+20	1.13E+20	9.44E+19	7.32E+19
29.35	1.69E+20	1.56E+20	1.41E+20	1.25E+20	1.07E+20	8.99E+19	6.97E+19
30.06	1.59E+20	1.47E+20	1.33E+20	1.18E+20	1.02E+20	8.52E+19	6.62E+19
30.68	1.51E+20	1.40E+20	1.27E+20	1.12E+20	9.72E+19	8.15E+19	6.34E+19
31.30	1.45E+20	1.34E+20	1.22E+20	1.08E+20	9.32E+19	7.82E+19	6.09E+19
32.10	1.37E+20	1.27E+20	1.16E+20	1.02E+20	8 87E+19	7.45E+19	5.80E+19
33.10	1.35E+20	1.25E+20	1.13E+20	1.00E+20	8.68E+19	7.28E+19	5.67E+19
34.09	1.37E+20	1.26E+20	1.15E+20	1.01E+20	8.74E+19	7.31E+19	5.68E+19
35 09	1.41E+20	1.30E+20	1.17E+20	1.04E+20	8.92E+19	7.45E+19	5.78E+19
36.08	1.46E+20	1.34E+20	1.21E+20	1.06E+20	9.13E+19	7.61E+19	5.87E+19
37.07	1.47E+20	1.35E+20	1.21E+20	1.06E+20	9.10E+19	7.57E+19	5.83E+19
37.94	1.38E+20	1.26E+20	1.14E+20	1.00E+20	8.58E+19	7.14E+19	5.50E+19
38.69	1.26E+20	1.16E+20	1.04E+20	9.20E+19	7.92E+19	6.60E+19	5.11E+19
39.43	1.13E+20	1.04E+20	9.46E+19	8.35E+19	7.20E+19	6 02E+19	4.67E+19
40.22	1.01E+20	9.36E+19	8.49E+19	7.51E+19	6.49E+19	5.44E+19	4.23E+19
41.04	9.10E+19	8.42E+19	7.65E+19	6.77E+19	5.86E+19	4.92E+19	3.84E+19
41.86	8.29E+19	7.68E+19	6.99E+19	6 20E+19	5.37E+19	4.52E+19	3.53E+19
42.73	7.65E+19	7.10E+19	6.47E+19	5.74E+19	4.99E+19	4.20E+19	3.28E+19
43.64	7.27E+19	6.73E+19	6.13E+19	5.45E+19	4.73E+19	3.98E+19	3.12E+19
44.55	7.09E+19	6.57E+19	5.98E+19	5.31E+19	4.61E+19	3.88E+19	3.04E+19

Table 12 Tabulation of Calculated Fluence (n/cm^2 above 1 MeV) for Weld H2 Projected to End of Cycle 8

Azimuthal Angle (Deg)	Distance Into Shroud from Inner Surface (inches)						
	0.00	0.333	0.667	1.00	1.333	1.667	2.00
0.50	3.06E+19	2.84E+19	2.59E+19	2.30E+19	1.99E+19	1.68E+19	1.32E+19
1.68	3.09E+19	2.86E+19	2.61E+19	2.32E+19	2.01E+19	1.70E+19	1.33E+19
3.00	3.17E+19	2.95E+19	2.68E+19	2.38E+19	2.07E+19	1.74E+19	1.37E+19
4.32	3.31E+19	3.07E+19	2.80E+19	2.49E+19	2.16E+19	1.82E+19	1.43E+19
5.75	3.53E+19	3.27E+19	2.98E+19	2.65E+19	2.30E+19	1.94E+19	1.52E+19
7.25	3.83E+19	3.55E+19	3.23E+19	2.87E+19	2.49E+19	2.10E+19	1.65E+19
8.75	4.25E+19	3.94E+19	3.58E+19	3.18E+19	2.76E+19	2.33E+19	1.82E+19
10.25	4.77E+19	4.42E+19	4.02E+19	3.57E+19	3.10E+19	2.61E+19	2.05E+19
11.75	5.42E+19	5.03E+19	4.57E+19	4.06E+19	3.52E+19	2.96E+19	2.32E+19
13.00	6.18E+19	5.73E+19	5.20E+19	4.61E+19	4.00E+19	3.36E+19	2.64E+19
14.00	6.90E+19	6.38E+19	5.80E+19	5.15E+19	4.46E+19	3.75E+19	2.94E+19
15.00	7.71E+19	7.15E+19	6.50E+19	5.76E+19	4.99E+19	4.20E+19	3.28E+19
16.00	8.70E+19	8.05E+19	7.30E+19	6.47E+19	5.60E+19	4.71E+19	3.68E+19
17.00	9.78E+19	9.04E+19	8.20E+19	7.27E+19	6.29E+19	5.28E+19	4.13E+19
17.97	1.10E+20	1.02E+20	9.21E+19	8.16E+19	7.06E+19	5.92E+19	4.62E+19
18.84	1.22E+20	1.13E+20	1.03E+20	9.07E+19	7.84E+19	6.57E+19	5.12E+19
19.75	1.36E+20	1.26E+20	1.14E+20	1.01E+20	8.70E+19	7.28E+19	5.66E+19
20.62	1.51E+20	1.39E+20	1.26E+20	1.11E+20	9.53E+19	7.97E+19	6.18E+19
21.40	1.63E+20	1.50E+20	1.35E+20	1.19E+20	1.03E+20	8.57E+19	6.64E+19
22.15	1.74E+20	1.60E+20	1.44E+20	1.27E+20	1.09E+20	9.10E+19	7.04E+19
22.88	1.85E+20	1.70E+20	1.53E+20	1.34E+20	1.15E+20	9.59E+19	7.41E+19
23.75	1.95E+20	1.79E+20	1.60E+20	1.40E+20	1.20E+20	9.98E+19	7.69E+19
24 63	1.97E+20	1.80E+20	1.61E+20	1.40E+20	1.20E+20	9.95E+19	7.66E+19
25.28	1.85E+20	1.70E+20	1.52E+20	1.34E+20	1.15E+20	9.53E+19	7.36E+19

Table 12 (cont) Tabulation of Calculated Fluence (n/cm^2 above 1 MeV) for Weld H2 Projected to End of Cycle 8

Azimuthal Angle (Deg)	Distance Into Shroud from Inner Surface (inches)						
	0.00	0.333	0 667	1.00	1.333	1.667	2.00
25.79	1.76E+20	1.61E+20	1.45E+20	1.28E+20	1.10E+20	9.16E+19	7.09E+19
26.31	1.66E+20	1.53E+20	1.38E+20	1.22E+20	1.05E+20	8.76E+19	6 81E+19
26.96	1.55E+20	1.43E+20	1.29E+20	1.14E+20	9.87E+19	8.26E+19	6.43E+19
27.76	1.46E+20	1.35E+20	1.22E+20	1.08E+20	9.34E+19	7.83E+19	6.09E+19
28.55	1.40E+20	1.29E+20	1.17E+20	1.03E+20	8.91E+19	7.46E+19	5.81E+19
29.35	1.33E+20	1.23E+20	1.11E+20	9.83E+19	8.48E+19	7.10E+19	5.53E+19
30.06	1.25E+20	1.16E+20	1.05E+20	9.29E+19	8.03E+19	6.73E+19	5.25E+19
30.68	1.19E+20	1.10E+20	1.00E+20	8.86E+19	7.67E+19	6.44E+19	5.03E+19
31.30	1.14E+20	1.05E+20	9.57E+19	8.49E+19	7.35E+19	6.18E+19	4.84E+19
32.10	1.08E+20	1.00E+20	9.10E+19	8.07E+19	7.00E+19	5.89E+19	4.60E+19
33.10	1.06E+20	9.84E+19	8.93E+19	7.91E+19	6.85E+19	5.75E+19	4.50E+19
34.09	1.08E+20	9.96E+19	9.02E+19	7.97E+19	6.89E+19	5.78E+19	4.51E+19
35.09	1.11E+20	1.02E+20	9.24E+19	8.16E+19	7.04E+19	5.89E+19	4.58E+19
36.08	1.15E+20	1.05E+20	9.50E+19	8.37E+19	7.20E+19	6.01E+19	4.66E+19
37.07	1.16E+20	1.06E+20	9.52E+19	8.36E+19	7.18E+19	5.98E+19	4.63E+19
37.94	1.09E+20	9.96E+19	8.97E+19	7.88E+19	6.77E+19	5.65E+19	4.37E+19
38.69	9.89E+19	9.11E+19	8.22E+19	7.25E+19	6.25E+19	5.22E+19	4.05E+19
39.43	8.92E+19	8.23E+19	7.45E+19	6.58E+19	5.68E+19	4.76E+19	3.70E+19
40.22	7.98E+19	7.37E+19	6.69E+19	5.92E+19	5.12E+19	4.30E+19	3.36E+19
41.04	7.16E+19	6.63E+19	6.02E+19	5.34E+19	4.63E+19	3.89E+19	3.05E+19
41.86	6.53E+19	6.05E+19	5.51E+19	4.89E+19	4.24E+19	3.57E+19	2.80E+19
42.73	6.02E+19	5.60E+19	5.10E+19	4.53E+19	3.94E+19	3.32E+19	2 61E+19
43.64	5.72E+19	5.31E+19	4.83E+19	4.30E+19	3.74E+19	3.15E+19	2.48E+19
44.55	5.58E+19	5.18E+19	4.71E+19	4.19E+19	3.64E+19	3.07E+19	2.41E+19

Table 13 Tabulation of Calculated Fluence (n/cm^2 above 1 MeV) for Welds V16 and V17 At End of Cycle 7

Height from BAF (in.)	Distance Into Shroud from Inner Surface (inches)						
	0.00	0.333	0.667	1.00	1.333	1.667	2.00
0	1.59E+19	1.49E+19	1.36E+19	1.21E+19	1.05E+19	8.91E+18	7.23E+18
0.55	1.72E+19	1.61E+19	1.47E+19	1.31E+19	1.14E+19	9.61E+18	7.79E+18
1.15	1.86E+19	1.75E+19	1.59E+19	1.42E+19	1.23E+19	1.04E+19	8.43E+18
1.88	2 07E+19	1.94E+19	1.77E+19	1.57E+19	1.37E+19	1.15E+19	9.32E+18
2.62	2.31E+19	2.16E+19	1.97E+19	1.75E+19	1.52E+19	1.28E+19	1.03E+19
3.75	2.64E+19	2.46E+19	2.24E+19	1.99E+19	1.73E+19	1.46E+19	1.17E+19
5.25	3.10E+19	2.90E+19	2.64E+19	2.34E+19	2.03E+19	1.71E+19	1.38E+19
7.07	3.64E+19	3.39E+19	3.09E+19	2.74E+19	2.37E+19	1.99E+19	1.60E+19

Table 14 Tabulation of Calculated Fluence (n/cm^2 above 1 MeV) for Welds V14 and V15 At End of Cycle 7

Height from BAF (in)	Distance Into Shroud from Inner Surface (inches)						
	0.00	0.333	0.667	1.00	1.333	1.667	2.00
7.07	2.00E+19	1.86E+19	1.70E+19	1.50E+19	1.30E+19	1.10E+19	8 80E+18
10.50	2.52E+19	2.36E+19	2.14E+19	1.90E+19	1.65E+19	1.38E+19	1.11E+19
15.00	3.08E+19	2.87E+19	2.61E+19	2.31E+19	2.00E+19	1.68E+19	1.35E+19
21.00	3.57E+19	3.34E+19	3.04E+19	2.69E+19	2.33E+19	1.96E+19	1.57E+19
27.00	3.96E+19	3.70E+19	3.36E+19	2.98E+19	2.58E+19	2.17E+19	1.74E+19
33.00	4.30E+19	4.01E+19	3.65E+19	3.24E+19	2.81E+19	2.36E+19	1.89E+19
39.00	4.64E+19	4.34E+19	3.95E+19	3.50E+19	3.03E+19	2.55E+19	2.04E+19
45.00	5.01E+19	4.68E+19	4.26E+19	3.78E+19	3.27E+19	2.75E+19	2.20E+19
51.00	5.42E+19	5.06E+19	4.60E+19	4.08E+19	3.54E+19	2.97E+19	2.38E+19
57.00	5.84E+19	5.45E+19	4.96E+19	4.40E+19	3.81E+19	3.20E+19	2.57E+19
63.00	6.28E+19	5.86E+19	5.33E+19	4 73E+19	4.10E+19	3.44E+19	2.76E+19
69.00	6.70E+19	6.26E+19	5.69E+19	5.05E+19	4.37E+19	3.67E+19	2.94E+19
75.00	7.11E+19	6.64E+19	6.04E+19	5.36E+19	4.64E+19	3.89E+19	3.12E+19
80.69	7.47E+19	6.97E+19	6.34E+19	5.62E+19	4.87E+19	4.09E+19	3.27E+19

Table 15 Tabulation of Calculated Fluence (n/cm^2 above 1 MeV) for Welds V12 and V13 At End of Cycle 7

Height from BAF (in.)	Distance Into Shroud from Inner Surface (inches)						
	0 00	0.333	0 667	1.00	1.333	1.667	2.00
80.687	1.35E+20	1.26E+20	1.15E+20	1.02E+20	8 80E+19	7.39E+19	5.92E+19
87.00	1.41E+20	1.32E+20	1.20E+20	1.06E+20	9.21E+19	7.73E+19	6.19E+19
93.00	1.46E+20	1.36E+20	1.24E+20	1.10E+20	9.50E+19	7.98E+19	6 39E+19
99.00	1.49E+20	1.39E+20	1.27E+20	1.12E+20	9.73E+19	8.17E+19	6.54E+19
105.00	1.51E+20	1.41E+20	1.28E+20	1.14E+20	9.86E+19	8.28E+19	6 62E+19
111.00	1.51E+20	1.41E+20	1.29E+20	1.14E+20	9.86E+19	8.28E+19	6.62E+19
117.00	1.49E+20	1.39E+20	1.26E+20	1.12E+20	9.67E+19	8.12E+19	6.49E+19
123.00	1.42E+20	1.32E+20	1.20E+20	1.06E+20	9.21E+19	7.73E+19	6.18E+19
129.00	1.28E+20	1.19E+20	1.08E+20	9.61E+19	8.31E+19	6.98E+19	5.58E+19
133 50	1.11E+20	1.04E+20	9.46E+19	8.38E+19	7.26E+19	6.09E+19	4.87E+19
136.50	9.72E+19	9.07E+19	8.24E+19	7.30E+19	6.32E+19	5.30E+19	4.24E+19
139.50	8.10E+19	7.57E+19	6.88E+19	6.10E+19	5.29E+19	4.44E+19	3.55E+19
142.00	6 80E+19	6.35E+19	5.78E+19	5.12E+19	4.44E+19	3.73E+19	2.99E+19
143.567	5.96E+19	5.57E+19	5.07E+19	4.50E+19	3.90E+19	3.28E+19	2.64E+19

Table 16 Tabulation of Calculated Fluence (n/cm^2 above 1 MeV) for Welds V6 to V11 At End of Cycle 7

Height from BAF (in.)	Distance Into Shroud from Inner Surface (inches)						
	0.00	0.333	0.667	1.00	1.333	1.667	2.00
Welds V6 and V9							
143.567	3.27E+19	3.05E+19	2.78E+19	2.46E+19	2.14E+19	1.80E+19	1.44E+19
144.30	3.06E+19	2.86E+19	2.60E+19	2.31E+19	2.00E+19	1.69E+19	1.36E+19
144.90	2.89E+19	2.70E+19	2.46E+19	2.18E+19	1.90E+19	1.60E+19	1.28E+19
145.45	2.74E+19	2.57E+19	2.34E+19	2.08E+19	1.80E+19	1.52E+19	1.22E+19
145.85	2.65E+19	2.47E+19	2.25E+19	2.00E+19	1.74E+19	1.46E+19	1.18E+19
146.067	2.59E+19	2.42E+19	2.20E+19	1.96E+19	1.70E+19	1.43E+19	1.15E+19
Welds V7, V8, V10, V11							
143.567	1.31E+20	1.22E+20	1.11E+20	9.77E+19	8.44E+19	7.06E+19	5.64E+19
144.30	1.23E+20	1.14E+20	1.04E+20	9.15E+19	7.90E+19	6.61E+19	5.29E+19
144.90	1.16E+20	1.08E+20	9.79E+19	8.65E+19	7.47E+19	6.26E+19	5.01E+19
145.45	1.10E+20	1.03E+20	9.30E+19	8.22E+19	7.11E+19	5.95E+19	4.76E+19
145.85	1.06E+20	9.88E+19	8.96E+19	7.92E+19	6.85E+19	5.74E+19	4.59E+19
146.067	1.04E+20	9.67E+19	8.77E+19	7.75E+19	6.70E+19	5.62E+19	4.50E+19

Table 17 Tabulation of Calculated Fluence Rate (n/cm²/s above 1 MeV) for Welds V16 and V17 Averaged over Cycle 7

Height from BAF (in.)	Distance Into Shroud from Inner Surface (inches)						
	0.00	0.333	0.667	1.00	1.333	1.667	2.00
0	5.83E+10	5.46E+10	4.98E+10	4.43E+10	3.86E+10	3.27E+10	2.66E+10
0.55	6.29E+10	5.90E+10	5.38E+10	4.80E+10	4.18E+10	3.54E+10	2.87E+10
1.15	6.84E+10	6.42E+10	5.86E+10	5.22E+10	4.55E+10	3.84E+10	3.11E+10
1.88	7.61E+10	7.13E+10	6.51E+10	5.79E+10	5.04E+10	4.26E+10	3.45E+10
2.62	8.51E+10	7.95E+10	7.25E+10	6 45E+10	5.61E+10	4.73E+10	3.83E+10
3.75	9.73E+10	9.10E+10	8.29E+10	7.37E+10	6.41E+10	5.41E+10	4.36E+10
5.25	1.15E+11	1.07E+11	9.78E+10	8.70E+10	7.55E+10	6.37E+10	5.12E+10
7.07	1.35E+11	1.26E+11	1.15E+11	1.02E+11	8.84E+10	7.44E+10	5.97E+10

Table 18 Tabulation of Calculated Fluence Rate (n/cm²/s above 1 MeV) for Welds V14 and V15 Averaged over Cycle 7

Height from BAF (in.)	Distance Into Shroud from Inner Surface (inches)						
	0.00	0.333	0.667	1.00	1.333	1.667	2.00
7.07	7.30E+10	6.81E+10	6.20E+10	5.50E+10	4.76E+10	4.00E+10	3.21E+10
10.50	9.23E+10	8.61E+10	7.84E+10	6.95E+10	6.02E+10	5.05E+10	4.05E+10
15.00	1.12E+11	1.04E+11	9.49E+10	8.41E+10	7.28E+10	6.11E+10	4.89E+10
21.00	1.28E+11	1.20E+11	1.09E+11	9.66E+10	8.36E+10	7.02E+10	5.62E+10
27.00	1.41E+11	1.31E+11	1.19E+11	1.06E+11	9.18E+10	7.71E+10	6.18E+10
33.00	1.53E+11	1.42E+11	1.30E+11	1.15E+11	9.96E+10	8.37E+10	6.71E+10
39.00	1.66E+11	1.55E+11	1.41E+11	1.25E+11	1.08E+11	9.08E+10	7.28E+10
45.00	1.80E+11	1.68E+11	1.53E+11	1.35E+11	1.17E+11	9.86E+10	7.90E+10
51.00	1.95E+11	1.82E+11	1.66E+11	1.47E+11	1.27E+11	1.07E+11	8.58E+10
57.00	2.12E+11	1.98E+11	1.80E+11	1.60E+11	1.39E+11	1.16E+11	9.33E+10
63.00	2.31E+11	2.15E+11	1.96E+11	1.74E+11	1.50E+11	1.26E+11	1.01E+11
69.00	2.49E+11	2.32E+11	2.11E+11	1.87E+11	1.62E+11	1.36E+11	1.09E+11
75.00	2.68E+11	2.50E+11	2.27E+11	2.02E+11	1.75E+11	1.47E+11	1.17E+11
80.69	2.85E+11	2.66E+11	2.42E+11	2.15E+11	1.86E+11	1.56E+11	1.25E+11

Table 19 Tabulation of Calculated Fluence Rate (n/cm²/s above 1 MeV) for Welds V12 and V13 Averaged over Cycle 7

Height from BAF (in.)	Distance Into Shroud from Inner Surface (inches)						
	0.00	0.333	0.667	1.00	1.333	1.667	2.00
80 687	5.28E+11	4.93E+11	4.49E+11	3.98E+11	3.45E+11	2.90E+11	2.33E+11
87.00	5.58E+11	5.21E+11	4.74E+11	4.20E+11	3.64E+11	3.06E+11	2.45E+11
93.00	5.77E+11	5.39E+11	4.90E+11	4.35E+11	3.77E+11	3.17E+11	2.54E+11
99.00	5.86E+11	5.47E+11	4.98E+11	4.42E+11	3.83E+11	3.22E+11	2.58E+11
105.00	5.91E+11	5.52E+11	5.02E+11	4.45E+11	3.86E+11	3.24E+11	2.60E+11
111.00	5.88E+11	5.49E+11	5.00E+11	4.43E+11	3.84E+11	3.23E+11	2.58E+11
117.00	5.72E+11	5.34E+11	4.85E+11	4.30E+11	3.73E+11	3.13E+11	2.51E+11
123.00	5.36E+11	5.00E+11	4.55E+11	4.04E+11	3.50E+11	2.93E+11	2.35E+11
129.00	4.71E+11	4.40E+11	4.00E+11	3.55E+11	3.07E+11	2.58E+11	2.06E+11
133.50	3 98E+11	3.71E+11	3.38E+11	2.99E+11	2.59E+11	2.18E+11	1.74E+11
136.50	3.35E+11	3.13E+11	2.84E+11	2.52E+11	2.18E+11	1.83E+11	1.47E+11
139.50	2.67E+11	2.50E+11	2.27E+11	2.02E+11	1.75E+11	1.47E+11	1.18E+11
142.00	2.18E+11	2.03E+11	1.85E+11	1.64E+11	1.43E+11	1.20E+11	9.67E+10
143.567	1.87E+11	1.75E+11	1.59E+11	1.41E+11	1.23E+11	1.04E+11	8.36E+10

Table 20 **Tabulation of Calculated Fluence Rate (n/cm²/s above 1 MeV) for Welds V6 to V11 Averaged over Cycle 7**

Height from BAF (in.)	Distance Into Shroud from Inner Surface (inches)						
	0.00	0.333	0.667	1.00	1.333	1.667	2.00
Welds V6 and V9							
143.567	1.02E+11	9.52E+10	8.67E+10	7.70E+10	6.69E+10	5.64E+10	4.54E+10
144.30	9.42E+10	8.81E+10	8.02E+10	7.13E+10	6.19E+10	5.22E+10	4.21E+10
144.90	8.80E+10	8.24E+10	7.51E+10	6.67E+10	5.80E+10	4.89E+10	3.95E+10
145.45	8.30E+10	7.78E+10	7.08E+10	6.29E+10	5.47E+10	4.61E+10	3.73E+10
145.85	7.97E+10	7.46E+10	6.79E+10	6.04E+10	5.25E+10	4.43E+10	3.58E+10
146 067	7.79E+10	7.28E+10	6.63E+10	5.89E+10	5.12E+10	4.32E+10	3.50E+10
Welds V7, V8, V10, V11							
143.567	4.82E+11	4 48E+11	4.06E+11	3.59E+11	3.10E+11	2.60E+11	2.08E+11
144.30	4.45E+11	4.14E+11	3.75E+11	3.32E+11	2.87E+11	2.40E+11	1.93E+11
144.90	4.15E+11	3.87E+11	3.51E+11	3.10E+11	2.69E+11	2.25E+11	1.81E+11
145.45	3.92E+11	3.65E+11	3.31E+11	2.93E+11	2.53E+11	2.12E+11	1.71E+11
145.85	3.76E+11	3.51E+11	3.18E+11	2.81E+11	2.43E+11	2.04E+11	1.64E+11
146 067	3.68E+11	3.42E+11	3.10E+11	2.74E+11	2.37E+11	1.99E+11	1.60E+11

Table 21 Tabulation of Calculated Fluence (n/cm^2 above 1 MeV) for Welds V16 and V17 Projected to End of Cycle 8

Height from BAF (in.)	Distance Into Shroud from Inner Surface (inches)						
	0.00	0.333	0.667	1.00	1.333	1.667	2.00
0	1.93E+19	1.80E+19	1.64E+19	1.46E+19	1.27E+19	1.08E+19	8.76E+18
0.55	2.08E+19	1.95E+19	1.78E+19	1.58E+19	1.38E+19	1.16E+19	9.44E+18
1.15	2.26E+19	2.12E+19	1.93E+19	1.72E+19	1.50E+19	1.26E+19	1.02E+19
1.88	2.51E+19	2.35E+19	2.14E+19	1.90E+19	1.66E+19	1.40E+19	1.13E+19
2.62	2.80E+19	2.61E+19	2.38E+19	2.12E+19	1.84E+19	1.55E+19	1.25E+19
3.75	3.19E+19	2.99E+19	2.72E+19	2.42E+19	2.10E+19	1.77E+19	1.42E+19
5.25	3.76E+19	3.51E+19	3.20E+19	2.84E+19	2.47E+19	2.08E+19	1.67E+19
7.07	4.41E+19	4.12E+19	3.75E+19	3.32E+19	2.88E+19	2.42E+19	1.94E+19

Table 22 Tabulation of Calculated Fluence (n/cm^2 above 1 MeV) for Welds V14 and V15 Projected to End of Cycle 8

Height from BAF (in.)	Distance Into Shroud from Inner Surface (inches)						
	0.00	0.333	0.667	1.00	1.333	1.667	2.00
7.07	2.42E+19	2.26E+19	2.05E+19	1.82E+19	1.58E+19	1.33E+19	1.06E+19
10.50	3.05E+19	2.85E+19	2.59E+19	2.30E+19	1.99E+19	1.67E+19	1.34E+19
15.00	3.72E+19	3.47E+19	3.15E+19	2.80E+19	2.42E+19	2.03E+19	1.63E+19
21.00	4.31E+19	4.03E+19	3.66E+19	3.25E+19	2.81E+19	2.36E+19	1.89E+19
27.00	4.77E+19	4.45E+19	4.05E+19	3.59E+19	3.11E+19	2.61E+19	2.09E+19
33.00	5.18E+19	4.83E+19	4.40E+19	3.90E+19	3.38E+19	2.84E+19	2.28E+19
39.00	5.59E+19	5.22E+19	4.75E+19	4.22E+19	3.65E+19	3.07E+19	2.46E+19
45.00	6.05E+19	5.64E+19	5.14E+19	4.56E+19	3.95E+19	3.32E+19	2.66E+19
51.00	6.54E+19	6.11E+19	5.56E+19	4.93E+19	4.27E+19	3.59E+19	2.87E+19
57.00	7.06E+19	6.59E+19	6.00E+19	5.32E+19	4.61E+19	3.87E+19	3.10E+19
63.00	7.61E+19	7.10E+19	6.46E+19	5.73E+19	4.96E+19	4.17E+19	3.34E+19
69.00	8.13E+19	7.59E+19	6.91E+19	6.12E+19	5.31E+19	4.46E+19	3.57E+19
75.00	8.65E+19	8.08E+19	7.35E+19	6 51E+19	5.64E+19	4.74E+19	3.79E+19
80.69	9.11E+19	8.50E+19	7.74E+19	6.86E+19	5.94E+19	4.99E+19	3.99E+19

Table 23 Tabulation of Calculated Fluence (n/cm^2 above 1 MeV) for Welds V12 and V13 Projected to End of Cycle 8

Height from BAF (in.)	Distance Into Shroud from Inner Surface (inches)						
	0.00	0.333	0.667	1.00	1.333	1.667	2.00
80.687	1.65E+20	1.54E+20	1.40E+20	1.24E+20	1.08E+20	9.05E+19	7.25E+19
87.00	1.73E+20	1.62E+20	1.47E+20	1.30E+20	1.13E+20	9.49E+19	7.60E+19
93.00	1.79E+20	1.67E+20	1.52E+20	1.35E+20	1.17E+20	9.80E+19	7.85E+19
99.00	1.83E+20	1.71E+20	1.55E+20	1.38E+20	1.19E+20	1.00E+20	8.02E+19
105.00	1.85E+20	1.73E+20	1.57E+20	1.39E+20	1.21E+20	1.01E+20	8.12E+19
111.00	1.85E+20	1.73E+20	1.57E+20	1.39E+20	1.21E+20	1.01E+20	8.11E+19
117.00	1.81E+20	1.69E+20	1.54E+20	1.36E+20	1.18E+20	9.92E+19	7.93E+19
123 00	1.72E+20	1.61E+20	1.46E+20	1.30E+20	1.12E+20	9.41E+19	7.53E+19
129.00	1.55E+20	1.45E+20	1.31E+20	1.16E+20	1.01E+20	8.46E+19	6.76E+19
133.50	1.34E+20	1.25E+20	1.14E+20	1.01E+20	8.75E+19	7.34E+19	5.87E+19
136.50	1.16E+20	1.09E+20	9.87E+19	8.75E+19	7.57E+19	6.36E+19	5.09E+19
139.50	9.64E+19	9.00E+19	8.19E+19	7.26E+19	6.29E+19	5.29E+19	4.23E+19
142.00	8.05E+19	7.52E+19	6.84E+19	6.07E+19	5.26E+19	4.42E+19	3.55E+19
143.567	7.04E+19	6.57E+19	5.98E+19	5.31E+19	4.61E+19	3.88E+19	3.12E+19

Table 24 Tabulation of Calculated Fluence (n/cm^2 above 1 MeV) for Welds V6 to V11 Projected to End of Cycle 8

Height from BAF (in.)	Distance Into Shroud from Inner Surface (inches)						
	0.00	0.333	0.667	1.00	1.333	1.667	2.00
Welds V6 and V9							
143.567	3.85E+19	3.60E+19	3.28E+19	2.91E+19	2.52E+19	2.12E+19	1.71E+19
144.30	3.60E+19	3.36E+19	3.06E+19	2.72E+19	2.36E+19	1.98E+19	1.60E+19
144.90	3.39E+19	3.17E+19	2.89E+19	2.57E+19	2.23E+19	1.88E+19	1.51E+19
145.45	3.22E+19	3.01E+19	2.74E+19	2.44E+19	2.12E+19	1.78E+19	1.44E+19
145.85	3.10E+19	2.90E+19	2.64E+19	2.35E+19	2.04E+19	1.72E+19	1.38E+19
146.067	3.04E+19	2.84E+19	2.59E+19	2.30E+19	1.99E+19	1.68E+19	1.36E+19
Welds V7, V8, V10, V11							
143.567	1.59E+20	1.48E+20	1.34E+20	1.18E+20	1.02E+20	8 55E+19	6.83E+19
144.30	1.48E+20	1.38E+20	1.25E+20	1.11E+20	9.55E+19	8 00E+19	6.40E+19
144.90	1.40E+20	1.30E+20	1.18E+20	1.04E+20	9.02E+19	7.55E+19	6.04E+19
145.45	1.33E+20	1.24E+20	1.12E+20	9.90E+19	8.56E+19	7.17E+19	5.74E+19
145.85	1.28E+20	1.19E+20	1.08E+20	9.53E+19	8.24E+19	6.91E+19	5.54E+19
146.067	1.25E+20	1.16E+20	1.05E+20	9.33E+19	8.06E+19	6.76E+19	5.42E+19